Investigation of Optical Properties of Metal and Conducting Polymer Nanocomposites

Thesis submitted by

Swatilekha Roy

Doctor of Philosophy (Engineering)

Department of Instrumentation & Electronics Engineering

Faculty Council of Engineering & Technology

Jadavpur University, Kolkata, India

2022

JADAVPUR UNIVERSITY

KOLKATA- 700032

INDIA

INDEX NO. 156/19/15/E

Title of the thesis: *Investigation of Optical Properties of Metal and Conducting Polymer Nanocomposites*

Name, Designation & Institute of the Supervisor:

Prof. Rajib Bandyopadhyay,

Professor,

Department of Instrumentation & Electronics Engineering, Jadavpur University, Salt Lake Campus, Sector-III, Block- LB, Plot-8, Kolkata-700106, India.

Phone : 08240235742; Fax: 03323357254

Paper published in International Journals

[1] Swatilekha Roy, K Asokan, P.V. Rajesh, JBM Krishna, *"Synthesis of metal-PolyAniline composites by ion implantation"* Indian Journal of Physics 96(10), November, 2021.

[2] Swatilekha Roy, Rajib Bandyopadhyay, "*Medium energy Silver and Nickel ion implantation into micrometer range PolyAniline film and observation of the structural changes*" --- under preparation.

[3] Swatilekha Roy, Rajib Bandyopadhyay, "*Preparation of Cu-Poly Aniline nanocomposite by Mechano-synthesis route (Ball-Milling) and checking frequency and temperature dependent electrical conductivity and dielectric relaxation*"---- under preparation.

[4] Swatilekha Roy, Rajib Bandyopadhyay, "*Study on dielectric relaxation of Ni doped PANI*" ---- under preparation.

Paper published in Conference proceeding

[1]Swatilekha Roy, Sachindranath Das, P. Asokan, P. V. Rajesh, J. B. M. Krishna, "*Synthesis of Metal-PolyAniline Composites by Ion Implantation*", Bose Tagore National Advanced Workshop on "Recent Advances in Condensed Matter Physics: Theory and Experiment" (NAWCMP - 2018) during 3 – 4 August, 2018 at the department of Physics, Visva-Bharati, West-Bengal, India.

[2] Swatilekha Roy, Shriya Chatterjee, JBM Krishna, Sachindranath Das, "*Electrical Properties of PolyAniline Nickel Nanocomposites prepared by Ball Milling method*",Condensed Matter Days (CMDAYS 2018) : A National Conference on Condensed Matter physics Bose

125Events, August 29 – 31, 2018 organized by The Department of Physics, The University of Burdwan.

[3] Swatilekha Roy, Sachindranath Das, JBM Krishna "*Study of Optical properties of PolyAniline-Gold nanocomposites*", National Symposium on Recent Trends in Instrumentation Science & Technology, organized by Department of Instrumentation Science, Jadavpur University Kolkata-32, March 19-21, 2015.

Statement of Originality

I, Swatilekha Roy, registered on 15/01/2015 do here by declare that this thesis entitled "*Investigation of Optical Properties of Metal and Conducting Polymer Nanocomposites*" contains literature survey and original research work done by the undersigned candidate as part of Doctoral studies.

All information in this thesis have been obtained and presented in accordance with existing academic rules and ethical conduct, I have fully cited and referred all the materials and results that are not original to this work.

I also declare that I have checked this thesis as per the "Policy on anti plagiarism, Jadavpur University 2019", and the level of similarity as checked by iThenticate software is 9%.

Swatilekha Roy

Index No. 156/19/15/E

Date:31/12/2022

Prof. Rajib Bandyopdhyay,

Professor,

Dept. of Instrumentation & Electronics Engineering

Jadavpur University, Salt lake Campus, Kolkata-700106, Kolkata, India.

Certificate from the Supervisor

Date:31/12/2022

This is to certify that the thesis entitled "Investigation of Optical Properties of Metal and Conducting Polymer Nanocomposites" submitted by Swatilekha Roy, who got her name registered on 15/01/2015 For the award of Ph.D. (Engineering) degree of jadavpur University, is absolutely based upon her own work under supervisor Prof. Rajib Bandyopadhyay and that neither her thesis nor any part of the thesis has been submitted for any degree/ diploma or any other academic award anywhere before.

Prof. Rajib Bandyopadhyay

Professor,

Dept. of Instrumentation & Electronics Engineering,

Jadavpur University,

Salt Lake Campus,

Kolkata-700106, India

Dedicated to

My Parents & My Guide, Prof.Rajib Bandyopadhyay

Acknowledgement

At the end of the path of PhD, when I look back I could still listen to my father encouraging me as he always used to, to take up any challenge sincerely, to face the hardship of life boldly, never to retreat. I can still hear my mother encouraging me my daily course of actions as usual. Even today, whenever, I earnestly need some guidance, I can still hear their voices deep from somewhere which encourage me in my daily life.

My supervisor, Prof. Rajib Bandyopadhyay always their standing as my true guide; his soft voice, firm and true instructions in work, his physical and strong presence at the darkest hours in my life, despite his own challenges has set an examplary milestone for me.I offer my utmost gratitude to Prof. Chiranjib Bhattacharjee for listening me intently to all my problems and worries and providing solutions for highest good. My heartfelt gratitude to our former Honorable Vice Chanellor, Prof. Suranjan Das sir, for standing there like a guardian figure, and taking necessary actions with best possible wayout, eventually forgiving my ignorance whenever I approached him, something beyond an authoritative figure. I am thankful to the Finance Officer of Jadavpur University for gving me appropriate guidance in right time. I am highly greateful to the staff members of Jadvpur University, specially Mr. Subrata Chakraborty, Mr. Kishalay Majumdar and others for supporting and encouraging me as elder brothers/ sisters. The members of Jadavpur University Research Scholar Association (JURSA) have been with me through thick and thin.

The faculties, staffs, my fellow scholars in my Department of Instrumentation & Electronics Engg. -- Prof. Bipan Tudu, Prof. Pachanan Pramanik, Prof. Sankar Narayan Patra, Prof. Runu Banerjee, Shrikanta Acharya, Shreya Nag, Mahua Banerjee, Debangana Das, Deepam Ganguly, Dilip Singh, Nilava Debabhuti for standing beside me in my dearth situation and providing me constant support for whom I could get back to normal life. I am thakful to the Department of Instrumentation Science and Dr. Sachindranath Das in the Department of Instrumentation Science for respective support in my work.

We would like to thank the Director of IUAC, New Delhi for providing the low energy ion beam facility. We also thank the Director and Prof. P V Satyam of IOP Bhubaneswar, for providing Medium energy ion beam facility and FESEM and other structural analysis facilities. We greatly acknowledge UGC-DAE CSR Kolkata Center for financial and infrastructure support. We are grateful to Department of Science & Technology for financial support through WOSA (Women Scientist-A) scheme.

In this scenario I would like to thank some more persons like Mr. Pradip Kumar and his pal and many others like him, may be they were just few passer bys in my life but they stood like guardian angels in dark, wee hours of life.

And above all I want to thank the almighty for surrounding me with wonderful people and opportunities.

Swatilekha Roy,
Department of Instrumentation & Electronics Engineering,
Jadavpur University, Salt Lake Campus
December 2022

Abstract

Metallic nanoparticles are best known for their unique optical, electronic, chemical and magnetic properties which are surprisingly different from the individual atoms and their bulk counterparts. It has been observed that nanoparticles with different sizes give rise to different colours which are quite different from their bulk intrinsic colours. There are a few metals which can survive as nanoparticles under atmospheric conditions whereas most metal nanoparticles are very reactive due to their large surface to volume ratio. However, certain metal nanoparticles can sustain in specific dielectric media and such studies have been carried out by embedding them into different matrices. Different methods like vapour deposition, thermal diffusion, sol-gel synthesis and dispersion in liquid media have been reported in the literature, but so far no studies have been carried out on nanoparticles embedded in conducting polymers. Therefore, we have chosen conducting polymers as our preferred matrix and metal nanoparticles were embedded in the matrix by ion implantation method.

The choice of conducting polymers is due to their emerging applications as transparent electrodes in electronic devices. These polymers are semiconducting in nature and their conductivity and optical behaviour can be tuned by appropriate doping. On the other hand, nanoparticles have many novel attributes which are well known and they can be manipulated in terms of shape and size to achieve the desired functionality. Therefore, nanoparticles embedded inside the conducting polymers are expected to exhibit interesting properties. It has been observed that metal nanoparticles are capable of forming organized structures and polymer ligands play an important role to influence this organized structure. Temperatures also have significance in controlling aggregate size and morphology. The dielectric constant of the surrounding medium has great influences on optical properties of the nanoparticles. Therefore, larger clusters and smaller distance between clusters provide higher optical response. Ion implantation method has been chosen as our preferred method because the depth of layer of nanoparticles can be controlled by choosing appropriate energy of the ion beam and the concentration of the metal ions can be controlled by the fluence. The process of nanoparticle formation inside a matrix is known as *Ostwald Ripening* where incorporation of metal ions in a matrix above the solubility limit causes agglomeration of particles. Our aim was to investigate the process of formation of optically active metal nanoparticles inside conducting polymer by ion implantation method and also study their optical and electrical behaviour.

In this thesis work, it was planned to use conducting polymer polyaniline (PANI)as our model system in which we planned to implant some transition metal and rare earth atoms. The choice of transition metals and rare earth metals is due to their well known optical properties. PANI is a well studied conducting polymer which has a well known as well as unique aromatic structure facilitating its doping by various kinds of dopants and it has a wide range of applications due to its good electrical conductivity and optical transmission characeristics. PANI wassynthesized by

chemical and in-situ method and doped to obtain desired conductivity of PANI films. The filmswere synthesized on ordinary glass and ITO coated glass by drop casting and spin coating techniques. Ion implantaion was carried out at different ion doses to investigate the formation of metal nanoparticles. The ion implanted samples were characterized to investigate the formation of metal naoparticles by XRD and electron microscopy techniques. The optical behaviour of the ion implanted samples was characterized using UV-Vis absorption, optical reflectance and spectroscopic ellipsometric techniques. The electrical behaviour of the samples was investigated by temperature dependence of electrical conductivity both in presence and absence of magnetic field to understand the dynamics of charge carriers. The obective of this study of the process of formation of metal nanoparticles in conducting polymers and the resulting optical and electrical properties was to find applications of these materials.

Lastly, we have tried lesser harvested technique of incorporating metal nanoparticles into conducting polymer PANI i.e., by the method of Ball milling which works on the principle of grinding and crushing fine metal powders into metallic nanoparticles and mixing uniformly with polymer in a planetary Ball –Mill system to obtain metal nanoparticle incorporated conducting polymer.

Contents

Page No.

Chapter 1: Introduction & Scope of the Thesis

1.1 Introduction……1
1.2 Conducting Polymers……3
1.3 Metal Nanoparticles……5
1.3.1Polymer-metal nanocomposites……6
1.4 Method of Ion Implantation……6
1.5 Spin Coating System……7
1.6 AFM Measurements……9
1.7 Thickness Measurements by UV-Vis……10
1.8 XRD Measurements & Grazing angle……11
1.9 Photoluminescence property of the composite materials……12
1.10 Ball-Milling System……12
1.11 Objective of the Thesis……13
1.12 Scope & Chapter wise Summary of the thesis……14
1.13 References……15

Chapter 2: Synthesis of Metal-PolyAniline nano-composites by Ion implantation

2.1 Introduction……17
2.2 Experimental Details……21
2.2.1 In-Situ Synthesis of PANI on Glass & Silicon wafers……21
2.2.2 Step 2:Ion Beam Implantation……22
2.3 Results & Discussions……23

2.3.1 XRD Measurements……23

2.3.2UV-Vis Absorbance measurements……24

2.3.3 FESEM measurements……25

2.3.4 Temperature Dependent DC Conductivity measurements……28

2.4 Conclusions……30

2.5 References……32

Chapter 3: Medium energy Silver and Nickel ion implantation into thick Poly-Aniline films and observation of structural changes& PANI-Au metal nanocomposites synthesis by Chemical route of fabrication

3.1 Introduction……34

3.2 Experimental Details……35

3.2.1 Synthesis of Poly-Aniline from Aniline monomer……35

3.2.2 Synthesis of protonated PANI……36

3.2.3 De-doping of PANI……37

3.2.4 Preparation of conducting solution of Poly-Aniline……38

3.2.5 Preparation of Thick film……38

3.2.6 Poly-Aniline thin film preparation……38

3.3. PolyAniline thick film thickness measurement……40

3.3.1 AFM Measurement……40

3.4. Ion implantation……42

3.4.1 SRIM Analysis……42

3.4.2 Discussions on XRD and SRIM Analysis……45

3.5 Optical Analysis of the implanted samples……45

3.5.1 Observations from Reflectance Curves……46

3.6 Cross-sectional FESEM Measurement……..47

3.6.1 Discussions on the FESEM images with EDAX Spectra……66

3.7 Poly-Aniline metal nanocomposites synthesis by Chemical-route of fabrication……..66

3.8 References……69

Chapter 4: Preparation of Cu-Poly Aniline nanocomposite by Mechano-synthesis route (Ball-Milling) and checking frequency and temperature dependent electrical conductivity and dielectric relaxation

4.1 Introduction……71

4.2 Experimental Details……73

4.2.1 Synthesis of Cu incorporated Poly-Aniline (PANI) nanocomposites……..73

4.2.2 Characterizations……74

4.3 Results & Discussions……75

4.3.1 UV-Vis study……75

4.3.2 FTIR analysis……76

4.3.3 Dielectric studies……77

4.3.4 Complex impedance study……79

4.3.5 AC conductivity study……82

4.6 Conclusions……83

4.7 References……84

Chapter 5: Study on dielectric relaxation of Ni doped PANI

5.1 Introduction……88

5.2 Experimental Details……88

5.2.1 Incorporation of Ni into PANI……89

5.3 Results & Discussions……89

5.3.1 UV-Vis study……90

5.3.2 XRD Analysis……90

5.3.3 FTIR Analysis……91

5.3.4 Dielectric Study……92

5.4 Conclusions……99

5.5 References……100

Chapter 6: Conclusions & Future Scope

6.1 Introduction……102

6.2 Questions aroused……103

6.3 Chapter wise summary of findings……104

6.4 Comparative studies with existing findings……105

6.5 Recommendations……107

6.6 Future scopes of the research……108

6.7Conclusions……108

List of Figures

Fig. 1.1	Applications of Metal-Polymer nanocomposites
Fig. 1.2	Conducting Polymers have linear backbone
Fig. 1.3	Classifications of Conducting Polymers
Fig. 1.4	Size dependent colour of Au nanoparticles
Fig. 1.5	Ion implantation System
Fig. 1.6	Photograph of a Spin Coating System with Temperature Control Unit
Fig. 1.7	Different modes of AFM measurements
Fig. 1.8	Thickness calculation from UV-Vis
Fig. 1.9	Photograph of a XRD Measurement System
Fig. 1.10	Planetary Ball Mill System
Fig. 2.1	Different Oxidation states of PolyAniline
Fig. 2.2	Schematic representation of surface plasmon in metallic nanoclusters of spherical shapes
Fig. 2.3	Substrate preparations for in-situ thin films
Fig. 2.4	In-situ synthesis of PANI thin films on substrates
Fig. 2.5(a)	XRD spectrum of Ag implanted samples at an angle of incidence of 0.5^{o}
Fig. 2.5(b)	XRD spectrum of Au implanted samples at an angle of incidence of 3^{0}
Fig. 2.6(a)	Absorbance spectra of Ag implanted samples
Fig. 2.6(b)	Absorbance spectra of Au implanted samples
Fig. 2.7(a)	Cross sectional view of unimplanted sample
Fig. 2.7(b)	Cross sectional view of implanted at a dose of 6×10^{16} ions/cm^2 (beads like features highlighted)
Fig. 2.7(c)	EDAX spectrum of selected area in the implanted region
Fig. 2.8	Cross sectional view of Au implanted sample at a dose of 1 x 1016/cm2 (Buried layer is indicated by the arrows)
Fig. 2.9	Fitting of temperature dependent DC conductivity to the Mott's 3D-VRH model
Fig. 3.1	Percentile description of research trends in polymer nanocomposites
Fig. 3.2	PolyAniline Distillation set up
Fig. 3.3	Vacuum filtration system
Fig. 3.4	AFM trace of Sample 1 (a) Topography (b) Deflection Traces
Fig. 3.5	AFM trace of Sample 2 (a)topography (b)deflection (c) friction traces
Fig. 3.6	AFM trace of Sample 3 (a)topography (b)deflection (c) friction traces
Fig. 3.7	AFM trace of Sample 4

	(a)topography
	(b)deflection
	(c) friction traces
Fig. 3.8	AFM trace of Sample 5
	(a)topography
	(b)deflection
	(c) friction traces
Fig. 3.9	AFM trace of Sample 6
	(a)topography
	(b)deflection,
	(c) friction traces
Fig. 3.10(a)	SRIM simulation of 2 MeV Silver ion implantation in PANI
Fig. 3.10 (b)	Defect distribution in 2 MeV Silver implanted PANI
Fig. 3.11 (a)	SRIM simulation of 2 MeV Nickel ion implantation in PANI
Fig. 3.11 (b)	Defect distribution in 2MeV Nickel implanted PANI
Fig. 3.12	XRD Spectra of gold implanted PANI
Fig. 3.13	XRD Spectra of Nickel implanted PANI
Fig. 3.14	Optical reflectance of Gold implanted Samples
Fig. 3.15(a)	Cross-sectional FESEM of Unimplanted Sample
Fig. 3.15 (b)	EDAX Spectrum of Unimplanted Sample
Fig. 3.15(c)	Beam Spectra
Fig. 3.16 (a)	Cross sectional FESEM 1 of implantation at a dose $1*10^{15}$ ions/cm^2
Fig. 3.16(b)	EDAX Spectrum-1 of dose 10^{15} ions/cm^2
Fig. 3.17(a)	Cross-sectional FESEM 2 at tilted angle of dose $1*10^{15}$ ions/cm^2
Fig. 3.17(b)	EDAX Spectrum-2 of dose 10^{15} ions/cm^2
Fig. 3.18(a)	Cross sectional FESEM 1 of implantation at a dose $5*10^{15}$ ions/cm^2
Fig. 3.18(b)	EDAX Spectrum-1 of dose $5*10^{15}$ ions/cm^2
Fig. 3.19(a)	Cross sectional FESEM 2 of implantation at a dose $5*10^{15}$ ions/cm^2
Fig. 3.19(b)	EDAX Spectrum-2 of dose $5*10^{15}$ ions/cm^2
Fig. 3.20(a)	Cross sectional FESEM 1 of implantation at a dose 10^{16} ions/cm^2
Fig. 3.20(b)	EDAX Spectrum-1 of dose 10^{16}ions/cm^2
Fig. 3.21(a)	Cross sectional FESEM 1 of implantation at a dose $5*10^{16}$ ions/cm^2
Fig. 3.21(b)	EDAX Spectrum-1 of dose $5*10^{16}$ions/cm^2
Fig. 3.22(a)	Cross sectional FESEM 2 of implantation at a dose $5*10^{16}$ ions/cm^2
Fig. 3.22(b)	EDAX Spectrum-2 of dose $5*10^{16}$ions/cm^2
Fig. 3.23(a)	Cross sectional FESEM 1 of implantation at a dose 10^{17} ions/cm^2
Fig. 3.23(b)	EDAX Spectrum of dose 10^{17}ions/cm^2
Fig. 3.24(a)	Cross sectional FESEM 2 of implantation at a dose 10^{17} ions/cm^2
Fig.3.25(a)-(d)	Cross-sectional FESEM of unimplanted samples at different angles
Fig.3.26(a)-(f)	Cross-sectional FESEM of implantation at a dose of $1*10^{15}$ ions/cm^2 at different angles
Fig.3.27(a)-(d)	Cross-sectional FESEM of implantation at a dose of $5*10^{15}$ ions/cm^2 at different angles
Fig.3.28(a)-(d)	Cross-sectional FESEM of implantation at a dose of $1*10^{16}$ ions/cm^2 at different angles
Fig.3.29(a)-(j)	Cross-sectional FESEM implantation at a dose of 5*1016 ions/cm2 at

different angles

Fig. 4.1 UV-Vis spectra of PANI and Cu-PANI nanocomposite
Fig. 4.2 FTIR spectra of PANI and Cu-PANI nanocomposite
Fig. 4.3(a) ε ′ vs Frequency of Cu incorporated PANI composites
Fig. 4.3(b) ε″ vs Frequency of Cu incorporated PANI composites
Fig. 4.4(a) Variation of real part of Z (Z ′) with frequency
Fig. 4.4(b) variation of imaginary part of Z (Z″) with imaginary part of frequency of Cu incorporated PANI
Fig. 4.5 Cole-Cole plots of Cu incorporated PANI composites
Fig. 4.6 Variation of ac conductivity with frequency of Cu incorporated PANI composites

Fig. 5.1 UV-Vis Spectra of PANI and Ni doped PANI
Fig. 5.2 XRD spectra of PANI and Ni doped PANI
Fig. 5.3 FTIR spectra PANI-Ni and PANI
Fig. 5.4 (a) Real impedance plot
(b) complex impedance plot
(c) Arrhenius plot
Fig. 5.5 (a) Real permittivity plot
(b) complex permittivity plot

List of Tables

Table No.	Title
Table 2.1	Relative elemental concentration in the cross sectional EDAX spectrum
Table 2.2	Characteristic Temperature
Table 3.1	FESEM Spectrum analysis table for unimplanted sample
Table 3.2	FESEM Spectrum analysis table for dose $1*10^{15}$ ions/cm^2
Table 3.3	FESEM Spectrum analysis table for dose $5*10^{15}$ ions/cm^2at tilted angle
Table 3.4	FESEM Spectrum analysis table for dose $1*10^{16}$ ions/cm^2
Table 3.5	FESEM Spectrum analysis table for dose $1*10^{16}$ ions/cm^2at tilted angle
Table 3.6	FESEM Spectrum analysis table for dose $5*10^{16}$ ions/cm^2
Table 3.7	FESEM Spectrum analysis table for dose $5*10^{16}$ ions/cm^2 at a different tilted angle
Table 3.8	FESEM Spectrum analysis table for dose 10^{17} ions/cm^2
Table 3.9	FESEM Spectrum analysis table for dose 10^{17} ions/cm^2at a different tilted angle

List of Abbreviations

AC	Alternate Current
AFM	Atomic Force Microscopy
Ag	Silver
APS	Ammonium Per Sulfate
Au	Gold
AuClO4H	Auro Chloric Acid
C	Carbon
C-60	Carbon 60
$CaCO_3$	Calcium Carbonate
CCR	Closed Cycle Refrigerator
CIS	Complex Impedance Study
CP	Conducting Polymer
CSA	Camphor Sulfonic Acid
Cu	Copper
DC	Direct Current
EB	Emaraldine Base
EDAX	Energy Dispersive X-ray Analysis
ES	Emeraldine Salt
FESEM	Field Effect Scanning Microscopy
FIB	Focused Ion Beam
FTIR	Fourier Transform Infra Red Spectroscopy
FWHM	Full Width at Half Maxima
GaAs	Gallium Arsenide
GCIB	Gas Cluster Ion Beams
Ge	Germanium
H2SO4	Sulfuric Acid
HCl	Hydro Chloric Acid
ITO	Indium Tin Oxide
IUAC	Inter University Accelaration Center
JRM	Jump Relaxation Model
KBr	Potassium Bromide
KeV	Kilo Electron Volt
LCR	Inductance, Capacitance, resistance meter
mCresol	Meta Cresol
MeV	Mega Electron Volt
Ni	Nickel
NiO	Nickel Oxide
NMP	n-Methyle Pyrrolidone
OLED	Organic Light Emitting Diode
PANI	Poly Aniline
Pt	Platinum
pTSA	p Toluene Sulfonic Acid

SEM	Scanning Electron Microscopy
Si	Silicon
SiO_2	Silicon Di Oxide
SPR	Surface Plasmon Resonance
SRIM	Stopping Range of Ions in Matter
UV-Vis	Ultra Violet-Visible spectroscopy
VRH	Variable Range Hopping
WO_3	Tungsten Oxide
XRD	X-Ray Diffraction spectrometry

Chapter 1

Introduction & Scope of the Thesis

1.1 Introduction:

The discovery of conductivity in conjugated polymer by Shirakawa and Heeger stimulated the development of a new emerging technology - organic electronics [1]. In earlier days, conventional inorganic semiconducting materials like Si, Ge, GaAs etc. were doped via ion implantation. Ion implantation was found to be a successful approach in modifying the properties of insulating polymers [2], [3]. Ion bombardment introduces radiation induced disruption of chemical bonds which effects in creating cavities and carbon-rich structures [3]–[8]. Depending on the polymer type and implantation parameters, the conductivity can be increased by 20 times than that of the pre-implanted insulated polymer[7], [9]. As the structure of polymer changes due to ion implantation, its optical, electrical and tribological characteristics undergo significant changes. Thus, by tuning the properties of conducting polymers in the desired way, various kinds of organic semiconductor devices like light filters, wave-guides and electro-optical modulators[10]–[13]. Another approach is to use this conducting polymers in bioligy and medicine based devices by altering the smoothness, hardness, adhesion, wettability, wear and chemical resistances of the polymer surfaces[3], [14]–[16]. The cavities and broken ligands play important sites to trap the ions, hence can lead to formation of nanoclusters depending on the shape and size of the cavities which promotes polymer-impurity composites. Shallow metal layers can be implanted into polymers which has great importance in plastic electronics. By varying the type of metal, ion fluenceand current, insulator to metal transition can be controlled. The earlier mechanism of charge transport in unimplanted conducting polymer can be like that of pure metal conductance through percolating metal inclusions.

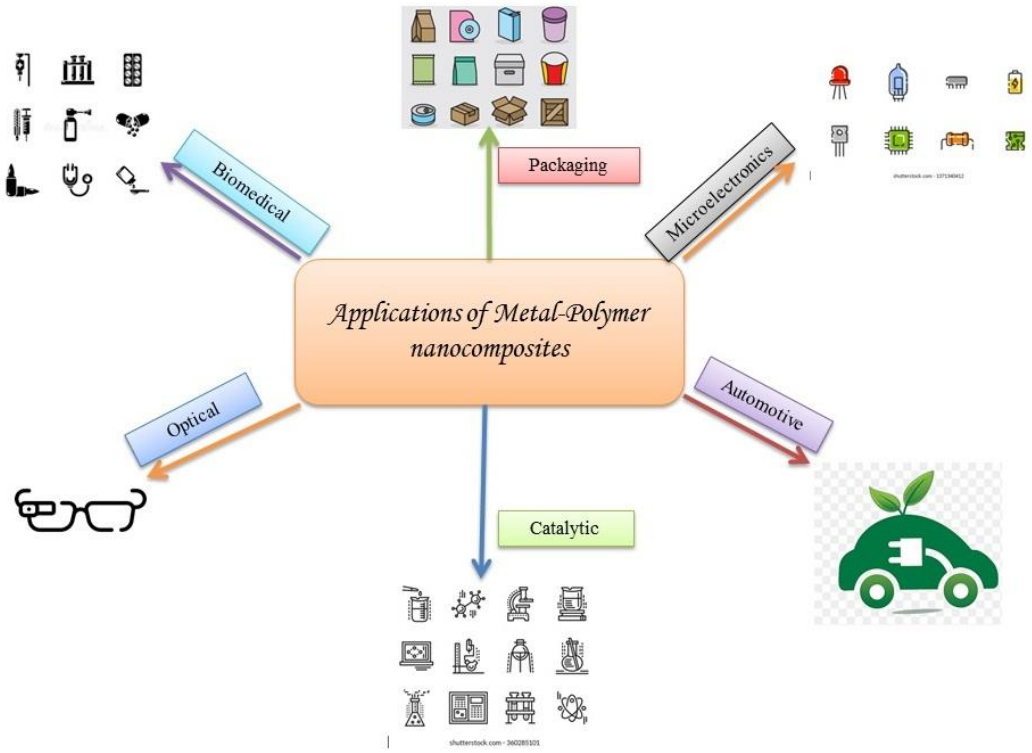

Fig. 1.1: Applications of Metal-Polymer nanocomposites

The researches in nanotechnology focus on incorporating nanoparticles into different conventional materials to improve its functional properties [17].Although colloidal metal nanoparticles are the key materials in many applications like catalysis, plasmonics, sensing and spectroscopy, but the size and shape can not be tuned accurately in colloidal form[18]. Since metal nanoparticles possess unique optical and electrical properties polymer metal nanocomposites have great deal of applications in biosensors, optical devices, micromechanical devices and advanced catalytic membranes as shown in Fig. 1.1. There are different approaches for synthesis of polymer-metal nanocomposites:---

- Incorporation of readily synthesized nanoparticles into polymer matrix using common blending solvents.
- Reduction of metal salts dispersed in polymer matrix using external reducing agent.
- Embedding nanoparticles in polymer using physical and chemical vapor deposition technique.
- Sol-gel route of synthesis.
- Ion Implantation is the preferred method, which is used to obtain precise depth.

1.2 Conducting Polymers:

Conducting polymers have some of the strikingly useful features, due to which and they are now used in place of traditional inorganic semiconductor materials. Most of the conducting polymers are linear in nature as shown in Fig.1.2 - this long chain is called backbone of the polymer and has alternate single and double bonds which germinates conducting nature in them[19]. Their conductivity changes upon amount and nature of the dopant, for example Camphor sulfonic Acid (CSA) doped PolyAniline (PANI) is more conducting than Hydro Chloric Acid (HCl) doped PANI. Conducting polymers also change their colours and hues upon application of different dopants. They are basically semiconducting in nature but can attain metallic conductivity upon doping. They are easy to fabricate and preparation method is cost effective compared to conventional inorganic semiconducting materials. They can be shaped easily and can form thin films.

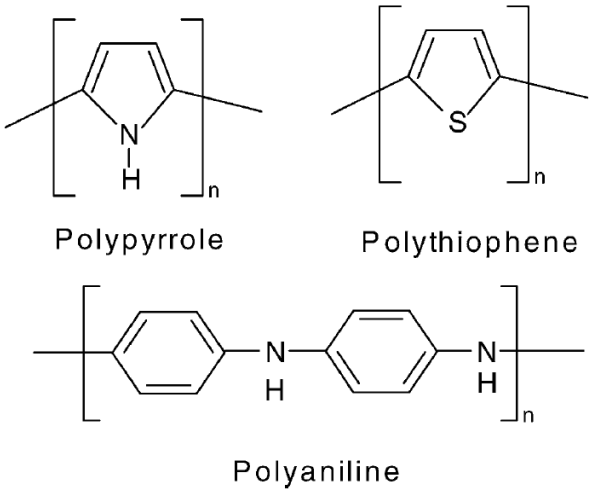

Fig. 1.2: Conducting Polymers have linear backbone

In a nutshell conducting polymers can be categorized in the following way (Fig. 1.3):-

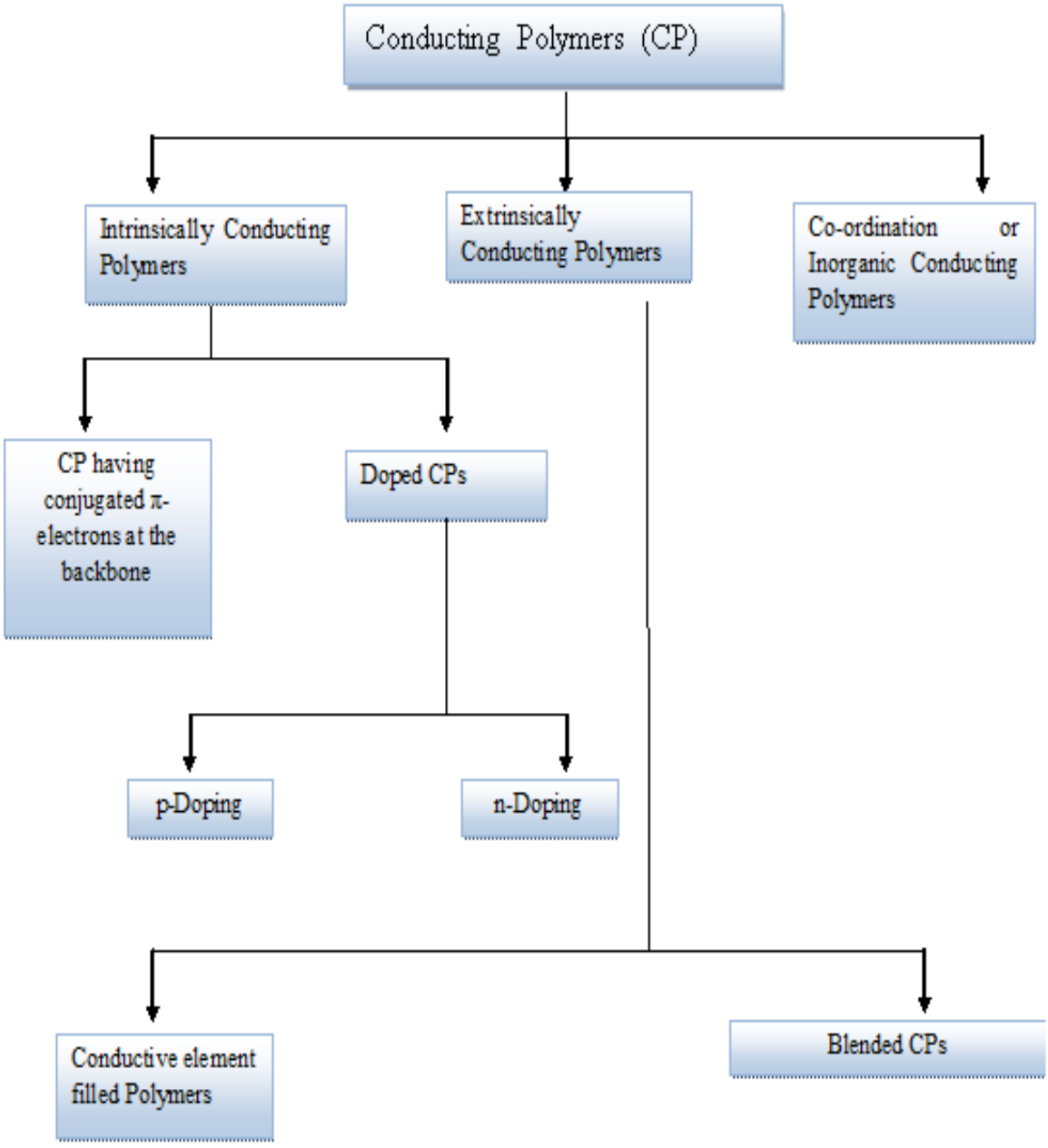

Fig. 1.3. Classifications of Conducting Polymers

1.3 Metal Nanoparticles:

Metallic nanoparticles possess unique optical, electrical and magnetic properties, which are strikingly different from their bulk counterparts. Again these properties can be tuned according to the requirement, because they depend on the sizes and shapes of the nanoparticles. Often they are in the size of 1-100nm, and approximately 10^6 atoms or molecules are bonded together. They cannot be called individual atoms nor they are bulk materials[20]–[22]. Because of this size aspect, they exhibit the intermediate behaviour. There are mainly three aspects, which playkey roles in their intermediate behaviour.

- High-surface to volume ratio.
- Quantum size effects.
- Electrodynamic interaction

Metallic nanoparticles show optical properties of great technological value. Colloidal solutions of nano particles, specially noble metal nanoparticles like gold, silver, copper etc. show interesting optical properties. They have strong absorption band at visible range of spectra. Moreover, they have size dependent optical properties (Fig. 1.4). This phenomenon is explained by Mie's theory.

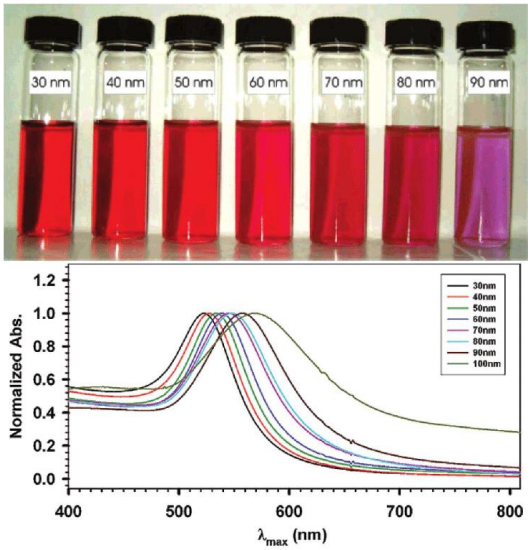

Fig. 1.4: Size dependent colour of Au nanoparticles

They have large surfaces to volume ratios and are very reactive in usual environmental conditions. According to Mie, plasmon excitations have strong effects whenever particle

radius becomes larger compared to the volume.Among all the metal nanoparticles, noble and coinagemetals and rare-earth elements are preferred for nanoparticles related applications as they can sustain for long in selective dielectric media.

1.3.1 Polymer-metal nanocomposites:

Insulated polymers implanted with metal nanoparticles have been studied extensively, but there is a good scope for using this method to alter the properties of conducting polymers. Polymer ligands play an important role to influence organized structure of metal nanoparticles; chain lengths affect particle size and gaps. Polymers containing metal inclusions have technologically important applications like light filters, waveguides, electro-optical modulators, bio sensors, optical devices, micromechanical devices, advanced catalytic membranes, memory devices etc.

1.4 Method of metal ion implantation:

Ion implantation is a non-equilibrium process. By this method, high metal filling factors can be reached in a matrix beyond the equilibrium solubility limit. System relaxes by precipitation of metal as nanoparticles. Energy of the ions can be chosen to control the depth of penetration and the ion current determines the concentration of particles in the matrix. We have chosen ion implantation method to prepare gold and silver nanoparticles embedded in PANI.

Advantage of this method is that purity of the implanted samples can be maintained to a high degree, depth of implantation and ion to matrix ratio can be controlled acutely.

And disadvantages are that it creates damages to the structure of the host material; and the process is a very costly process.However, defects caused by ion implantation play important role in nanoparticle formation. Defects play as traps to metal inclusions.

According to mode of implantation there are different types of ion beams:

A. Sputter Beams

This type of beam has high current, large spot size and wide field of view. It has a large dose of ions over a wide range of area. It sputters the targeted surface thus removing material before analysis.

B. Analytical Beams

It has wide range, small spot size and variable current control; precisely low current. It is also used as focused ion beam.

C. C60 Beams

Carbon-60 or C60 is a fullerine molecule consisting of 60 carbon atoms used for smoother sputtering which reduces the fragmentation of larger molecules.

D. Gas Cluster Ion Beams (GCIB)

GCIBs are high energy ion beams of cluster ions. They consist of versatile ion sources; here both the ion species and beam properties can be varied.

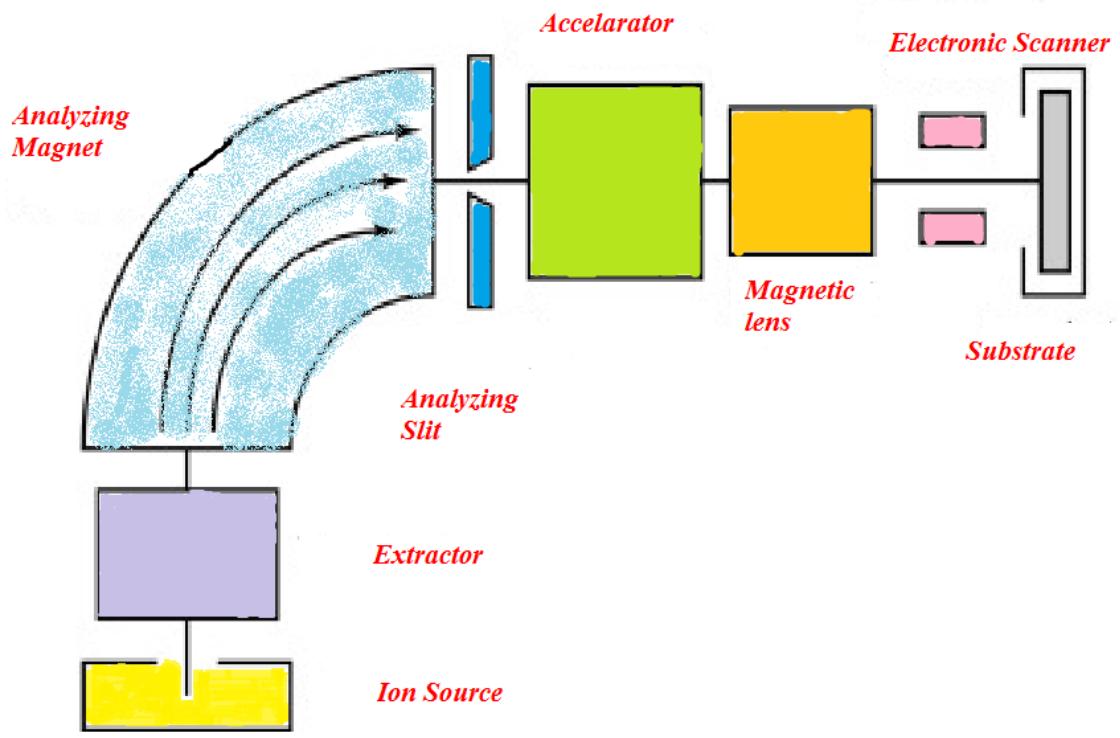

Fig. 1.5: Ion implantation System

1.5 Spin Coating System:

Spin coating is a technique to obtain a thin film of desired thickness. The apparatus used for this technique is called a Spin coater or a spinner. Few drops of solution dispersed over a flat substrate or wafer and a thin film is spread by centrifugal force. Sometimes, different sets of speeds with different time limits is set to wet the surface, uniform spreading, thickness control and finally, drying. Sometimes a heating system is also used simultaneously for fast evaporation of the solvent. The higher the angular speed, thinner is the film. Below in Fig. 1.6 a Spin coater along with Temperature control units have been used in our lab shown below.

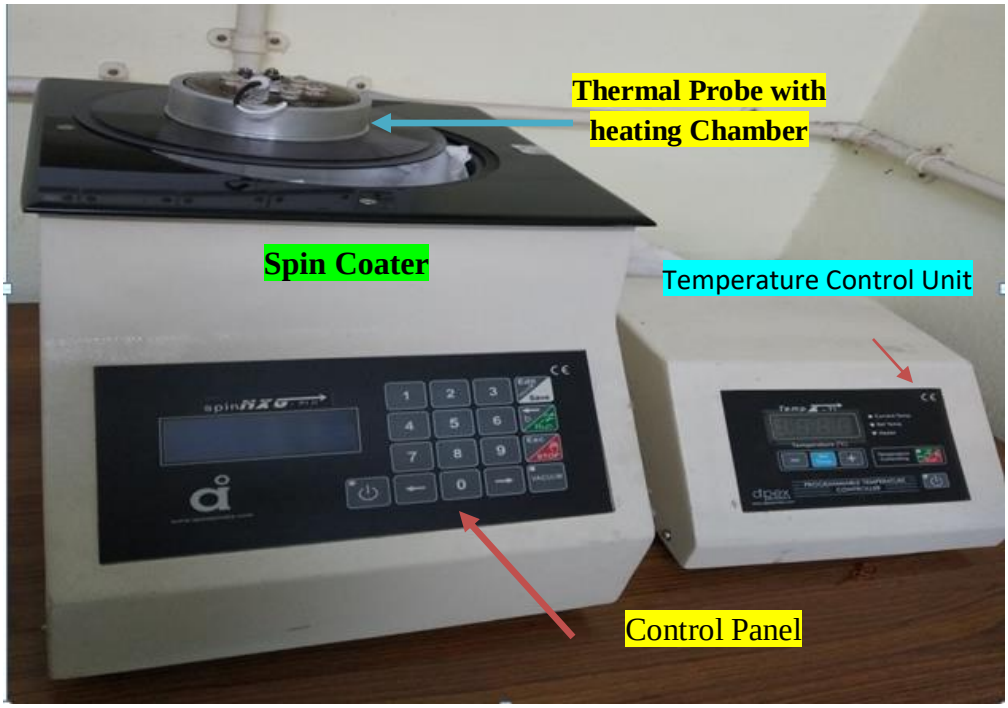

Fig. 1.6: Photograph of a Spin Coating System with Temperature Control Unit

Temperature control unit:

Along with the Spin Coater, a separate tempeature control unit is used for fast drying and uniform, smoother films.

Thick films & Thin films:

In view of thin film technology, a polymer film is called thick when it has a thickness of greater than 0.1μm and below which a film is called thin film. Both the films have their own significances as per applications are concerned. Thick films can be used as free standing film. Upon metal ion implantation its structural, electrical and magnetic properties change; optical property may or may not change. Thin films are mostly suitable for coating materials. Generally, we obtain thick films by repeated drop casting on substrates placed on horizontal surfaces. Thinfilms are prepared by spin coating or dip coating where varying different parameters we can obtain desired thicknesses and films prepared in this way are reproducible.

1.6 AFM Measurements:

Atomic Force Microscopy (AFM) which is a powerful technology for imaging any type of surfaces was used here to detect the surface topology and film thickness. Although we can measure thickness by UV-Vis spectrometry, but AFM gives clearer picture of surface roughness.

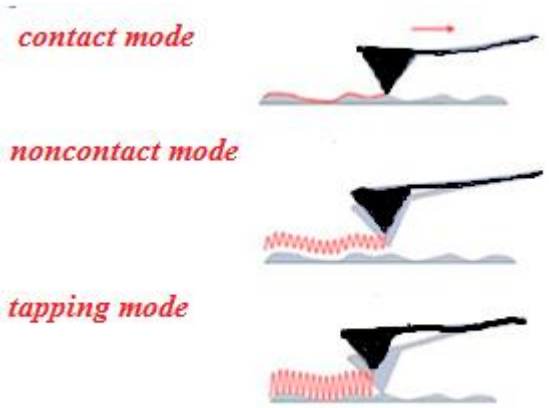

Fig. 1.7: Different modes of AFM measurements

According to nature of tip motion, AFM operation can be divided into three types of mode of operation as shown in Fig. 1.7:

i. **Contact Mode**: here the tip is dragged onto the surface of the sample and its contour and measurement is done by the deflection signal of the cantilever as feedback.

ii. **Noncontact mode**: in noncontact mode the tip of the cantilever does not touch the sample surface; instead it works on decreasing the resonance frequency due to Van der Waals force which is very strong near the surface

iii. **Tapping mode**: in this mode the cantilever moves up and down at oscillating frequency of a piezoelectric crystal. Here frequency and amplitude of oscillation is kept constant; the interaction of different forces acting on the cantilever like Van der waals, dipole-dipole, electrostatic forces cause change in amplitude. This mode creates less damage than contact mode.

1.7 Thickness measurement by UV-Vis:

Thickness of a single layer film in the range of 0.3 to 60 µm and with a known refractive index can be measured with the help of UV-Vis spectrometry.

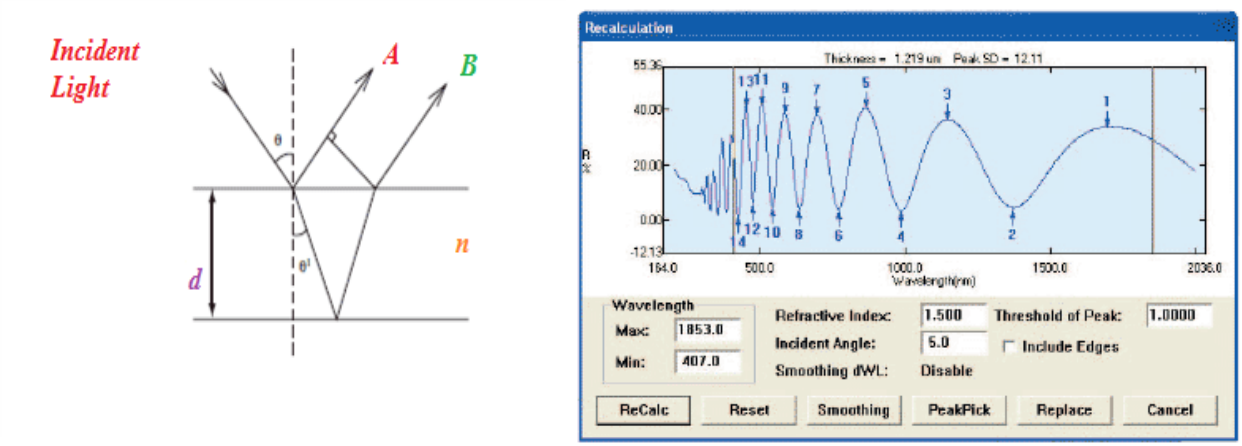

Optical path difference between A and B
= (λ/2) *2n → Reinforce
Optical path difference between A and B
= (λ/2) * (2n+1) → Cancel out
Where λ : wavelength; m: Integer

Recalculation window of film thickness

Fig. 1.8: Thickness calculation from UV-Vis

In the above fig. 1.8, it is ahown that in case of a film, there are interferences between light reflected from incident surface (A) and light reflected from opposite surface (B) as the incident light strikes the film.

The film thickness *"d"* is calculated by counting the number of peaks or valleys in the interference spectrum as found within some specified wavelength range as shown below:

$$\boldsymbol{d} = \frac{\boldsymbol{\Delta m}}{2\sqrt{\boldsymbol{n^2 - sin^2\theta}}} \times \frac{1}{\left(\frac{1}{\lambda_2} - \frac{1}{\lambda_1}\right)} \quad \text{.....(1)}$$

Where "Δm" is the number of peaks in the defined wavelength range; "n" is the refractive index, "Θ" is the angle of incidence with respect to the sample; λ_1 and λ_2 are the start and end wavelengths of the range considered.

In case of opaque films reflection measurement is considered and for transparent films, transmission measurement is considered.

1.8 XRD Measurements & Grazing angle:

As we all know that *XRD* or X-ray diffraction analysis technique is used mainly to determine the structure of a material. This is done by exciting a material by incident X-rays and then insenties of the scattered rays are measured at some specific angles. If the XRD pattern of the existing material is already known, then by judging the obtained plot, we can affirm any structural change or presence of any foreign element. We used XRD technique in our work to investigate the structural change of polyaniline due to ion beam exposure and formation of metal nanoparticles.

During the process of ion implantation, metal ions are located near the surface of pristine polymer; also, ratio of metal fillers to polymer matrix is very small. For these reasons, we have chosen grazing incidence X-ray diffraction technique for our XRD analysis. Also, grazing angle XRD can neglect scatterings from the substrates onto which the polymer film has been coated.Here, in this case, the angle of incidence of X-rays with sample surface ranges from0.1° to 1°;where as in normal XRD measurementit is Θ-2Θ variation. Grazing angle XRD is very useful specifically in thin film study. It is a non-destructive process. Fig. 1.9 shows a typical XRD system:

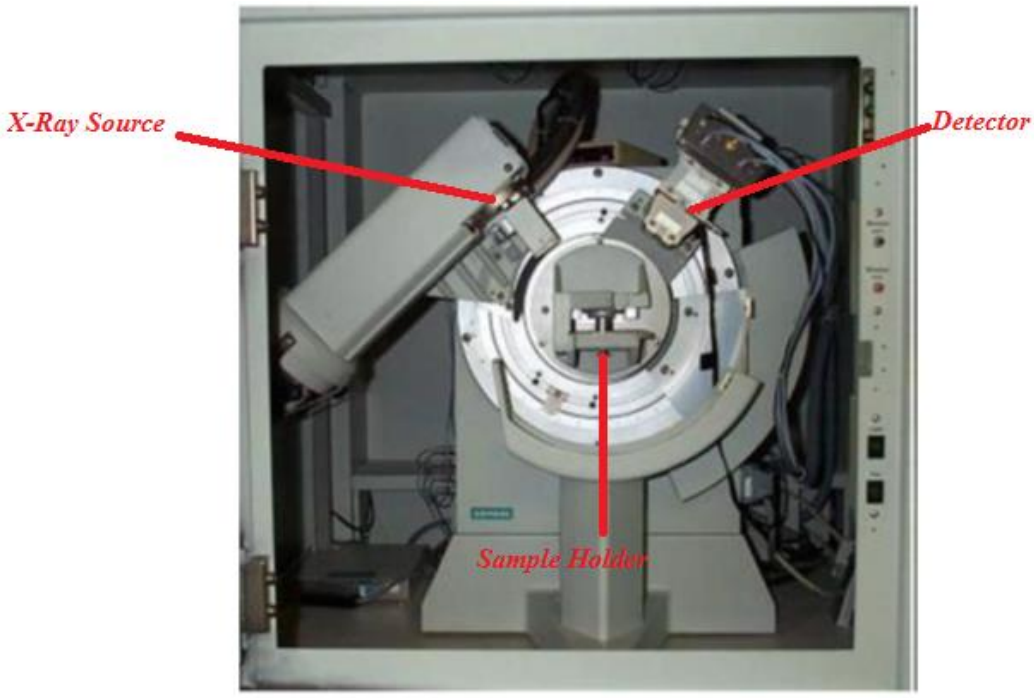

Fig. 1.9: Photograph of a XRD Measurement System

1.9 Photoluminescence property of the composite materials

Photoluminescence is an optical phenomenon where a molecule emits light by absorbing a photon in the visible region; here an electron absorbs incident light and upon returning it emits light of less energy. We have studied photoluminescence property of metal ion embedded poly-aniline. But due to adequate damage of the polymer matrix during ion implantation and comparatively less amount of filler materials, we did not get strong photoluminescence spectra for our metal- PANI composite material.

1.10 Ball Milling System

A ball-mill is a grinder, used for grinding and blending bulk materials into powdered material, specifically for nanomaterials or quantum dots. The working principle is impact and attrition. The size of the nanoparticles can be tailored by varying number and size of the balls, materials of the balls and rotation speed. In our work we have used typical planetary ball-Milling system.

Planetary ball-Mill system:

The motion of the planetary ball-milling system is like our typical solar planetary system. It consists of several cylindrical grinding jars filled with loose grinding balls. The grinding jar rotates on an orbit around the centre of the jar. Along with it rotates on its own axis. These two rotational movements of the jar are superimposed which result in centrifugal and acceleration forces leading to strong grinding effects. Moreover, there are forces working according to the coriolis acceleration, the way particles move on the surface of the earth which results in intensive grinding. There are different rotational ratios. For example a rotational ratio of 1:-2 imply that the grinding jar rotates twice during a sun wheel turn. The negative sign here indicates opposite direction of rotation.

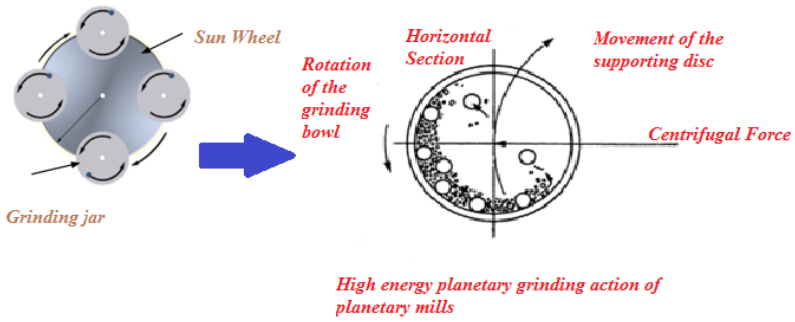

Fig. 1.10: Planetary Ball Mill System

Above Fig. 1.10 depicts schematic diagram of planetary Ball-Mill system used in our lab.

1.11 Objective of the thesis:

In this thesis work our quest began with the combination of conducting polymer and metal nanoparticles and how it can be implemented in practice so that the composite material could be a good replacement of conventional inorganic semiconducting device. A novel approach of ion implantation has been carried out. The previous studies show that there were uses of conducting polymer thin films including PolyAniline, and some of them blended metal nanoparticles as well. But, the process of mixing polyaniline with metal nanoparticles leaves space for doubt as in practice we find, that PANI lost its conducting property eventually in the process of conventional chemical route of fabrication. Also, the mixture is not a homogeneous one; there are higher numbers of undesirable impurities introduced in the process. By means of ion implantation we can introduce chosen impurities into the stand alone or coated PANI films and it can introduce highest amount of metal nanoparticles. The method created holes which can act as sites for receiving as well growth place of nanoparticles. By choosing the appropriate energy implantation can be ascertain at a certain depth. But the method of ion implantation is obviously a costly method. To ward off the high cost method of ion implantation and complexity and less promising other methods of composite fabrications, we have introduced a more simple technology of Ball-Milling, where a homogenous mixture of metal and polymer can be obtained. This method is well known to break macromolecules into nanomolecules introducing a homogeeous nanocomposite.In a nutshell the objectives are the followings:

1. *Preparation of thin films of conducting polymer Poly-Aniline doped by various acids on different substrates to obseve its morphology at pre and post ion implantation, and obtain semiconducting junctions.*

2. *Optimization of films aiding different technologies, like drop-casting, spin coating and in-situ film fabrication*

3. *Metal ion implantaion and formation of nanoparticles within the conducting polymer matrix; optimizing different parameters of ion implantation, i.e., dose, current, energy etc.*

4. *Study of the changes in the optical, electrical properties of the polymer matrix due to ion beam implantation.*

5. *Preapration of conducting polymer PANI and coinage metal nanocomposites by Ball-Mill method and study the dielectic properties of the composite material.*

1.12 Scope & Chapterwise Summary of the thesis:

Based on the above objectives, this thesis is divided into five chapters and they are narrated briefly as follows:

Chapter 1presents the theoretical background and objectives of the thesis.

Chapter 2 describes process of PANI thin film fabrication by in-situmethod. These films were then undergone low energy (~KeV) gold and silver ion beam implantation. Then structural, optical and electrical studies were carried out on the implanted samples.

Chapter 3deals with thick films of PANI. They were bombarded by two different kinds of ions, namely, silver and nickel. Structural and electrical properties of the films were observed.Here we preaped thick films of PANI in the micrometer range which were opaque, so reflectance property was observed.

Chapter 4 ventures into Ball-Mill method. In this work, small copper clusters were included into HCl doped PANI in powdered form and crushed by planetary Ball-Mill system. We called this physical-mechanical route of fabrication. Frequency and temperature dependent electrical conductivities and dielectric measurements were carried out on them.

Chapter 5 repeats same set of experiments as depicted in chapter 4 keeping nickel as our included element.

1.13References

[1] V. N. Popok, "No Title," *Rev.Adv.Mater.Sci.*, vol. 301, 2012.

[2] G. F. L.Compagnini, G.Calcagno, "Section VII Polymers and organics," *Nucl. Instruments Methods Phys. Res. Sect. B Beam Interact. with Mater. Atoms*, vol. 65, no. 1–4, pp. IN7, 413–422, 1992, [Online]. Available: https://www-sciencedirect-com.proxy.lib.umich.edu/science/article/pii/0168583X92950775?via%3Dihub.

[3] A. Tóth, I. Bertóti, V. S. Khotimsky, G. Marletta, J. L. Sullivan, and S. O. Saied, "Modification of gas separation membranes on a nanometric scale," *Nucl. Instruments Methods Phys. Res. Sect. B Beam Interact. with Mater. Atoms*, vol. 122, no. 3, pp. 547–549, 1997, doi: 10.1016/S0168-583X(96)00760-4.

[4] A. P. Micolich *et al.*, "Superconductivity in metal-mixed ion-implanted polymer films," *Appl. Phys. Lett.*, vol. 89, no. 15, 2006, doi: 10.1063/1.2358190.

[5] A. Chapiro, "Chemical modifications in irradiated polymers," *Nucl. Inst. Methods Phys. Res. B*, vol. 32, no. 1–4, pp. 111–114, 1988, doi: 10.1016/0168-583X(88)90191-7.

[6] D. V Sviridov, "Ion Implantation in polymers: chemical aspects," *Chem. Probl. Dev. New Mater. Technol.*, no. i, pp. 88–106, 2003.

[7] V. N. Popok *et al.*, "Radiation-induced change of polyimide properties under high-fluence and high ion current density implantation," *Appl. Phys. A Mater. Sci. Process.*, vol. 78, no. 7, pp. 1067–1072, 2004, doi: 10.1007/s00339-003-2166-9.

[8] E. H. Lee, "Ion-beam modi®cation of polymeric materials ± fundamental principles and applications." [Online]. Available: www.elsevier.nl/locate/nimb.

[9] M. Iwaki, "Ion surface treatments on organic materials." [Online]. Available: www.elsevier.nl/locate/nimb.

[10] D. Fink, M. Moller, L. T. Chadderton, P. H. Cannington, R. G. Elliman, and D. C. Mcdonald, "OPTICALLY ABSORBING LAYERS ON ION BEAM MODIFIED POLYMERS: A STUDY OF THEIR EVOLUTION AND PROPERTIES," 1988.

[11] P. Cottin, R. A. Lessard, E. J. Knystautas, and S. Roorda, "Polymer waveguides under ion implantation: optical and chemical aspects." [Online]. Available: www.elsevier.nl/locate/nimb.

[12] D. M. Rück, "Ion induced modification of polymers at energies between 100 keV and 1 GeV applied for optical waveguides and improved metal adhesion," *Nucl. Instruments Methods Phys. Res. Sect. B Beam Interact. with Mater. Atoms*, vol. 166–167, pp. 602–609, May 2000, doi: 10.1016/S0168-583X(99)01175-1.

[13] F. F. Komarov, A. V Leontyev, V. V Grigoryev, and M. A. Kamishan, "Ion implantation for local change of the optical constants of polymer films." [Online]. Available: www.elsevier.com/locate/nimb.

[14] J. D. Carlson, J. E. Bares, A. M. Guzman, and P. P. Pronko, “SURFACE PROPERTY CHANGES INDUCED IN POLY(l-HEXENE) ELASTOMER BY HIGH ENERGY ION IRRADIATION,” 1985.

[15] Y. Suzuki, “Ion beam modification of polymers for the application of medical devices,” in *Nuclear Instruments and Methods in Physics Research, Section B: Beam Interactions with Materials and Atoms*, May 2003, vol. 206, pp. 501–506, doi: 10.1016/S0168-583X(03)00808-5.

[16] A. Kondyurin, B. K. Gan, M. M. M. Bilek, D. R. McKenzie, K. Mizuno, and R. Wuhrer, “Argon plasma immersion ion implantation of polystyrene films,” *Nucl. Instruments Methods Phys. Res. Sect. B Beam Interact. with Mater. Atoms*, vol. 266, no. 7, pp. 1074–1084, Apr. 2008, doi: 10.1016/j.nimb.2008.02.063.

[17] S. K. Ghosh and T. Pal, “Interparticle coupling effect on the surface plasmon resonance of gold nanoparticles: From theory to applications,” *Chem. Rev.*, vol. 107, no. 11, pp. 4797–4862, 2007, doi: 10.1021/cr0680282.

[18] V. Mankad, K. K. Mishra, S. K. Gupta, T. R. Ravindran, and P. K. Jha, “Low frequency Raman scattering from confined acoustic phonons in freestanding silver nanoparticles,” *Vib. Spectrosc.*, vol. 61, pp. 183–187, Jul. 2012, doi: 10.1016/j.vibspec.2012.02.004.

[19] A. K. Haghi, “Conducting polymers,” *Monomers, Oligomers, Polym. Compos. Nanocomposites*, no. October, pp. 193–207, 2021, doi: 10.1201/9781315101217-2.

[20] S. K. Ghosh, A. Pal, S. Nath, S. Kundu, S. Panigrahi, and T. Pal, “Dimerization of eosin on nanostructured gold surfaces: Size regime dependence of the small metallic particles,” *Chem. Phys. Lett.*, vol. 412, no. 1–3, pp. 5–11, Aug. 2005, doi: 10.1016/j.cplett.2005.06.059.

[21] S. Sinha, S. K. Chatterjee, and J. Ghosh, “Dielectric relaxation and ac conductivity behaviour of polyvinyl alcohol – HgSe quantum dot hybrid films,” doi: 10.1088/0022-3727/47/27/275301.

[22] S. K. Ghosh, A. Pal, S. Kundu, S. Nath, and T. Pal, “Fluorescence quenching of 1-methylaminopyrene near gold nanoparticles: Size regime dependence of the small metallic particles,” *Chem. Phys. Lett.*, vol. 395, no. 4–6, pp. 366–372, Sep. 2004, doi: 10.1016/j.cplett.2004.08.016.

Chapter 2

Synthesis of Metal-PolyAniline nano-composites by Ion implantation

2.1 Introduction

The conducting polymers are very good replacements of conventional inorganic semiconducting materials and some important areas of applications of conducting polymers are

- Corrosion resistance [1]
- Gas sensors [2]
- Transistors [3]
- Hybrid solar cells [4]
- OLEDs [5]

The reasons behind chosing conducting polymers in various electronics applications are because of the following facts:

i. They possess tunable semiconducting properties [6]
ii. The raw materials are inexpensive.
iii. Ease to fabrication.
iv. Oxidation state depended optical & electrical properties, i.e., tunable opto-electric property [7]-[10]

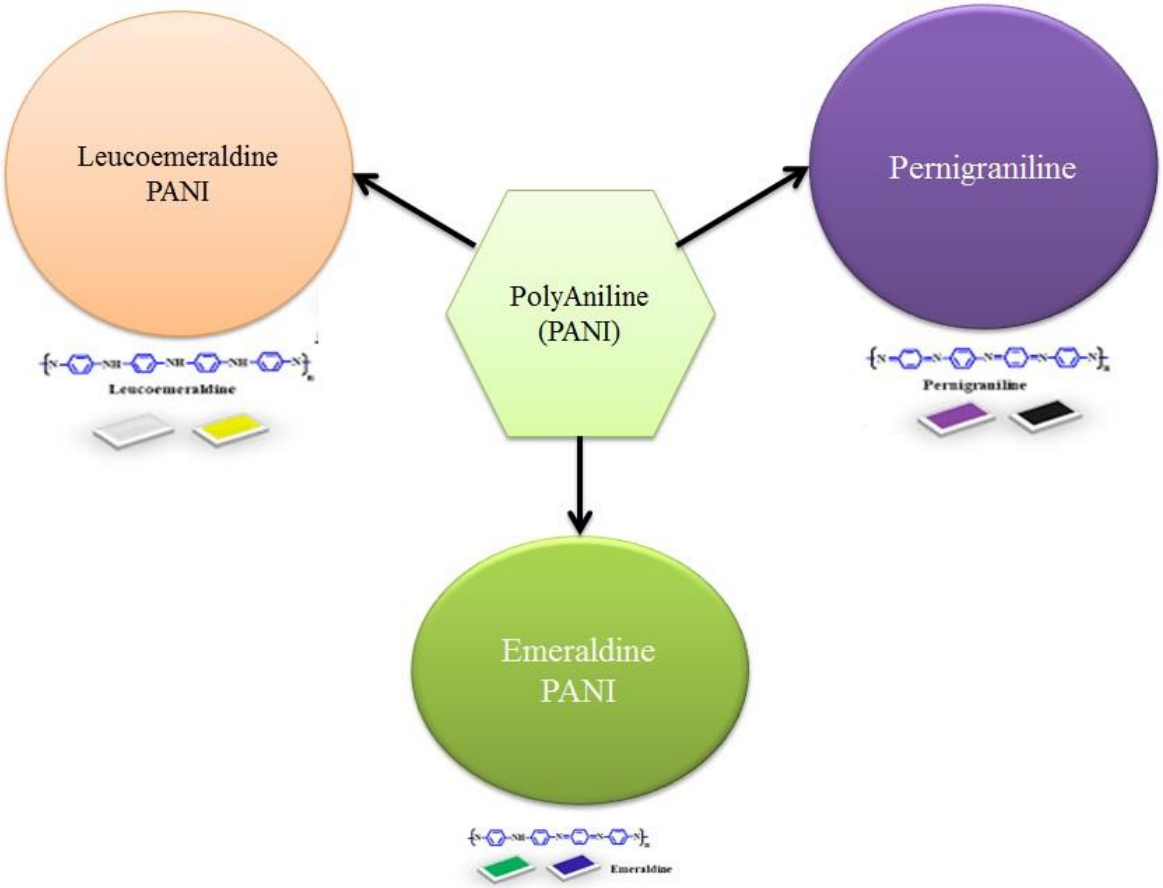

Fig. 2.1: Different Oxidation states of PolyAniline

As shown in Fig. 2.1, depending on oxidation states, there are three forms of PANI,

1) Leucoemeraldine PANI – fully undoped form which appears as white or yellow,

2) Pernigraniline – fully doped form of PANI which is violet in colour and

3) most useful form of PANI – emeraldine PANI, which are of mainly two forms---

a) Emeraldine Salt (ES) which is green in colour because of doping by acids and it possesses conductivity property.

b) Emeraldine Base (EB) which is dark blue in colour and generally doped by base.

But the understanding developed so far by the researchers have not resulted in exploiting the optical properties in real applications. Though the development and the translation of the technology to the consumer market are the major important steps in utilizing the electro-optical behaviour of these materials, lot of work is still going on with regard to the functionalizing the polymer chains to tailor the optical properties [11]. One simple method of tailoring the optical

properties could be to incorporate optically active nanoparticles in conducting polymers.Mie theory predicts the Surface Plasmon Resonance (SPR) of nanoparticles embedded in dielectric matrix and it is well known that the dielectric constant of the medium also affects the position of the SPR peak [2].

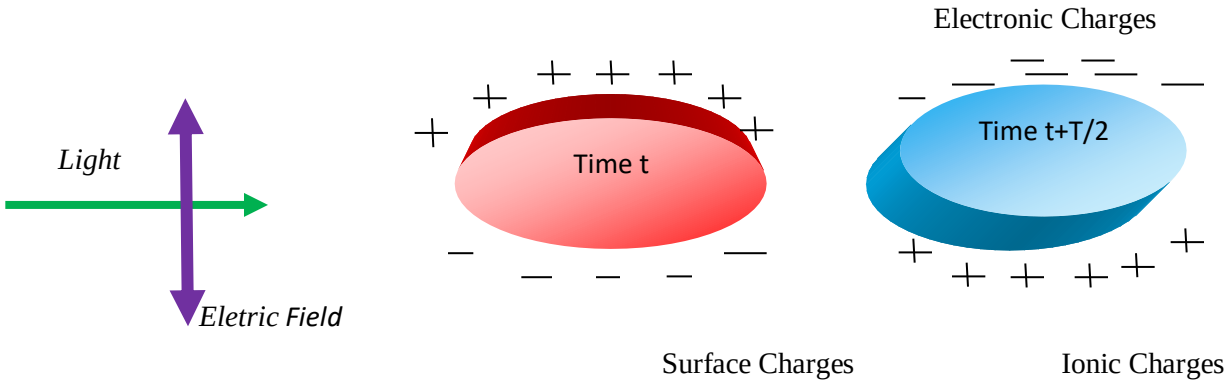

Fig. 2.2: Schematic representation of surface plasmon in metallic nanoclusters of spherical shapes

In case of bulk solids, as the particles sizes grow, the energy levels start splitting and gradually they merge into a quasi continuous band.On the other hand, for smaller particles quantization of energy level becomes prime factor, which is called quantum effect. As shown in Fig. 2, incoming electric field of light wave polarizes the conduction electrons against heavier ionic core. As a consequence dipolar oscillation is created which is otherwise known as plasmon resonance.

Studies have been reported by chemically incorporating nanoparticles of Au [3], Ag [4] and SiO_2, Pt, WO_3[5] during the polymer synthesis. Such nanocomposites have been found to exhibit improved mechanical and electrical properties and also could have possible electrocatalytic applications.

An alternative method of incorporating nanoparticles in conducting polymers could be by using ion implantation techniques. The advantages of this method are…..

i. High purity of the nanoparticle phase that can be achieved.
ii. By choice of the energy of the ion beam the layer of nanoparticles can be embedded at a specified depth.

iii. Ion implantation also introduces defects which result from the broken bonds due to the energy deposited by the ion beam.
iv. Ion implantation in conducting polymers introduce electrical and optical behaviour of the defects which can be tailored by tuning the energy and dose of the ion beam[6]–[9].

Ion implantation could also be viewed as a method of introducing defects in conducting polymers and by controlling the energy and dose the desired defect states can be achieved[9]–[15]. Particularly, low energy (few tens of KeV) ion beams can be very useful in incorporating a near surface layer which is modified with the desired defects while leaving rest of the polymer unaffected. Such layered structure can be used to fabricate devices once the methodology is optimized. In this study an attempt has been made to study the properties of such layered composite material by utilizing low energy ion beams of Au and Ag. We have used polyaniline (PANI) as our model system as it is a well-studied conducting polymer [16] and can be easily synthesized in the form of thin films. The choice of Au and Ag was with an idea to explore the possibility of studying the conditions to grow embedded nanoparticles and investigate the optical properties of the composite material. Conducting polymer Poly-Aniline (PANI) was implanted with 75 KeV Gold (Au) and 30KeV Silver (Ag) ions to study the optical and electrical properties of the composite materials. The projected range of 75 KeV Au was calculated as 65nm and that of Ag as 32 nm in PANI by SRIM analysis prior to implantation. Post implantations, optical absorption behaviour of the composites have been studied intensively and they were found to bestrikingly different from the pristine ones which are due to combined effects of the defects produced by ion bombardment and presence of metal fillers in the polymer matrix. The possibility of formation of metal nanoparticles due to phase segregation was investigated but due to the strong optical absorption of PANI the respective Surface Plasmon Resonance (SPR) peaks of Au or Ag nanoparticles appeared to be overlapped by response from PANI.

However, cross-sectional FESEM (Field Effect Scanning Electron Microscopy) revealed the presence of a buried layer of small Au clusters in the Au implanted samples. In case of Ag implanted samples small clusters of Ag were found to be randomly dispersed throughout the targeted area. This indicates difference in the diffusion behaviour of Au and Ag in the samples. XRD measurements show the development of small peaks over the amorphous hump, which evolve with the implantation dose. However, the positions of the peaks differ in case of Au and Ag implanted samples and these could be ascribed to the defect regions containing short range ordered structures created during ion implantation. It is also noted that the defect states produced in the two cases are not identical; as a result they appeared at different positions in the XRD spectrum.The difference in the optical absorption behaviour also corroborates difference in the nature of defects created in the two types of samples. Temperature dependent DC conductivity study was carried out to investigate the role of the defects and the metal fillers on the charge transport behaviour. A comprehensive analysis of all the measurements reveals that the defect states created by Au and Ag implantation have different behaviours which

incorporate all the factors of ion implantations. The diffusion behaviour of the defects and the implanted ion species both seem to be responsible for the difference in the observed properties of the implanted samples. The dose dependence of optical absorption combined with the FESEM analysis indicates the probability of radiation enhanced diffusion in case of the Ag implanted samples. The results of this study indicate it is possible to tailor the optical and electrical properties of the composite materials by the choice of ion species and also implantation dose and energy.

2.2 Experimental Details:

2.2.1. In-Situ Synthesis of PANI on Glass & Silicon wafers

Step 1:*Substrate Preparation*

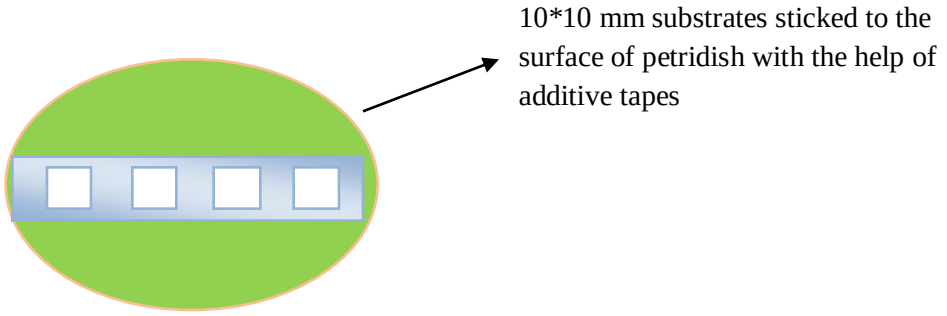

Fig. 2.3:Substrate preparations for in-situ thin films

- PANI thinfilms were synthesized on three different substrates by in-situ polymerization [17].
- For Au ion implantation films synthesized on ITO coated glass substrates were used and Ag ion implantation was carried out on films synthesized on glass substrates.
- For carrying out FESEM measurements identical PANI films were synthesized on polished and cleaned Si wafers.
- 2.59 g of Aniline hydrochloride and 5.71 g Ammonium Per Oxy Sulphate (APS) was dissolved separately in 50 ml distilled water and both solutions were cooled to about 5^0C.

- 10mm x 10 mm substrates were stuck to an adhesive tape and placed in a petri dish and the cooled solutions of Aniline Hydrochloride and APS were added to it, as shown in Fig. 2.3.

- Both the solutions as mentioned in above poured into the petridish containing the substrates as shown in Fig. 2.4. The substrates remained immersed in the reaction mixture on which the polymerization took place forming films. Earlier reports and detailed studies have shown that perpendicular growth of PANI chains on the substrates starts initializing providing an almost horizontal smooth film with almost equal thickness throughout the surface. The typical reaction time is about 15 minutes after which the substrates were removed and washed in HCl and Acetone and then dried in vacuum desiccator. The dark green films are known to be in 50% oxidized state of PANI and they show high electrical conductivity.

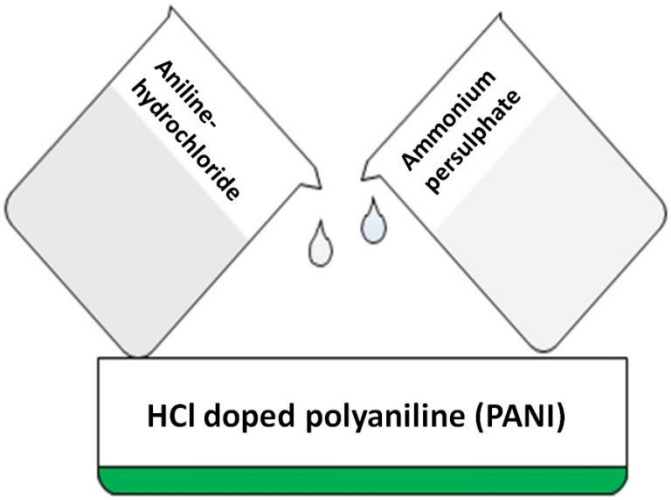

Fig. 2.4: In-situ synthesis of PANI thin films on substrates

2.2.2 *Step 2:Ion Beam Implantation:*

Au ion implantation was carried out on thus formed PANI thin films using the low energy ion beam facility at IUAC, New Delhi. The energy of the ion beam was 75 KeV and the samples were implanted in the dose range of $5x\ 10^{15}$ions/cm^2 to $1\ x\ 10^{17}$ ions/cm^2. Ag ion implantation was carried out using the low energy ion beam facility at Institute of Physics, Bhubaneswar. The energy of the ion beam was 30 KeV and the implantation dose has been varied in the range $1\ x\ 10^{15}$ions/cm^2 to $4\ x\ 10^{16}$ions/cm^2. In both cases the ambient pressure of the sample chamber was kept around $3\ x\ 10^{-7}$ Torr. The implanted samples were characterized by X-ray Diffraction using Bruker D8 X-ray diffractometer to study the structural changes due to ion implantation. UV-Vis absorbance studies were carried out using Perkin Elmer to understand the change in the optical absorbance. FESEM measurements were carried out using Jeol system at Institute of

Physics, Bhubaneswar. Temperature dependent DC conductivity studies were carried out in the temperature range of 100K to 300K to assess the defects generated by ion implantation.

2.3 Results & Discussions:

2.3.1 XRD Measurements:

XRD measurements were carried out on the films deposited on Si wafers. The results of the XRD measurements carried out on Ag implanted PANI at an angle of incidence of 0.5^0 or grazing angle are shown in Figure-5 (a). The XRD spectra of Au implanted samples are shown in and Figure 5 (b). In general the peaks at 13.7^0 and 16.5^0, correspond to the short range crystalline regions found in the unimplanted sample [18], are seen to broaden and diminish in intensity as the implantation dose increases as can be seen in Figure-5b. In case of Ag implanted samples, the peak at 30^0 was found to develop as a function of increasing implantation dose. In the case of Au implantation this peak doesn't seem to be affected by ion implantation. Now, there were two unimplanted samples of PANI, one on ordinary glass slide another on Si wafers which are taken at the first and at the last of Fig. 2.5(a) to check any anomality present. It was found to be same everywhere. So, if we take two samples keeping all the parameters same, one on ordinary glass and another Silicon wafer there must not be any structural ambiguities and we can take any one of them for characteristic studies suitable for the involving system, like glass has a problem of reflecting or refracting lights. Therefore, we can take Si wafer for XRD measurements instead of glass samples.

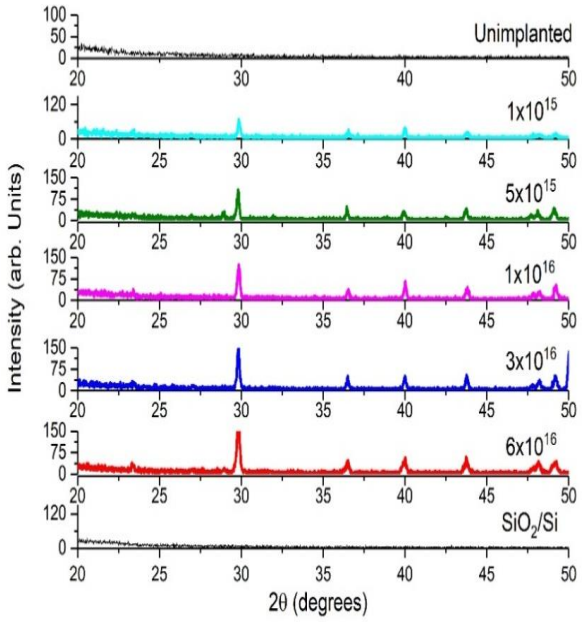

Fig. 2.5(a): XRD spectrum of Ag implanted samples at an angle of incidence of 0.5^o

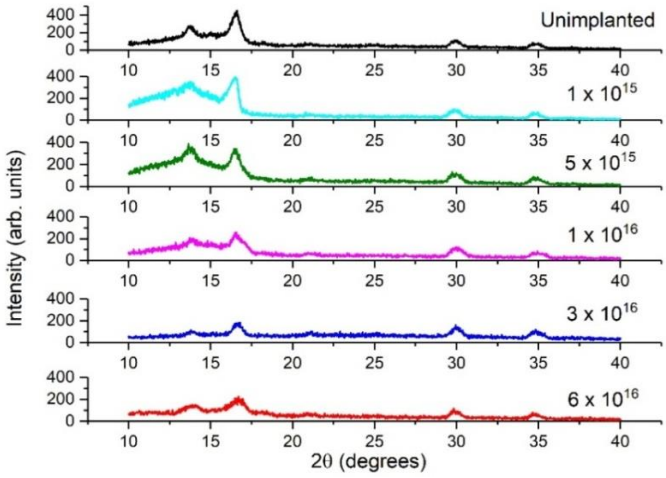

Fig. 2.5(b): XRD spectrum of Au implanted samples at an angle of incidence of 3^0

The difference in the structural changes in the case of Au and Ag implantation can be clearly seen from the XRD spectrum in the two cases. This could be due to the difference in the energy of the two ion beams used and also the mass of the implanted ion. Au being larger in size is expected to create more structural damage than the Ag ion.

2.3.2 UV-Vis Absorbance measurements:

The optical absorbance of the Ag implanted samples is shown in Fig. 2.6(a). The optical absorbance of the unimplanted films is consistent with the earlier reported work [17], [18]. Ag implantation can be seen to change the absorbance behaviour significantly in the region around 540 nm. The SPR peak of Ag nanoparticles is known to be around 420 nm[19], so in this case the observed increase in the absorbance does not seem to be due to the formation of Ag nanoparticles.

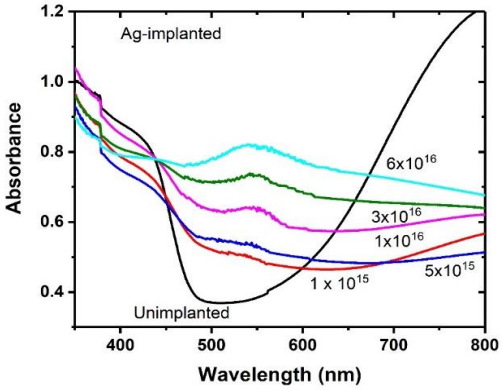

Fig. 2.6(a): Absorbance spectra of Ag implanted samples

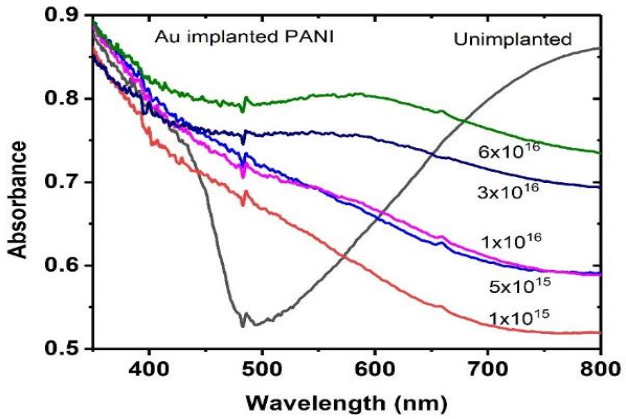

Fig. 2.6(b): Absorbance spectra of Au implanted samples

The absorbance of Au implanted samples is shown in Fig. 2.6(b). In this case also Au implantation gives rise to a dose dependent change in absorbance in the region around 590 nm. It may be noted that the SPR peak for 5-10 nm sized Au nanoparticles is around 520 nm with the peak shifting to higher wavelengths as the particle size increases beyond 100 nm [20]. In the present case, we did not observe any peak developing in this wavelength range however; the absorbancecan be seen to increase in the range of 500 to 600 nm regions with a broad hump developing around 590 nm for the highest implantation dose. We cannot ascribe this feature to the formation of Au nanoparticles since our SEM analysis does not show the presence of Au nanoparticles of sizes greater than 100 nm which could give rise to this kind of optical behaviour. Hence it can be presumed that in the case of Ag implantation as well as Au implantation the observed optical behaviour is due to the superposition of the effects of radiation induced defects and the presence of metallic fillers. It is worth noting that the observed optical behaviour is systematic and definitely dependent on the implantation dose dependent and also on the ion species being implanted.

2.3.3 FESEM measurements:

Ag and Au implanted PANI films synthesized on Si wafers were studied using FESEM measurements. The ion implanted samples were cut through the middle using a diamond saw and FESEM measurements were carried out on the cross sections of the samples to see the depth distribution of implanted ions. A typical cross sectional view of the unimplanted and Ag implanted sample is shown in Fig. 2.7(a) and Fig. 2.7(b) respectively and Fig. 2.7(c) shows the EDAX spectrum.

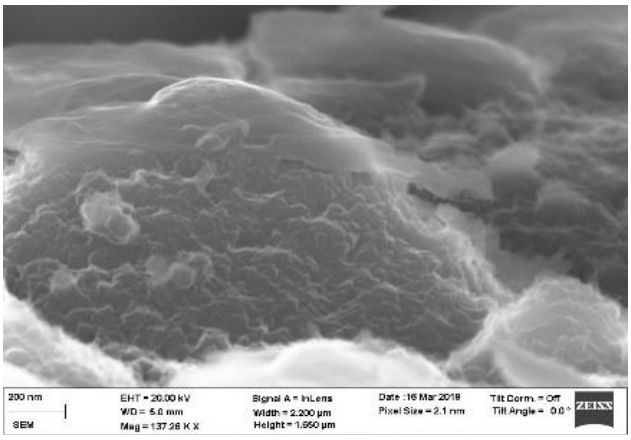

Fig. 2.7(a): Cross sectional view of unimplanted

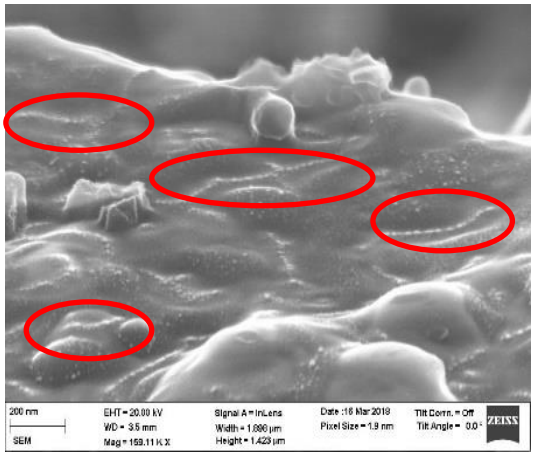

Fig. 2.7(b): Cross sectional view of sample implanted at a dose of 6 x 10^{16}ions/cm^2 (bead like features highlighted)

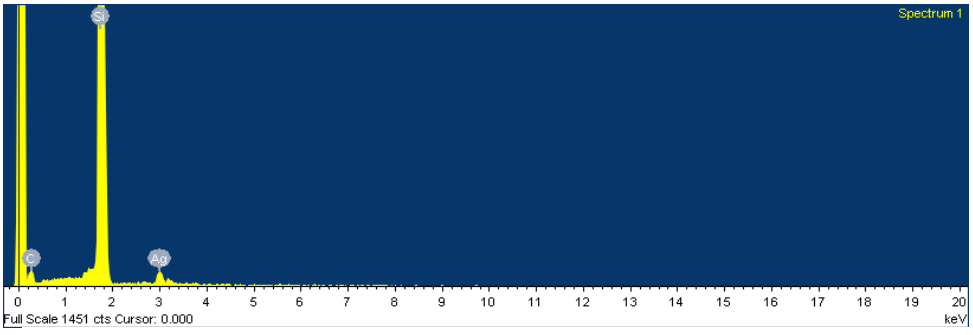

Fig. 2.7(c): EDAX spectrum of selected area in the implanted region

The cross sectional FESEM analysis shows formation of bead like structures dispersed throughout the depth as the implantation dose increases. The beads can be clearly seen at the dose of 3 x 10^{16}ions/cm^2 and become more prominent at the dose of 6 x 10^{16}ions/cm^2. While it cannot be unambiguously pointed out that these beads are Ag nanoparticles, the EDAX spectrum does show the presence of Ag atoms in the selected regions. Table- 2.1 shows the relative elemental concentration in the selected regions around the bead like structures. The presence of the bead like structures throughout the implantation zone and their dose dependence suggests that there is significant diffusion of the implanted ions and also the defects produced during the implantation process.

Element	App Conc.	Intensity Corrn.	Weight %	Weight % Sigma	Atomic %
C K	2.30	0.1694	31.20	2.71	52.47
Si K	32.3	1.1434	65.12	2.58	46.84
Ag L	1.08	0.6793	3.68	0.45	0.69
Totals			100.00		

Table 2.1: Relative elemental concentration in the cross sectional EDAX spectrum

Fig. 2.4 shows the FESEM picture of Au implanted sample. The cross section in this case shows a layer of possibly clusters of Au atoms. It may be noted that in this case, at higher dose significant sputtering was observed. This could be the reason that the depth of the buried layer was less than the range of the 75 KeV ions in the samples and it decreased as the dose increased. Therefore, the possibility of self-sputtering of the implanted atoms cannot be ruled out. This observation is also confirmed by SRIM calculations which show the sputtering yield isconsiderably high at 75 KeV, which points out that this energy is not suitable for ion implantation for synthesizing nanoclusters of Au in Polyaniline.

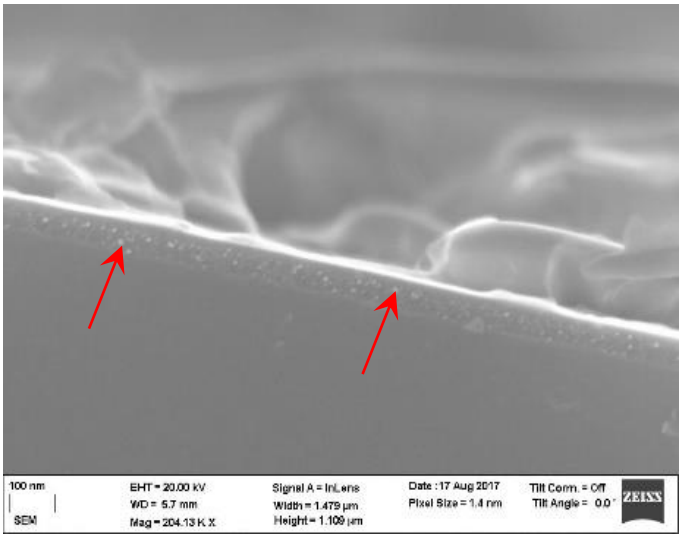

Fig. 2.8: Cross sectional view of Au implanted sample at a dose of 1 x 10^{16}/cm^2 (Buried layer is indicated by the arrows)

2.3.4 Temperature dependent DC conductivity measurements:

- Temperature dependent DC conductivity measurements were carried out in a CCR based cryostat in four probe geometry.
- The DC conductivity was seen to follow the well-known Variable Range Hopping (VRH) model. According to Mott's VRH model the variation of DC conductivity with temperature is given by [21]

$$\sigma = \sigma_0 \left(-\frac{T_0}{T} \right)^{\gamma} \qquad \textbf{(1)}$$

- Where σ_0 is the conductivity at infinite temperature and T_0 is the characteristic temperature which is related to the density of states at Fermi energy and localisation length and T is the absolute temperature.
- The exponent $\gamma = \frac{1}{d+1}$ is related to the dimensionality (d) of the hopping process.
- For 1D VRH d=1, for 2D VRH d=2 and for 3D VRH d=3.

- The DC conductivity data was fitted with this model keeping T_o and γ as free variables and it was found that in all the samples the data matches with 3D hopping as shown in figure-9. T_0 is related to the density of states at Fermi energy, Average hopping distance and Hopping energy as follows [22].

$$T_0 = \frac{16\alpha^3}{k_B N(E_F)} \quad \textbf{(2)}$$

$$R_{hop} = \left[\frac{9}{8\pi\alpha k_B T_0 N(E_F)}\right]^{\frac{1}{4}} \quad \textbf{(3)}$$

$$W = \frac{3}{4\pi R_{hop}^3 N(E_F)} \quad \textbf{(4)}$$

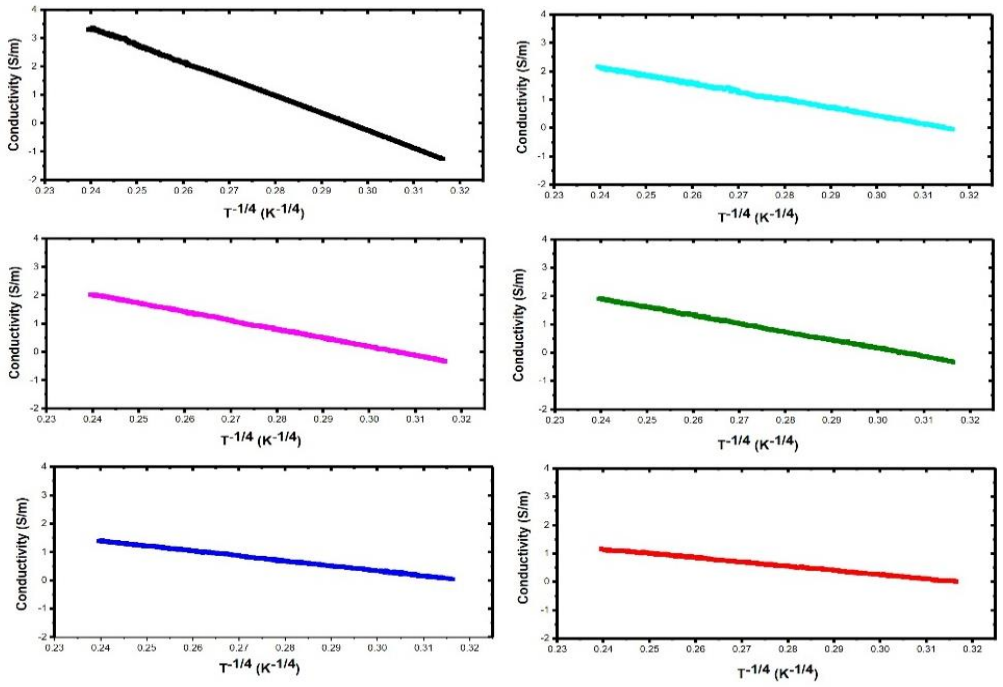

Fig. 2.9: Fitting of temperature dependent DC conductivity to the Mott's 3D-VRH model

The values of T_0 calculated from the slope of the plots in Fig. 2.9 are given in Table-2.2.

Sample/Dose	T_0 (K)
Unimplanted	1.9×10^4
1×10^{15}	2.2×10^4
5×10^{15}	2.8×10^4
1×10^{16}	2.4×10^4
3×10^{16}	5.5×10^3
6×10^{16}	3.2×10^3

Table 2.2: Characteristic Temperature

The deductions from the above observations are as follows----

- ✓ The values of T_0 are rather high, but that could be an indication that the samples are on the insulator side of the metal-insulator transition.

- ✓ In earlier reports the DC conductivity was found to increase with implantation dose [], but in the present study we have observed the conductivity decreased with increasing dose. This could be because of the radiation induced disorder in the samples.

- ✓ The values of T_0 increased till the dose of 5×10^{15} and then there is a decrease with increasing dose.

- ✓ The lower values of T_0 are indicative of an increase in the density of states near Fermi level but, as can be seen, it did not lead to increase in conductivity. This could be due to the decrease in the localization length which is expected from the increase in the disorder due to the energy deposited during the implantation process.

- ✓ Some independent measurements are needed to estimate the density of states, which will be carried out and reported elsewhere.

2.4 Conclusions

Finally, in conclusion we may say that

1. Au-polyaniline and Ag-polyaniline composites can be synthesized using ion implantation method.

2. In both the cases remarkable changes in the optical absorbance was observed.

3. Although the optical behaviour could not be related to the formation of Au and Ag nanoparticles but from FESEM images the existence of some cluster formations have been confirmed.

4. In case of Ag ion implantation small bead like structures were found to be dispersed throughout the implanted zone.

5. This observation leads us to believe that in case of Ag ion implantation there is considerable diffusion of the implanted ions and also the defects associated with it. On the other hand a layer of small clusters were seen buried deeper inside the samples in the case of Au ion implantation.

6. XRD measurements indicate that the difference in the radiation induced damage in the samples could be a combination of the effects of ion mass and the incident energy.

7. DC conductivity measurements show that all the samples were on the insulator side of the metal-insulator transition, while there is an indication of increase in the density of states near the Fermi energy at higher implantation doses.

2.5 References

[1] Zarras*P, AndersonN, WebberC, IrvinD.J, IrvinJ.A, GuenthnerA,Stenger-J.D,Smith, *Radiat. Phys. **Chem*68**, 387, 2003

[2] BaiHua and ShiGaoquan, *Sensors*, ***7***, 267, 2007

[3] PeierlsR. E, *Quantum Theory of Solids* (Oxford University Press, London, 1955

[4] TangC. W, *Appl. Phys. Lett*. **48,** 183, 1986.

[5] PronA, RannouP, *Prog. Polym. Sci*.**27**, 135, 2002

[6] HuangW.S. and MacDiarmidA.G, *Polymer*, **34(9)**, 1833, 1993

[7] SalaneckW. R, StrafströmS, and BrédasJ. L, *Conjugated polymer surfaces and interfaces: electronic and chemical structure of interfaces for polymer light emitting devices (Cambridge Unversity Press, Cambridge, 1996).*

[8] SalaneckW. R, FriendR. H, and Brédas J. L, *Phys. **Rep***.**319,** 231 (1998).

[9] SalaneckW. R and BrédasJ. L, *Adv. Mater*.**8,** 48 (1996).

[10] SalaneckW. R, SekiK, KahnA, and PireauxJ.-J, *Conjugated polymer and molecular interfaces: Science and technology for photonic and optoelectronic applications (Marcel Dekker, New York, 2002).*

[11] Roger J. Mortimer, Aubrey L. Dyer, John R. Reynolds, *Displays***27,**2, 2006

[12] PileniM.P, New J. Chem. **22**, 693, 1998

[13]BogdanovićU, Pašti I, MarjanovićG Ć, MitrićM, Scott P. Ahrenkiel, and VodnikV, *ACS Appl. Mater. Interfaces*, **7 (51)**, 28393, 2015

[14] Reda[1]*S M, Al-Ghannam[2]S M,*AMPC*, **2**, 75,2012

[15] GangopadhyayR and DeA, *Chem. Mater.***, 12**, 608,2000

[16] BogdanovicU, Pasti I, MarjanovicG Ć, MitricM, Scott P. Ahrenkiel, and VodnikV, *Appl. Mater. Interfaces*, **7**, 28393, 2015

[17] AleshinA. N, MironkovN. B, SuvorovA. V, ConklinJ. A, SuT. M and KanerR. B, *Phys. Rev. B***54 (16)**, 11638, 1996

[18] ParkS. K, LeeS. Y, LeeC. S, KimH. M,JooaJ,BeagY. W and KohS. K, *J. Appl. Phys.***96 (4)**, 1914, 2004

[19] LiuZ.M, ZhuJ.L, GuoY.P, YuZ.W, QianP.P and MaZ.T,*Nucl.Instrum.& Meth. B***91**,465, 1994

[20] ZhuJ.L, LiuZ.M, YuZ.W, GuoY.P, MaZ.T and BengR.Z, *Nucl.Instrum.& Meth. B* **91**,469, 1994

[21] WangW, LinS, BaoJ, RangT, WanH and SunJ, *Nucl. Instrum.& Meth. B***74**, 514-518, 1993

[22] LungK.G ,SchultzeW, and HuchalCh, *Nucl. Instrum.& Meth. B***80/81**, 1076, 1993

[23] TongZ S, WuM Z, i:rtgJ L, HuQ H, ZhuM and ChenL, XuX L, WanM X and ZhouH X*Nucl. Instrum.& Meth. B***71**, 26, 1992

[24] YAOQ, LIUL and LrC, *Radiat. Phys. Chem.* **Vol. 44**, **No. 4**, 381, 1994

[25] YAOQ, LIUL and LrC, *Radiat. Phys. Chem*. **41,(6),** 791, 1993

[26] SrivastavaM.P, MohantyS.R, AnnapoorniS, RawatR.S, *Phys. **Lett**. A***215**, 63, 1996

[27] KANGE. T, NEOHK. G and TANK. L, *Prog. Polym. Sci.,* **Vol. 23**, 211, 1998

[28] Pouget J.P., Josefowicz M.E., Epstein A.J., Tang X. and MacDiarmid A.G., *Macromolecules*, **24**, 779, 1991
[29] STEJSKALJ AND SAPURINAI, *Pure Appl. Chem.*, **77 (5),** 815, 2005
[30] Das R, NathSS. , ChakdarD, GopeG&BhattacharjeeR, *J. Exp. Nanosci.*,**5:4**, 357, 2010
[31] ZuberA, PurdeyaM, SchartnerE, ForbesC, Benjamin van der Hoek, GilesD, AbellA, MonroT, HeidepriemH E, ***SENSOR*** *ACTUAT* ***B****-CHEM***227**, 117, 2016

[32] Mott N.F. and Davis E.A., 1979, *Electronic Processes in Non Crystalline Materials* 2nd edn. (Oxford: Clarendon)
[33] Campos M., Bello B. Jr., *J. Phys. D: Appl. Phys.*,**30**, 1531, 2006

[34]Vladimir N. Popok, *Rev.Adv.Mater.Sci.***30**1 2012

[35] StepanovA.L andKhaibullinR.I,*Rev.Adv.Mater.Sci*.**7** 108 2004

Chapter 3

Medium energy Silver and Nickel ion implantation into thick Poly-Aniline films and observation of structural changes& PANI-Au metal nanocomposites synthesis by Chemical route of fabrication

3.1 Introduction:

Time since its discovery in the 18th Century PolyAniline (PANI) have been known as Aniline Black after it was derived by oxidizing the liquid Aniline [1]–[3]. As time progressed PANI gained its popularity because of

i. Ease of synthesis
ii. Environmental stability
iii. It has a unique feature of redox depandant colouring effect
iv. It shows tunable conductivity

PANI is majorly synthesized in two steps processes; it may be in-situ method as described in the earlier chapter or bulk fabrication which will be discussed shortly in this chapter. Polyaniline also can be synthesized electrochemically but our knowledge and purpose limited to simple chemical route of fabrication of PANI.

PANI has basically three oxidative forms namely; *emeraldine*, *leucoemeraldine*, *pernigraniline*. PANI becomes conductive in its emeraldine form. At the very early stage of PANI synthesis it is available as HCl doped PANI which is conducting at fully doped ($\sigma \geq 1$ S/cm); it is dark green in colour. It can be dedoped by appropriate amount of *Base* and PANI becomes insulating ($\sigma \leq 10^{-10}$ S/cm). It can be again redoped by applying any kind of dopant acids. With each change in type of dopant the conductivity changes along with the hue of doped PANI. This quality of tuning the conductivity of PANI is applied in many practical devices such as sensors, batteries, actuators, antistatic coatings, corrosion protection, electro-optic and electro-chromic device, electromagnetic shielding [4], [5],[6],[7].

Moreover, current trend in research is focusing on nanostructured and nanocomposite of PANI which is increasing year by year as shown in Fig. 3.1.

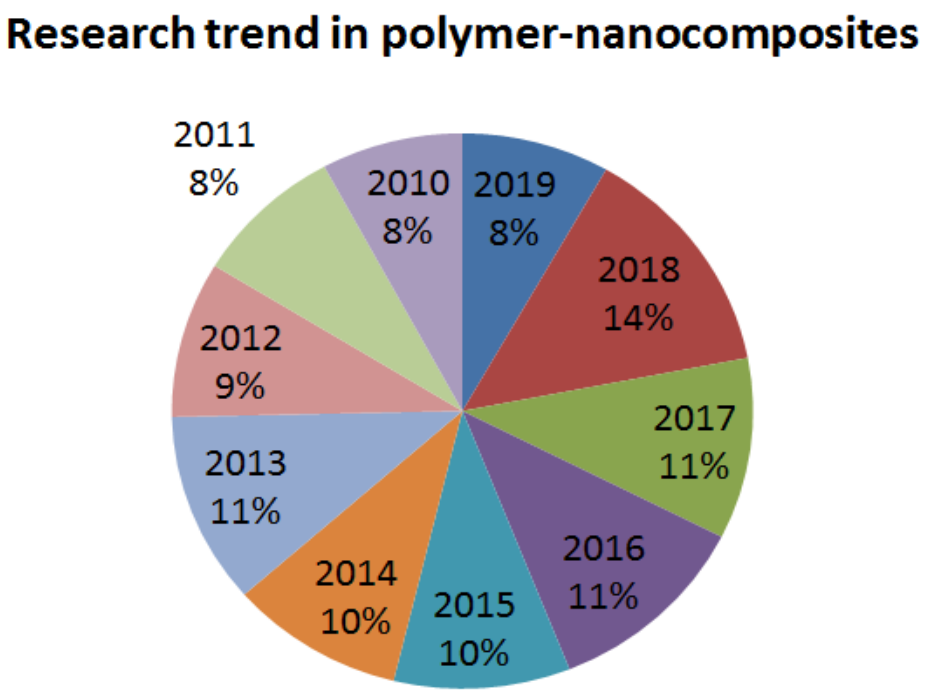

Fig. 3.1: Percentile description of research trends in polymer nanocomposites

3.2 Experimental Details:

3.2.1 Synthesis of Poly-Aniline from Aniline monomer

The chemical Aniline is hygroscopic and thus it is readily oxidized when purchased from regular and reputed sources. So, first of all aniline monomer was deoxidized using Zinc dust. A distillation set up was used for this purpose. Temperature raised to around 100°-150^0 C for distillation. Oxidized Aniline is reddish in color; after distillation it becomes colorless and clear. The schematic diagram of the experimental set up is shown below in the Fig. 3.2

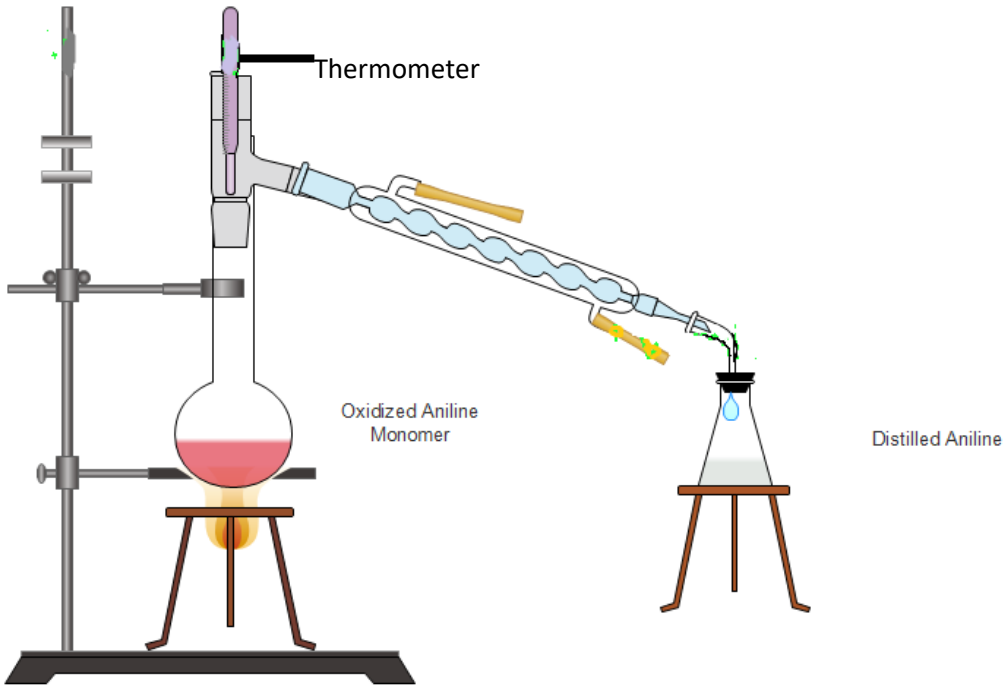

Fig. 3.2: PolyAniline Distillation set up

3.2.2 Synthesis of Protonated PANI:

- 200ml of Aniline monomer was dissolved in 300ml of 1 molar Hydro Chloric Acid (HCl).
- In another container 11.5gm of Ammonium per sulphate was dissolved in 200ml of 1M HCl.
- The abovetwo solutions were mixed in a large beaker set in an ice bath so that the temperature could be maintained at 0-5^0 C as the reaction is exothermic.
- The mixture is stirred for half an hour to complete the reaction so that maximum precipitate could be collected.
- The precipitate was dark green in colour, with a high amount of acid, untreated monomer and oligomers.
- It was then washed with 0.2M HCl and acetone to remove untreated oligomers and monomers; and then washed with plenty of deionized water to remove the traces of acid and the excretion was checked repeatedly in order to bring the pH level to normal.
- After that it was dried in vacuum desiccator to obtain a green powdery substrate which is known as HCl-doped PANI[8]–[10].

For our purpose, we used HCl as purchased from Merck with the strength of 13 (N).

By using the formula $C_1V_1 = C_2V_2$,

Where C_1, V_1, are initial concentration and volume respectively and C_2, V_2 are desired concentration and volume respectively,we used 23ml of 13 Molar solutions of HCl to prepare 300ml of 1M.

3.2.3 De –doping of PANI:

The process of getting De-doped PANI or reduced PANI follows also very simple steps without much requirement of knowledge of Chemistry.

- About 2gm of HCL-doped PANI was added to 200ml of 0.1M Ammonia solution purchased from Merck.
- The mixture was stirred for 3-4 hours. De-doped PANI so obtained was dark blue in colour.
- The mixture was filtered out and precipitate is collected.
- It was then washed repeatedly with de-ionized water to remove the traces of Ammoniaand later, it was vacuum dried and preserved for future applications.

The schematic diagram vacuum filtration set up is shown in below Fig. 3.3

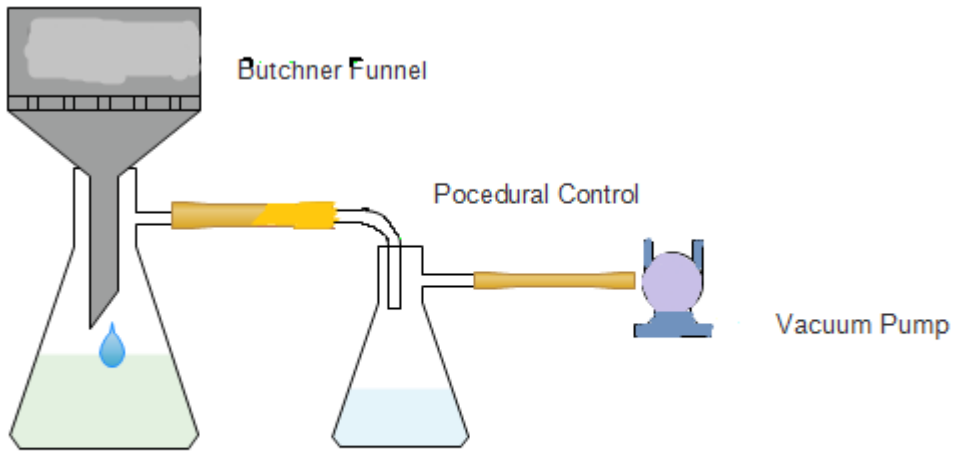

Fig. 3.3: Vacuum filtration system

3.2.4 Preparation of conducting solution of Poly-Aniline:

Preparation of solution of poly-Aniline was being a challenge, as PANI being insoluble in common solvents.

A) Poly Aniline in n-Methyle Pyrrolidone (NMP):

As mentioned in earlier reports for preparation of both doped and de-doped PANI solutions were tried with 1-2 gm of PANI dissolved in 30 ml of 1-Methyle, 2-Pyrrolidone (NMP). Solubility found to be very poor and the solution was not appropriate for film preparation. Moreover, solution of green colored doped PANI turned out to be blue,which implies PANI lost its conducting property.

B) Camphor Sulfonic Acid (CSA) doped PANI:

According to previous literature Poly-Aniline has highest solubility in m-Cresol and Camphor Sulfonic Acid (CSA).

- 0.4 gm de-doped PANI was mixed with 2 gm CSA in a Morter Pestle.
- As found from literature, CSA works well as a doping reagent for PANI at the time of making the paste.
- After that this mixture was dissolved in 30ml m-Cresol and it was stirred for 72 hours continuously to obtain a homogeneous solution.
- *m*-Cresol straightens curled up PANI chain. So, conductivity of PANI further enhanced while dissolving in m-Cresol.

3.2.5 Preparation of thick film:

To prepare thick films, different substrates of dimensions 10mm * 10mm made of glass, Indium Tin Oxide (ITO) coated glass and n-type Silicone wafer were cut from the bulk. This dimension was selected as it was appropriate for the substrate holder in ion beam implantation system.

After checking with a mercury level, on a horizontal surface, about 10 µl of this solution was drop casted on the substrates and it was left for semi-drying. This process was repeated for 3-4 times until a few tens of microns thick film is obtained. It was then left in vacuum desiccators to become fully dry. These films can now be used as free standing films also. Thicknesses of the films were measured with the help of the screw gauge meter.

3.2.6 Poly-Aniline thin film preparation:

A) Thin film by in-situ method:

2.59 g of Aniline hydrochloride and 5.71 g Ammonium per Oxy Sulfate (APS) was dissolved separately in 50 ml de-ionized water and both solutions were cooled to about 5^0C. 10mm x 10

mm substrates were stuck to an adhesive tape and placed in a Petri dish and then the cooled solutions of Aniline Hydrochloride and APS were added to it. The substrates remained immersed in the reaction mixture on which the polymerization took place forming films. According to literature survey the poly aniline chains so grown in this way are vertical in nature.

B) Thin film by spin coater:

Thin films can be prepared by mainly three ways…..a) Drop casting, b) Dip Coating, c) Spin Coating. Among these three methods precise control can be achieved by Dip coating and Spin coating. In our lab we followed spin coating method. In the spin coating method,

- We applied a few drops of solutions on substrates of 10mm*10mm diameter suitable for ion beam implantation.
- Substrates were of mainly three kinds namely laboratory grade biological glass slides, ITO coated glass slides and *n*-type Silicon wafers.
- Laboratory grade biological glass slides were used to observe optical properties.
- ITO coated glass slides were used for electrical property studies.
- And *n*-type Silicon wafers were used for structural studies.
- The solutions werekept for few minutes to wet the substrate surface.
- This wetting time found to becomelonger as the surface smoothness increases.
- Then different spreading and drying speeds were tried to optimize the uniform and smooth thick films.
- Uniformity was checked by applying voltages across the samples.

The following wetting and spreading speeds are were attempted:

SPREADING / wetting Speed	Drying Speed
600	900
800	1000
700	1200
900	1500
900	2000
1000	3000
800	1500

After many iterations, we found that the film with 700rpm wetting speed and 1200 rpm drying speed was the most suitable ones.

3.3 Poly-Aniline thick film thickness measurement:

3.3.1 AFM Measurement:

Atomic Force Microscopy measurements were carried out for the prepared samples to observe the surface topography and obtain the sample thicknesses. We could obtain an average thickness of all the prepared samples as all the samples were prepared in the same way. This thickness estimation was carried out for SRIM analysis which is calculated before ion beam implantations. Below are the AFM images:

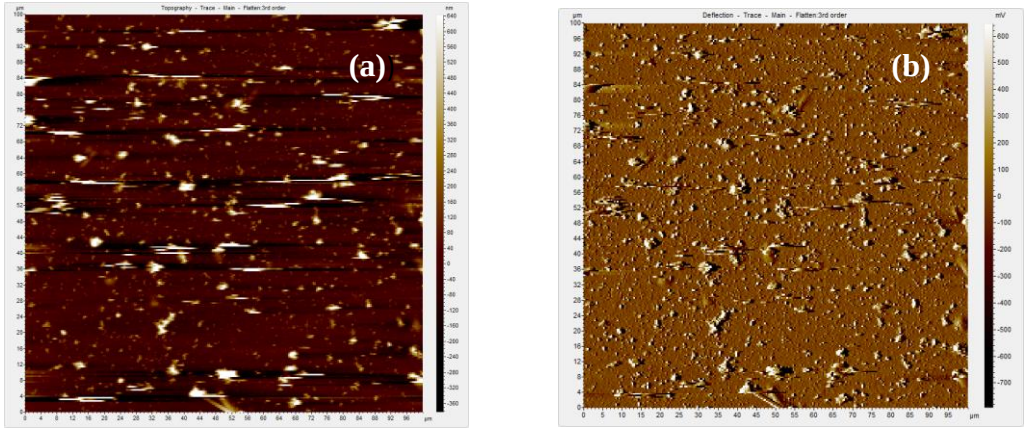

Fig. 3.4: AFM trace of Sample 1[(a) Topography, (b) Deflection Traces]

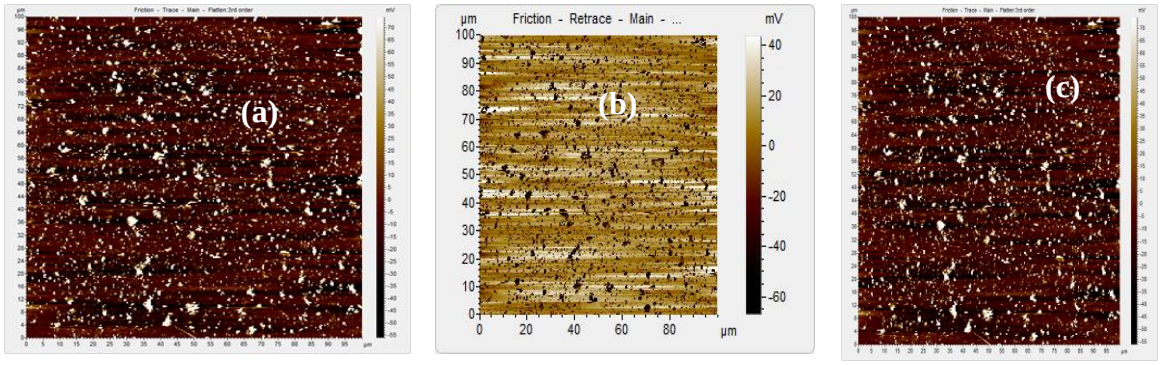

Fig. 3.5: AFM trace of Sample 2 [(a)topography, (b)deflection, (c) friction traces]

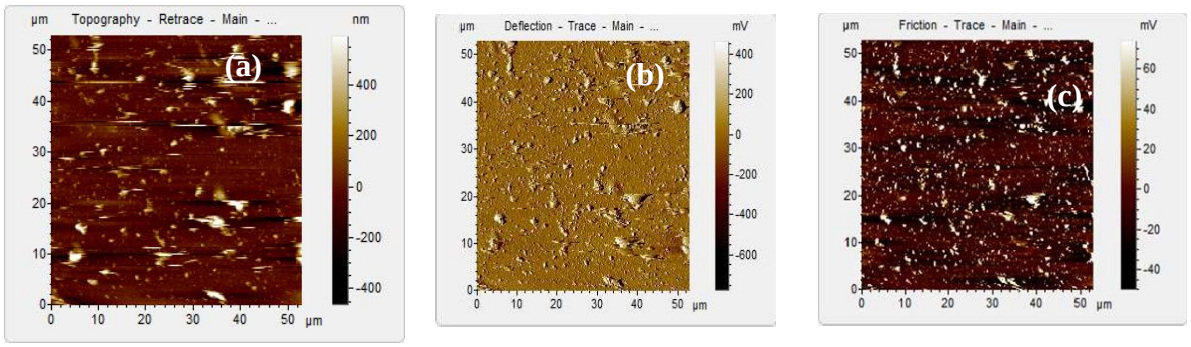

Fig. 3.6: AFM trace of Sample 3 [(a)topography, (b)deflection, (c) friction traces]

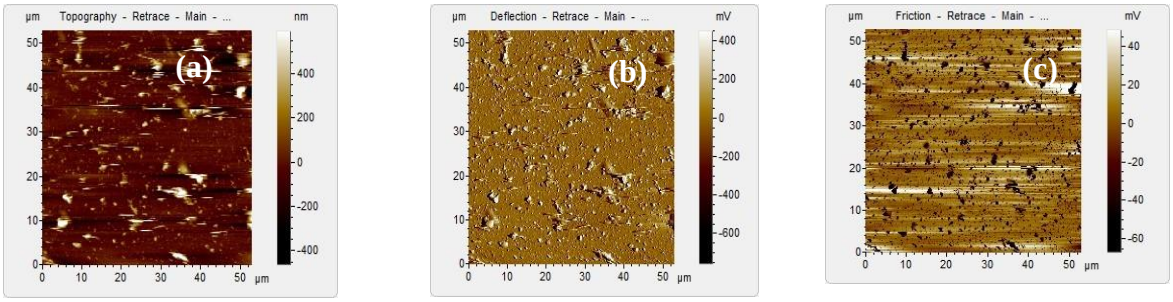

Fig. 3.7:AFM trace of Sample 4 [(a)topography, (b)deflection, (c) friction traces]

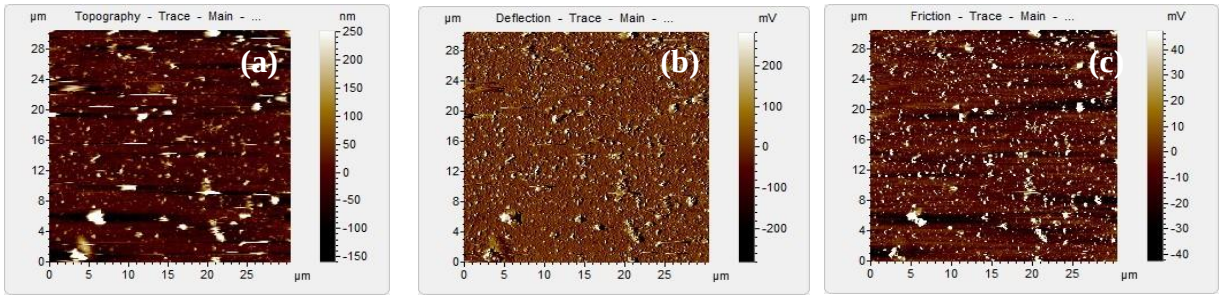

Fig. 3.8: AFM trace of Sample 5 [(a)topography, (b)deflection, (c) friction traces]

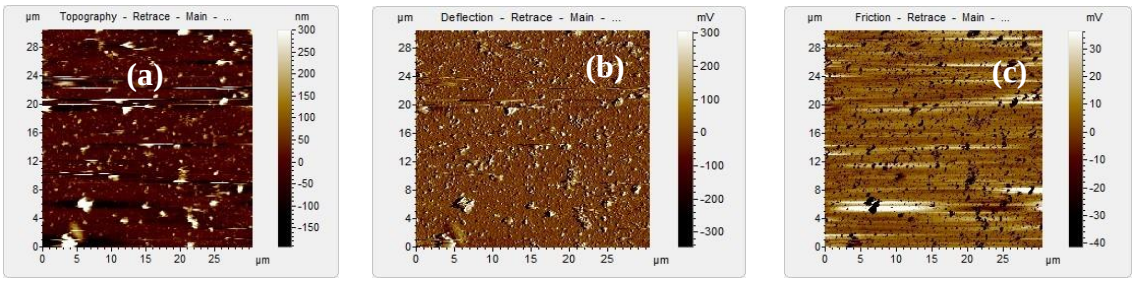

Fig. 3.9 AFM trace of Sample 6 [(a)topography, (b)deflection, (c) friction traces]

Fig. 3.8 and Fig. 3.9 are taken for thin films separately. From the above plots it is inferred that thick films are around 50µm and thin films are around 10µm thick. Once the film thicknesses were estimated, the ion implantation was carried out.

Also by means of ellipsometry we could measure the thickness but due to smooth transparent substrate this method was discarded.

3.4 Ion implantation:

For thick films, MeV range ion implantation is preferred ones and for thin films KeV range ion implantations have been opted the details of which is provided in the previous chapter.

3.4.1 SRIM Analysis:

The SRIM analysis spectra and collision event spectra are shown below in Fig. 3.10 (a) and (b) respectively for Silver ions.

Fig. 3.11 (a) and (b) depicts same analysis in for Nickel ions respectively.

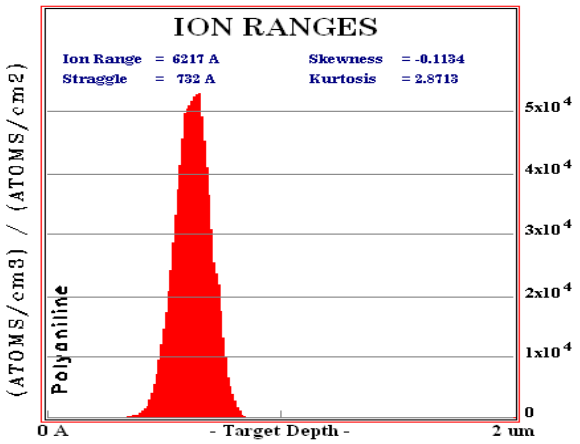

Fig. 3.10(a) : SRIM simulation of 2 MeV Silver ion implantation in PANI

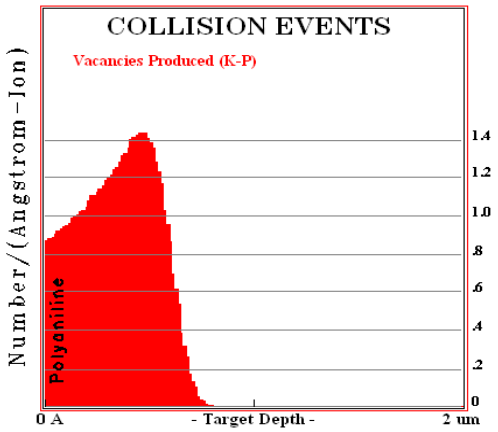

Fig. 3.10 (b): Defect distribution in 2 MeV Silver implanted PANI

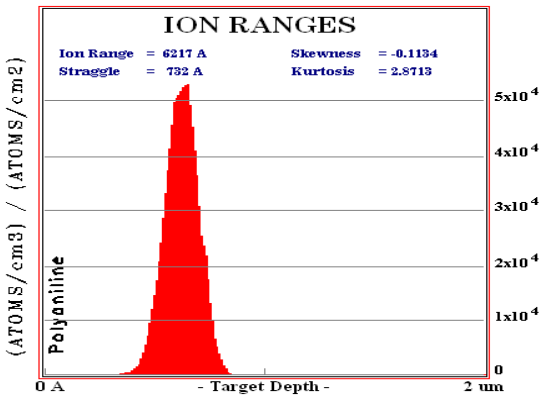

Fig. 3.11 (a): SRIM simulation of 2 MeV Nickel ion implantation in PANI

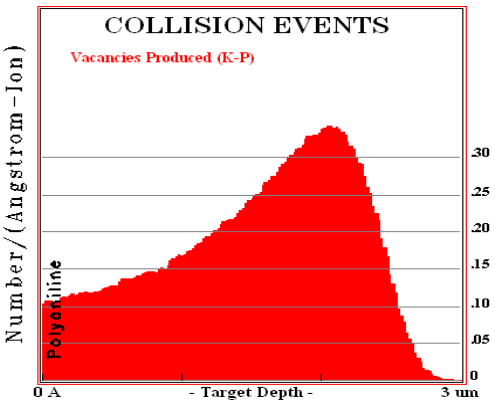

Fig. 3.11 (b): Defect distribution in 2MeV Nickel implanted PANI

The work of ion implantation was executed at Institute of Physics (IOP, Bhubaneswar).

The doses varied from 10^{15} to 10^{17}ions/cm^2. Later these samples were analyzed under XRD and reflectance spectra as transmittance spectra could not be observed because of the opaque samples.

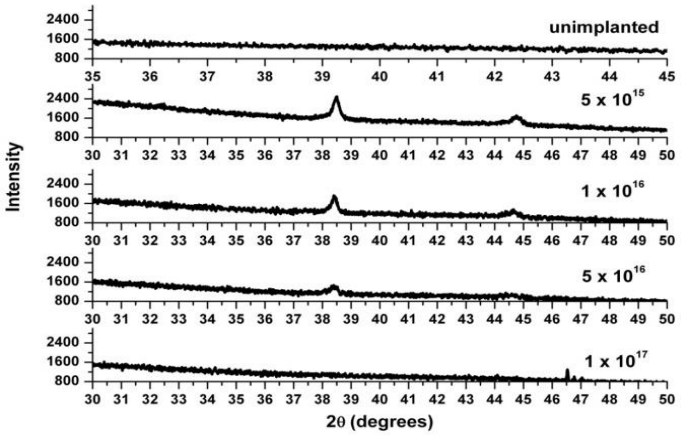

Fig. 3.12: XRD Spectra of gold implanted PANI

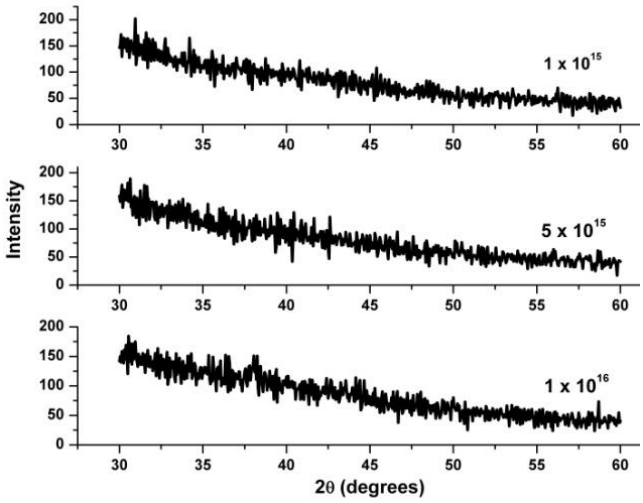

Fig. 3.13: XRD Spectra of Ni implanted PANI

Fig. 3.12 and 3.13 in the above depicts the XRD Spectra of gold and nickel implanted polyaniline films taken on (101) plane of Si wafer. In case of Ni implanted samples, as shown in Fig. 3.13 as the amount of impurity is very less compared to the overall host matrix amount and Ni particles are smaller in size compared to Silver or gold particles, a feeble signal from amorphous Ni could be observed, on the other hand Ni particles within the matrix must be very small to be detected by XRD spectra.

3.4.2 Discussions on XRD and SRIM Analysis:

- The peak defect densities in case of gold implanted samplesare about 4 times larger than that of Ni implanted samples.
- The XRD spectrum of unimplanted sample is typical of an amorphous material as expected
- In case of gold implanted samples distinct peaks appear at 38.2° and 44.5°
- The intensity of the peaks and particle sizes reduce with the increase in fluence and completely disappear at the highest dose of 1 x $10^{17}/cm^2$.
- There is no feature to show formation of Ni nanoparticle.
- Higher defect density and larger atomic size seems to favor the formation of nanoparticles.

3.5 Optical Analysis of the implanted Samples:

Since the implanted samples are opaque due to micro level thicknesses we could not perform transmittance spectroscopy, instead we observed reflectance spectroscopy which is given below:

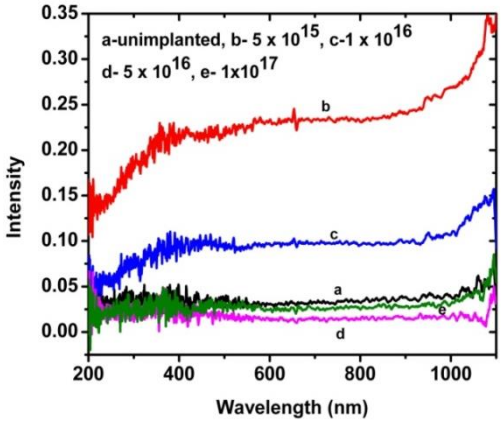

Fig. 3.14(a): Optical reflectance of Gold implanted Samples

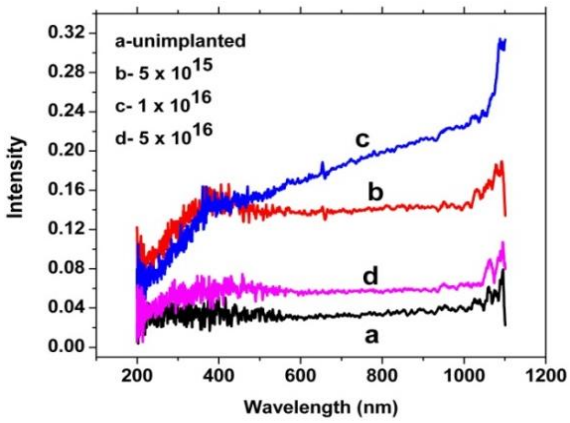

Fig. 3.14(b): Optical reflectance of Nickel implanted Samples

3.5.1 Observations from Reflectance curves:

- Ion implanted samples showed dose dependent optical reflactance.
- The samples acquired metallic lustres after implantations.
- In case of Au implanted samples reflectivity remained almost constant in the visible region for each implantation dose.
- For all implanted samples reflectivity increased sharply near IR region which might be due to free carriers.
- In case of gold implanted samples, reflactance increases with lowest dose of implantation but it gradually, decreases with higher doses, one reason for this may be carbonification caused by ion bombardment. Thus, at highest dose (curve e) reflectance diminishes to the level of unimplanted sample.
- In case of Ni implanted samples the reflectivity shows a different kind of behavior. Upto the dose of 1 x 10^{16}/cm^2 it increased with the dose and then it lost metallic lustre at higher dose due to energy imbued carbonification. Such behavior is expected from dipolar radiation.

From the literature study [11], [12] this phenomenon can be explained as the impact of ion bombardment. In the thick polymer films carbonifactions and graphite like structures appear due to the impulse of ion implantations which brings metallic lusters to the samples.
The different nature of the two graphs may be due to the size difference of the two metals.

The different nature of the two graphs in Fig. 3.14(a) and (b) respectively may be due to the size difference of the two metals.

3.6 Cross-sectional FESEM Measurement:

For FESEM measurements samples were prepared on n-type Silicon wafers (101) in the same way like samples prepared on glass substrates. As in this present work of chapter 3 we were mainly focusing on thick film and medium energy ion beam implantation, the films on Silicon wafers were prepared by drop casting method.

Post implantation Silicon wafers were broken from the middle and its cross section was examined as in Fig. 3.15 to Fig. 3.24.

Sample 1:*Unimplanted Sample*

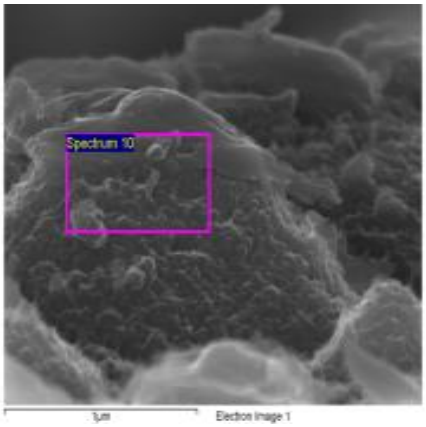

Fig. 3.15(a): Cross-sectional FESEM of Unimplanted Sample

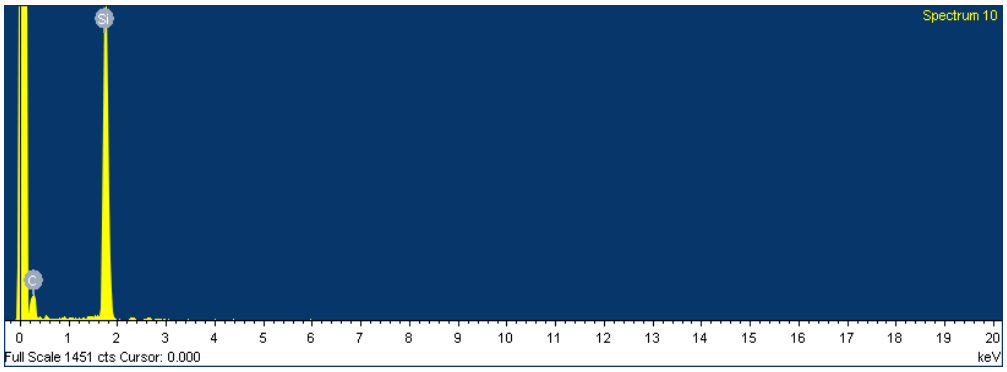

Fig.3.15 (b): EDAX Spectrum of Unimplanted Sample

Fig. 3.15(c): Beam Spectra

Element	App Conc.	Intensity Corrn.	Weight %	Weight % Sigma	Atomic %
C K	8.88	0.3470	70.61	1.08	84.89
Si K	11.46	1.0763	29.39	1.08	15.11
Totals			**100.00**		

Table 3.1: Spectrum analysis table for unimplanted sample

Spectrum processing:

Peaks possibly omitted: 0.520, 2.290 keV

Processing option: All elements analyzed (Normalized)

Number of iterations = 7

Standard:

C $CaCO_3$ 1-Jun-1999 12:00 AM

Si SiO_2 1-Jun-1999 12:00 AM

Sample 2 A:*Ag implanted at a dose of 10^{15} ions/cm^{2}at Horizontal plane*

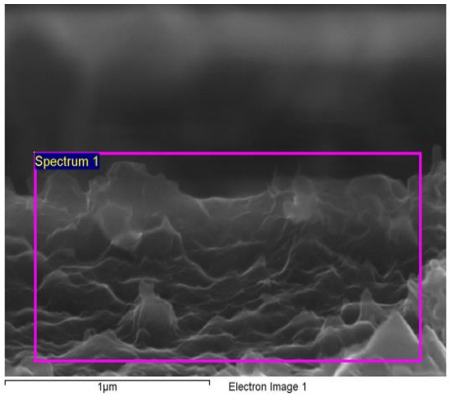

Fig. 3.16 (a): Cross sectional FESEM 1 of implantation at a dose $1*10^{15}$ ions/cm^2

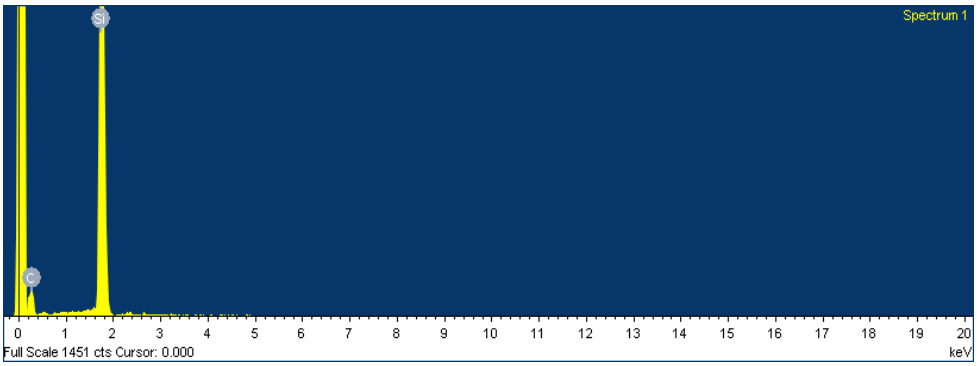

Fig. 3.16(b): EDAX Spectrum-1 of dose 10^{15} ions/cm^2

The Details of scanning parameters are as follows:

Spectrum processing:

Peak possibly omitted: 2.300 KeV

Processing option: All elements analyzed (Normalized)

Number of iterations = 4

From the above scanning no significant evidence could be observed because of very low ratio of metal fluence to polymer matrix volume.

Below fig is scanned at different tilted angle:

Sample 2B:*Ag implanted at a dose of 10^{15} ions/cm^{2}at tilted plane*

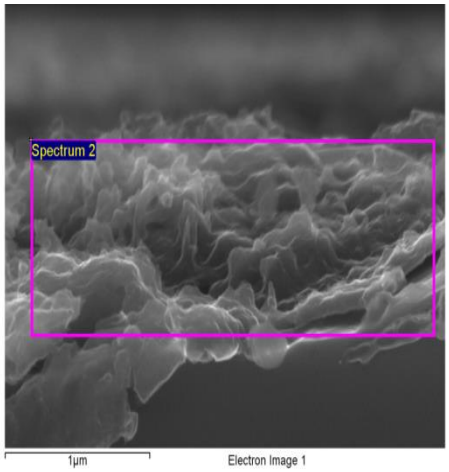

Fig. 3.17(a): Cross-sectional FESEM 2 at tilted angle of dose 1*10^{15} ions/cm^2

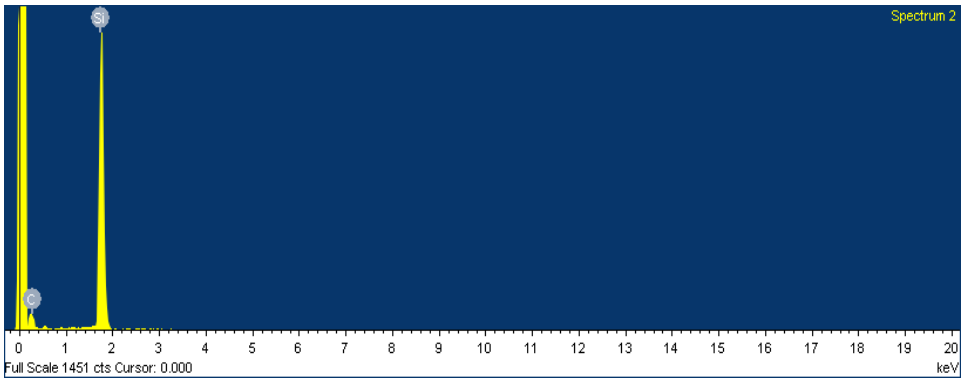

Fig. 3.17(b): EDAX Spectrum-2 of dose 10^{15} ions/cm^2

The Details of scanning parameters are as follows:

Spectrum processing:

Peak possibly omitted: 0.530 keV

Processing option: All elements analyzed (Normalized)

Number of iterations = 6

Standard:

C $CaCO_3$ 1-Jun-1999 12:00 AM

Si SiO_2 1-Jun-1999 12:00 AM

Element	App Conc.	Intensity Corrn.	Weight %	Weight % Sigma	Atomic %
C K	6.05	0.3122	67.05	1.39	82.63
Si K	10.33	1.0844	32.95	1.39	17.37
Totals			100.00		

Table 3.2: Spectrum analysis table for dose $1*10^{15}$ ions/cm^2

With the tilted angle also no such strong evidence of metal inclusion and formation of nanoparticles are found.

Sample 3 A:*Ag implanted at a dose of $5*10^{15}$ ions/cm^2at Horizontal plane*

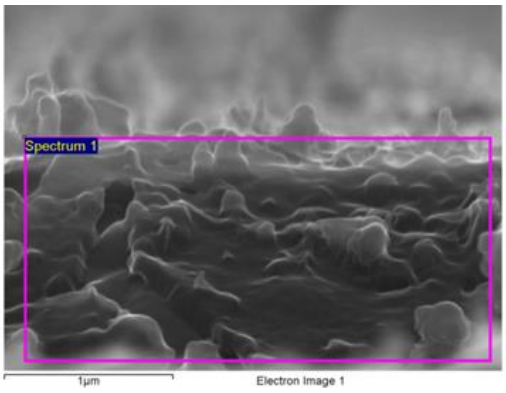

Fig. 3.18(a): Cross sectional FESEM 1 of implantation at a dose $5*10^{15}$ ions/cm^2

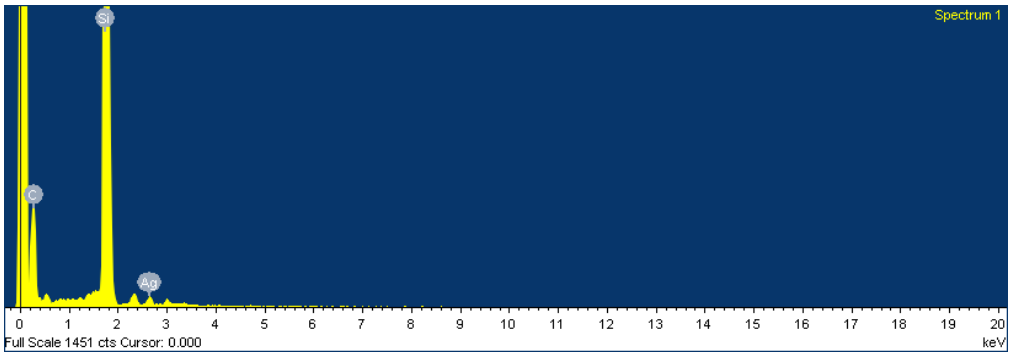

Fig. 3.18(b): EDAX Spectrum-1 of dose $5*10^{15}$ ions/cm^2

Spectrum processing:

No peaks omitted

Processing option: All elements analyzed (Normalized)

Number of iterations = 5

Standard:

C $CaCO_3$ 1-Jun-1999 12:00 AM

Si SiO_2 1-Jun-1999 12:00 AM

Ag Ag 1-Jun-1999 12:00 AM

Element	App Conc.	Intensity Corrn.	Weight %	Weight % Sigma	Atomic %
C K	9.07	0.2737	61.23	1.38	78.94
Si K	22.45	1.0933	37.99	1.35	20.94
Ag L	0.31	0.7273	0.78	0.20	0.11
Totals			100.00		

Table 3.3: FESEM Spectrum analysis table for dose $5*10^{15}$ ions/cm^2

Spectrum taken at a different tilted angle:

Sample 3 b:*Ag implanted at a dose of 5*10^{15} ions/cm^{2}at tilted plane*

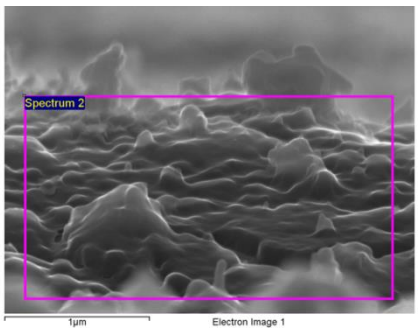

Fig. 3.19(a): Cross sectional FESEM 2 of implantation at a dose 5*10^{15} ions/cm^2

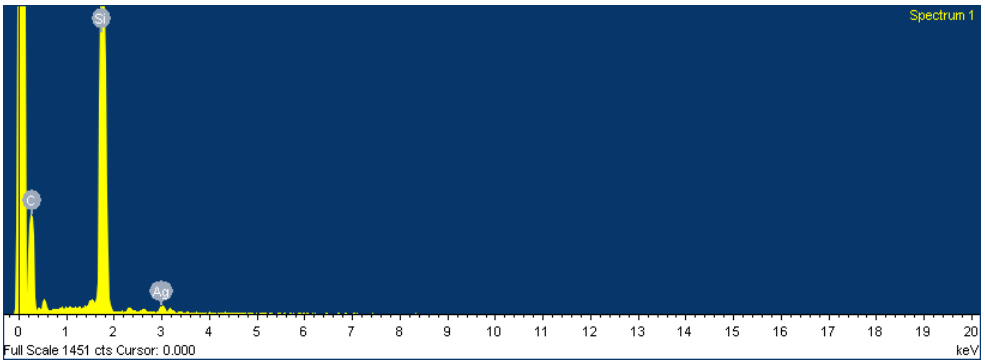

Fig. 3.19(b): EDAX Spectrum-2 of dose 5*10^{15} ions/cm^2

Spectrum processing:

No peaks omitted

Processing option: All elements analyzed (Normalized)

Number of iterations = 6

Standard:

C $CaCO_3$ 1-Jun-1999 12:00 AM

Si SiO_2 1-Jun-1999 12:00 AM

Ag Ag 1-Jun-1999 12:00 AM

Element	App Conc.	Intensity Corrn.	Weight %	Weight % Sigma	Atomic %
C K	10.25	0.2903	63.74	1.33	80.61
Si K	21.54	1.0888	35.71	1.31	19.31
Ag L	0.22	0.7320	0.55	0.19	0.08
Totals			100.00		

Table 3.4: FESEM Spectrum analysis table for dose $5*10^{15}$ ions/cm^2 at tilted angle

Sample 4: *Ag implantation at a dose of 10^{16}*

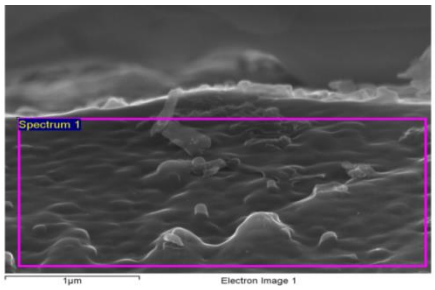

Fig. 3.20(a): Cross sectional FESEM 1 of implantation at a dose 10^{16} ions/cm^2

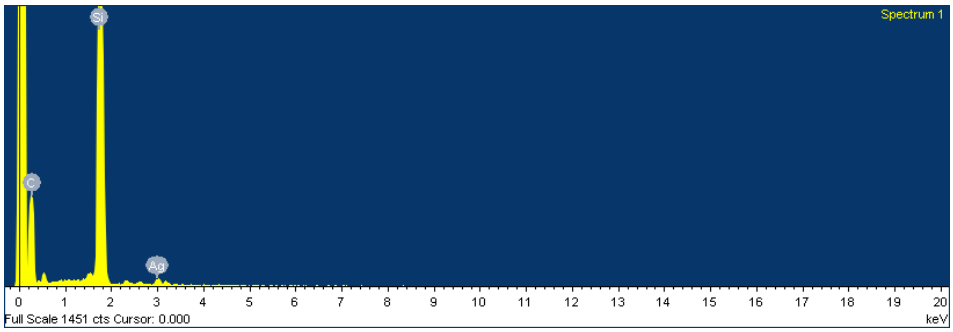

Fig. 3.20(b): EDAX Spectrum-1 of dose 10^{16}ions/cm^2

Spectrum processing:

Peak possibly omitted: 2.309 keV

Processing option: All elements analyzed (Normalized)

Number of iterations = 6

Standard:

C $CaCO_3$ 1-Jun-1999 12:00 AM

Si SiO_2 1-Jun-1999 12:00 AM

Ag Ag 1-Jun-1999 12:00 AM

Element	App Conc.	Intensity Corrn.	Weight %	Weight % Sigma	Atomic %
C K	9.96	0.3166	65.62	1.25	82.20
Si K	16.98	1.0787	32.83	1.19	17.59
Ag L	0.55	0.7402	1.56	0.25	0.22
Totals			100.00		

Table 3.5 FESEM Spectrum analysis table for dose $1*10^{16}$ ions/cm^2 at tilted angle

Sample 5: *Ag implantation at a dose of $5*10^{16}$*

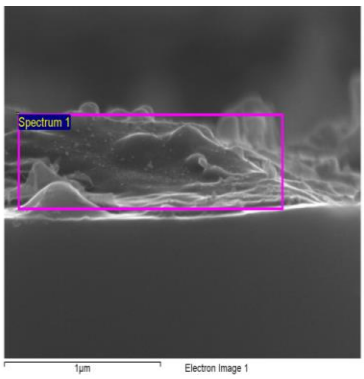

Fig. 3.21(a): Cross sectional FESEM 1 of implantation at a dose $5*10^{16}$ ions/cm^2

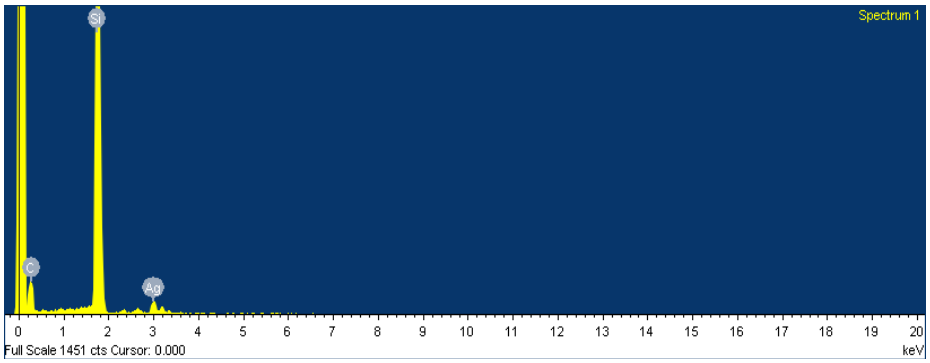

Fig. 3.21(b): EDAX Spectrum-1 of dose $5*10^{16}$ions/cm^2

Spectrum processing:

Peak possibly omitted: 2.300 keV

Processing option: All elements analyzed (Normalized)

Number of iterations = 4

Standard:

C $CaCO_3$ 1-Jun-1999 12:00 AM

Si SiO_2 1-Jun-1999 12:00 AM

Ag Ag 1-Jun-1999 12:00 AM

Element	App Conc.	Intensity Corrn.	Weight%	Weight% Sigma	Atomic%
C K	3.43	0.2531	53.31	2.19	74.11
Si K	11.77	1.0907	42.44	2.00	25.23
Ag L	0.78	0.7243	4.24	0.50	0.66
Totals			100.00		

Table 3.6: FESEM Spectrum analysis table for dose $5*10^{16}$ ions/cm^2

Spectrum taken at different tilted angle

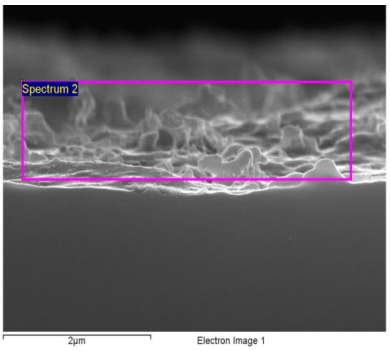

Fig. 3.22(a): Cross sectional FESEM 2 of implantation at a dose $5*10^{16}$ ions/cm^2

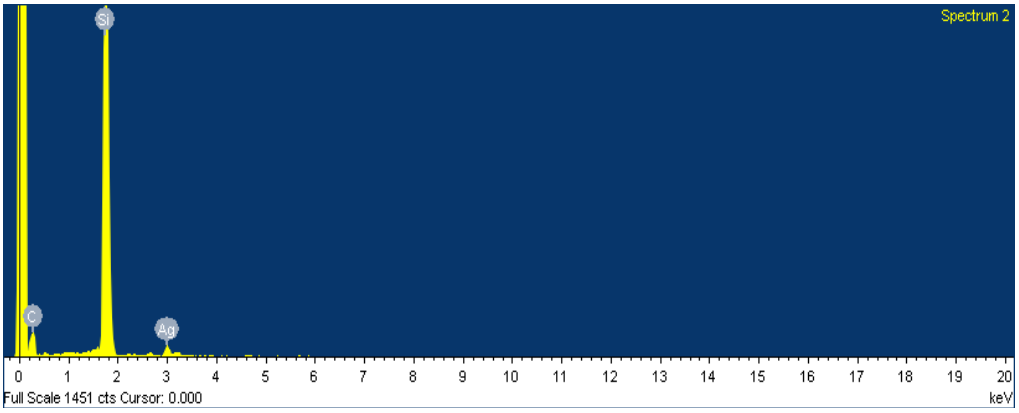

Fig. 3.22(b): EDAX Spectrum-2 of dose $5*10^{16}$ions/cm^2

Spectrum processing:

No peaks omitted

Processing option: All elements analyzed (Normalized)

Number of iterations = 6

Standard:

C $CaCO_3$ 1-Jun-1999 12:00 AM

Si SiO_2 1-Jun-1999 12:00 AM

Ag Ag 1-Jun-1999 12:00 AM

Element	App Conc.	Intensity Corrn.	Weight %	Weight % Sigma	Atomic %
C K	8.53	0.3209	64.58	1.06	81.91
Si K	14.42	1.0741	32.64	0.98	17.70
Ag L	0.85	0.7428	2.78	0.37	0.39
Totals			100.00		

Table 3.7: FESEM Spectrum analysis table for dose $5*10^{16}$ ions/cm^2 at a different tilted angle

Sample 7: ***Ag implantation at a dose of 10^{17}ions/cm^2***

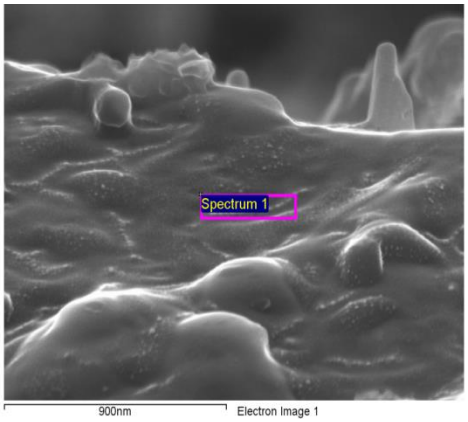

Fig. 3.23(a): Cross sectional FESEM 1 of implantation at a dose 10^{17} ions/cm^2

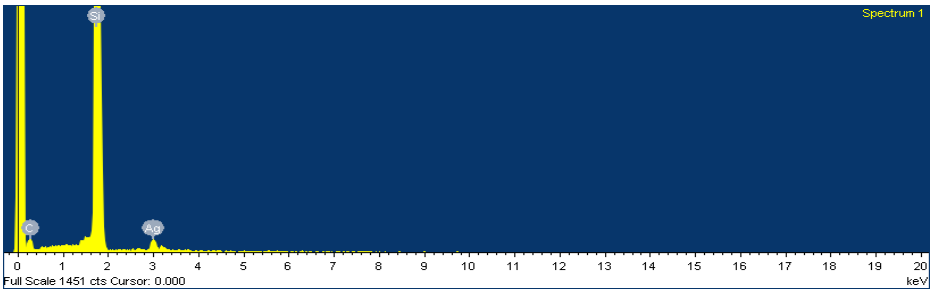

Fig. 3.23(b): EDAX Spectrum of dose 10^{17}ions/cm^2

Spectrum processing:

No peaks omitted

Processing option: All elements analyzed (Normalized)

Number of iterations = 3

Standard:

C $CaCO_3$ 1-Jun-1999 12:00 AM

Si SiO_2 1-Jun-1999 12:00 AM

Ag Ag 1-Jun-1999 12:00 AM

Element	App Conc.	Intensity Corrn.	Weight %	Weight % Sigma	Atomic %
C K	2.30	0.1694	31.20	2.71	52.47
Si K	32.32	1.1434	65.12	2.58	46.84
Ag L	1.08	0.6793	3.68	0.45	0.69
Totals			100.00		

Table 3.8: FESEM Spectrum analysis table for dose 10^{17} ions/cm^2 at a different tilted angle

Spectrum taken at different tilted angle:

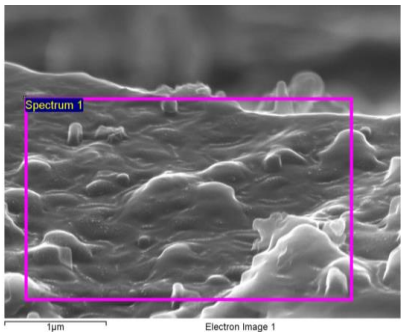

Fig. 3.24(a): Cross sectional FESEM 2 of implantation at a dose 10^{17} ions/cm^2

EDAX Spectrum of the Sample:

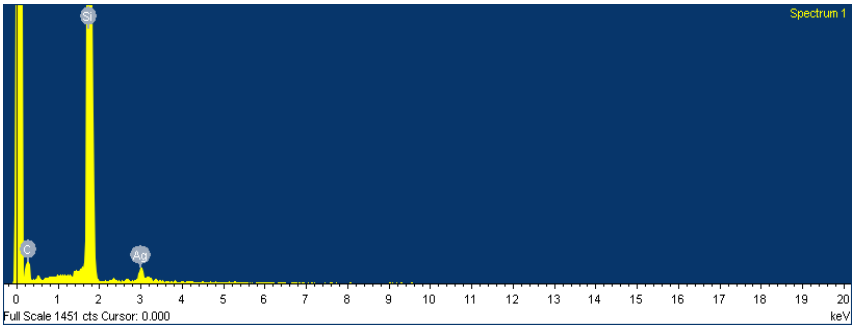

Fig. 3.24(b): EDAX Spectrum 2 of dose 10^{17}ions/cm^2

Spectrum processing:

No peaks omitted

Processing option: All elements analyzed (Normalized)

Number of iterations = 3

Standard:

C $CaCO_3$ 1-Jun-1999 12:00 AM

Si SiO_2 1-Jun-1999 12:00 AM

Ag Ag 1-Jun-1999 12:00 AM

Element	App Conc.	Intensity Corrn.	Weight %	Weight % Sigma	Atomic %
C K	2.92	0.1872	38.45	2.47	60.35
Si K	26.61	1.1292	58.19	2.34	39.06
Ag L	0.94	0.6914	3.36	0.43	0.59
Totals			100.00		

Table 3.9:FESEM Spectrum analysis table for dose 10^{17} ions/cm^2

Now we have taken some more Cross-sectional FESEM images for observation purposes only, whose details strengthens previous deductions. They are given as follows:

Unimplanted Sample

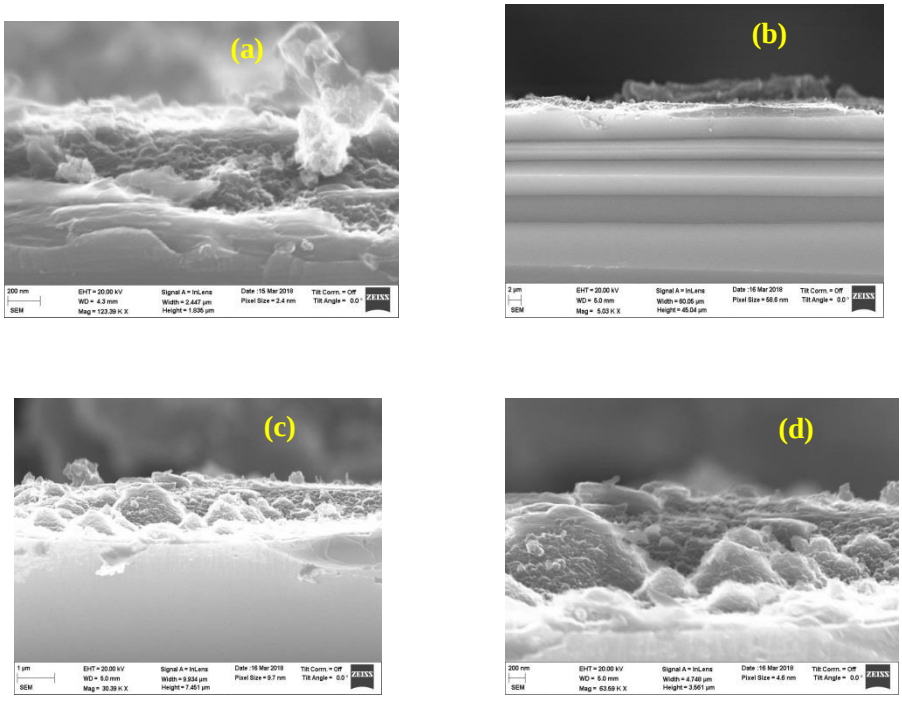

Fig. 3. 25(a), 3.25(b), 3.25(c), 3.25(d) Cross-sectional FESEM of unimplanted samples

Ag implantation at a dose of 1*10^{15}ions/cm^{2}

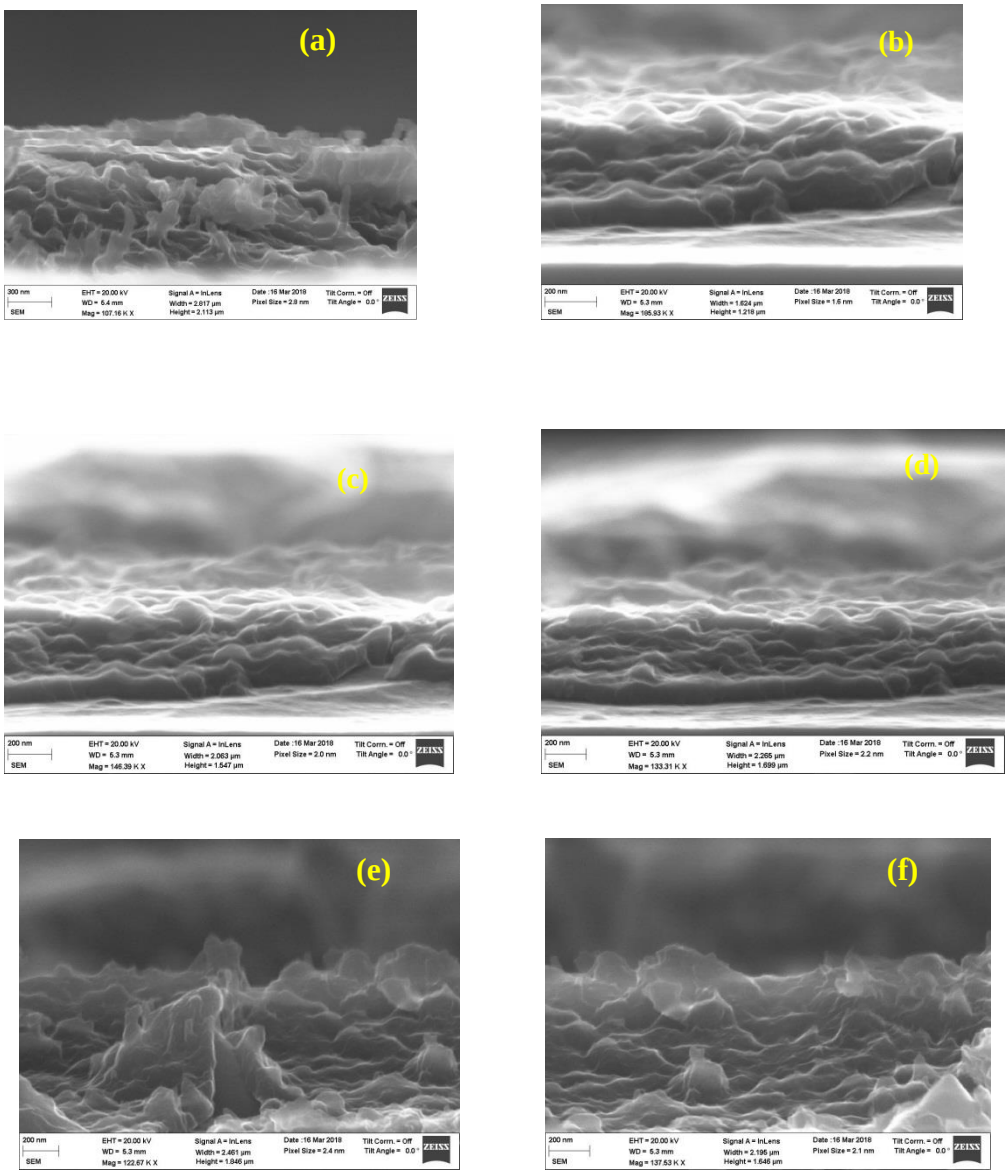

Fig. 3.26(a),3.26(b), 3.26(c), 3.26(d), 3.26(e), 3.26(f) Cross-sectional FESEM of implantation at a dose of 1*10^{15} ions/cm^{2} at different angles

Ag implantation at a dose of 5*10^{15}

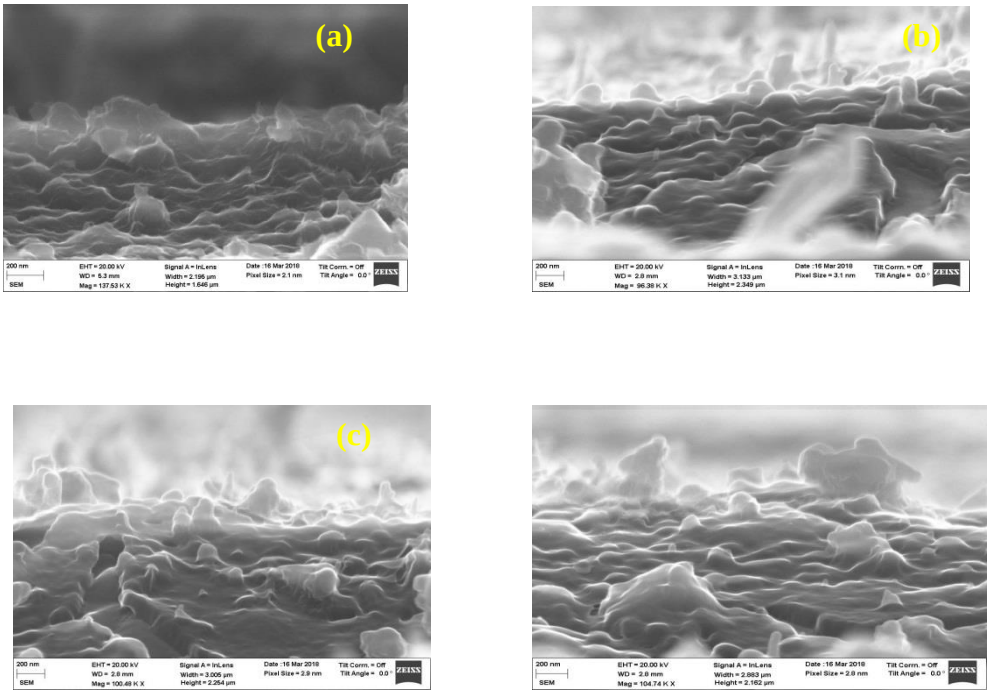

Fig. 3.27(a), 3.27(b), 3.27(c), 3.27(d) Cross-sectional FESEM of implantation at a dose of 5*10^{15} ions/cm^2

Ag implantation at a dose of 10^{16} ions/cm^2

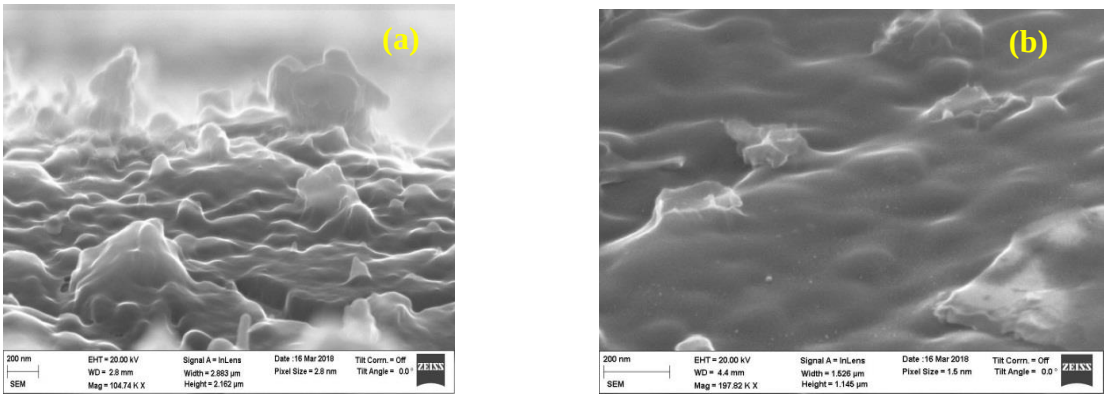

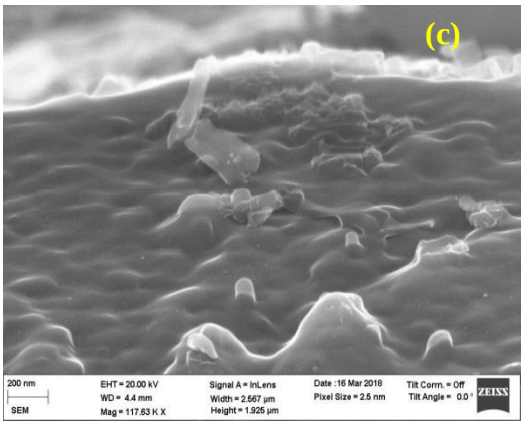

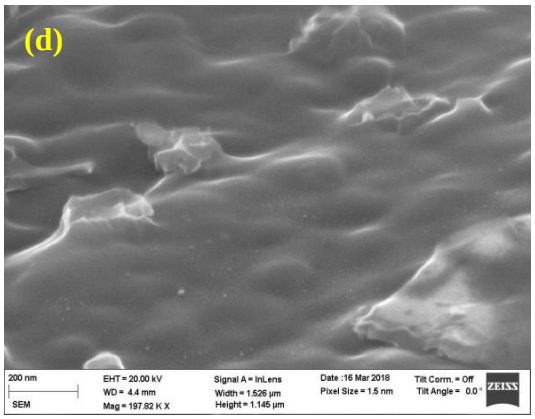

Fig. 3.27(a), 3.27(b), 3.27(c), 3.27(d) Cross-sectional FESEM of implantation at a dose of $5*10^{15}$ ions/cm^2

Ag implantation at a dose of 10^{16} ions/cm^2

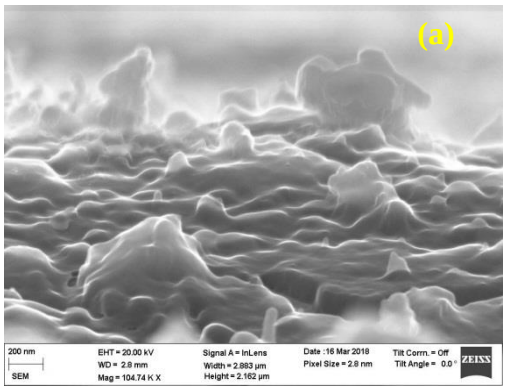

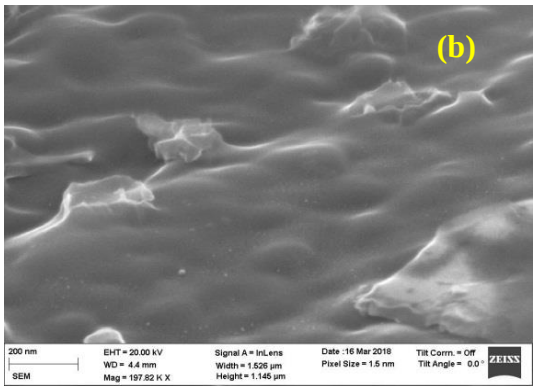

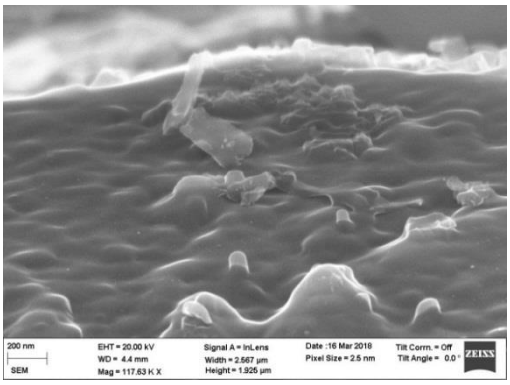

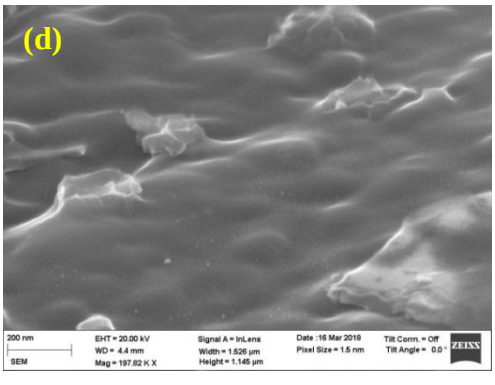

Fig. 3.28(a), 3.28(b), 3.28(c), 3.28(d) Cross-sectional FESEM of implantation at a dose of $1*10^{16}$ ions/cm^2

Ag implantation at a dose of 5*10^{16} ions/cm^2

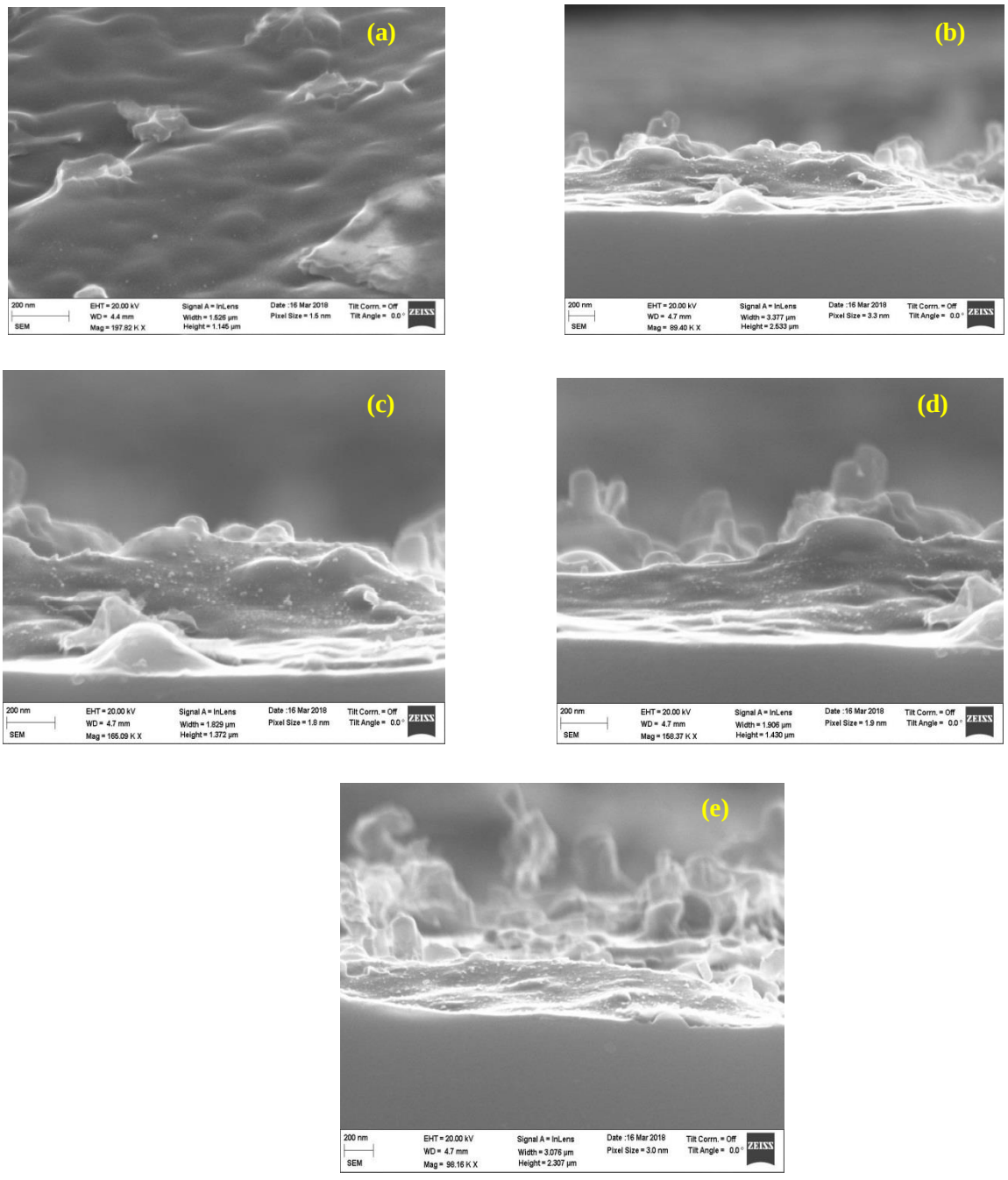

Fig. 3.29(a), 3.29(b), 3.29(c), 3.29(d), 3.29(e) Cross-sectional FESEM implantation at a dose of 5*10^{16} ions/cm^2 at different

3.6.1 Discussions on the FESEM images and EDAX spectra

❖ It is evident from the above images and spectra from [Figures 3.15 - 3.29]that Silver inclusions were observed in the polyaniline matrix due to ion implantation and they are trapped into the pores and defects formed due to the process of polymerization and ion bombardments respectively.

❖ More importantly, close observations revealed, at lower doses the probabilility formation of nanoparticle was very less. So nothing could be observed from at the lower doses or very few metal trapped sites could be observed compared to the overall volume.

❖ At higher doses formation of metal clusters is evident. To know the exact size of the metal clusters cross-sectional TEM analysis is needed, but due to inavailability of the facility and required arrangements, it could not be carried out.

❖ Some images above were taken at tilted angles, to enhance the observation, or to find more traps in other directions.

❖ The EDAX spectra above were taken for material analysis of the samples as found from the FESEM pictures and the same results are ploted in the corresponding tables .

❖ However, in thick films medium energy ion beam was implanted in the MeV energy range which is Focused Ion beam (FIB) unlike the Raster Scanning Beam discussed in previous chapter used for thin film implantaion.Here the impurities are scattered through out the volume of the matrix, rather than restricted to a particular area.

❖ Moreover, as the matrix becomes opaque here, UV-Vis study couldnot be performed, we rather opted for reflctance study in case of optical study and structural study.

3.7 PolyAniline-metal nanocomposite Synthesis by Chemical route of fabrication:

For our purpose we chose PANI- Gold nanocomposites by chemical route of synthesis in one pot method and the following points illustrates the previous research reports and findings:

- Although known for more than 150 years research trends [1][3], [13], [14] with PANI grew since 1980 after discovery of conductivity in conjugated polymers. Earlier times PolyAniline was known as ‘Aniline Black’ as people used to get PANI by oxidizing Aniline.

- Emeraldine PANI becomes conducting by doping acid; by controlling the pH of the dopant acid solution doping level can be tuned. The undoped insulating base has conductivity as low as $\sigma \leq 10^{-10}$ S/cmand fully doped conducting salt conductivty $\sigma \geq$ 1 S/cm.

- Nanostructured PANI offers new properties compared to bulk PANI.

- It is believed that PANI synthesized at different times keeping all the reation conditions same are of different chain structures.

- PANI is insoluble in water thus polymerization of PANI takes place by precipitating polymerized products. Formation of PANI initiated by nucleation i.e, by formation of small molecular agglomerates. Thus it can form on parent phase or any other surface.

- Traditional reactions provide PANI growth on earlier formed agglomerates leading to coral like structures.

- The reason for PANI being doped with different acids provides different conductivities is that different acids elongates differentlywith PANI. For example, PANI doped with hydrochloric acids have diameter about 30nm, those with camphor sulfonic acid produces nanofibers of diameters of 120nm and that with perchloric acid 150nm. Further, conductiviy becomes more when dissolved in *m*-Cresol. This is due to the reason that curled up chains straightened up which eases up electron conduction.

- Earlier reports show plenty of research works have been carried out done using gold, silver, copper, palladium, platinum, nickel to obtain metal-polymer nanocomposites.These metals are good at electrical conduction as well show surface plasmon resonance at visible range of spectra [15], [16],[17].

- Gold nanoparticles are useful for a wide range of applications like catalysis, photocatalysis, imaging, sensing, drug delivery, gene targeting etc.The nanocomposites exhibit both organic and inorganic behaviour.

- Interaction betweenTetra HydroChloric Acid ($AuClO_4H$) salt and highly sorption conducting polymer can create metal-polymer composite material[18], [19]. In the process conducting polymer acts as reducing agent to the chloroaurate salt , resulting in high amount of gold accumulation in the polymer matrix due to sorption property.

- But in these process the rate of reaction cannot be controlled acurately. In the sorption process of gold and PANI imino nitrogen plays a key factor in controlling the reaction. Actually, $AuCl_4^-$ gets reduced at the point of contact with Aniline rather than polymerizing the whole chain. For this reason monomer doesnot transfer into polymer but it creates oligomers.

- So conducting polymer loses its intrinsic conductivity. This process doesnot produce homogeneous mixture rather chemical and electrochemical route of fabrication require a subtle knowledge of chemistry.

There are mainly two ways of approach for obatining metal-polymer composite by chemical route of fabrication:

i. ***Chemical polymerization of PANI with pre-formed particles, and***

ii. ***One-pot synthesis approach where aniline monomer acts as reductant for metal ions.***

iii. ***There are another two-step approach to fabricate Au-PANI core-shell structutre(jie han).***

- In our lab, we primarily dissolved 20mg PANI in 10ml DMSO and then this solution in dispersed formed added to 100µl Au nanoparticles [20] and the solution is vortex. We found this strategy not satisfactory one as Au precipitates after sometimes.

- In another approach we have tried Au-PANI nanocomposite [21] by using the Lewis Acid ($HAuCl_4$) as an oxidative doping agent in two different acid media Sulfuric Acid (H_2SO_4) and p-Toluene Sulfonic Acid (pTSA). But this approach also could not meet our expectation.

Therefore, from practical view point, we found that although there are many reports on PANI-Au nanocomposites have been grown in laboratory, but they lack the conducting property of polyaniline as in most of the cases oligomers are produced instead of polymer. These oligomers are short chain formed by connecting few monomers and they are insulating in nature. Besides, desired concentration and depth of nanoparticle layer cannot be precisely controlled in this approach.

3.8 References:

[1] D. Li, J. Huang, and R. B. Kaner, "Polyaniline Nanofibers: A Unique Polymer Nanostructure for Versatile Applications," 2009, doi: 10.1021/ar800080n.

[2] A. G. Macdiarmid, J. C. Chiang, A. F. Richter, and A. J. Epstein, "Polyaniline: a new concept in conducting polymers," *Synth. Met.*, vol. 18, no. 1–3, pp. 285–290, Feb. 1987, doi: 10.1016/0379-6779(87)90893-9.

[3] E. M. Geniès, A. Boyle, M. Lapkowski, and C. Tsintavis, "Polyaniline: A historical survey," *Synth. Met.*, vol. 36, no. 2, pp. 139–182, Jun. 1990, doi: 10.1016/0379-6779(90)90050-U.

[4] L. Hu, G. Gruner, D. Li, R. B. Kaner, and J. Cech, "Patternable transparent carbon nanotube films for electrochromic devices," *J. Appl. Phys.*, vol. 101, no. 1, 2007, doi: 10.1063/1.2402330.

[5] E. Song and J. W. Choi, "Conducting polyaniline nanowire and its applications in chemiresistive sensing," *Nanomaterials*, vol. 3, no. 3, pp. 498–523, 2013, doi: 10.3390/nano3030498.

[6] R. J. Tseng *et al.*, "Charge transfer effect in the polyaniline-gold nanoparticle memory system," *Appl. Phys. Lett.*, vol. 90, no. 5, pp. 5–8, 2007, doi: 10.1063/1.2434167.

[7] J. Huang and R. B. Kaner, "A General Chemical Route to Polyaniline Nanofibers," *J. Am. Chem. Soc.*, vol. 126, no. 3, pp. 851–855, 2004, doi: 10.1021/ja0371754.

[8] H. Noby, A. H. El-Shazly, M. F. Elkady, and M. Ohshima, "Novel preparation of self-assembled HCl-doped polyaniline nanotubes using compressed CO2-assisted polymerization," *Polymer (Guildf).*, vol. 156, pp. 71–75, Nov. 2018, doi: 10.1016/J.POLYMER.2018.09.060.

[9] P. Kong *et al.*, "Conjugated HCl-doped polyaniline for photocatalytic oxidative coupling of amines under visible light," *Catal. Sci. Technol.*, vol. 9, no. 3, pp. 753–761, 2019, doi: 10.1039/c8cy02280a.

[10] Sewench N. Rafeeq & wasan Z.Khalaf, "Preparation, characterization and electrical conductivity of doped polyaniline with (HCL and P - TSA)," *Eng. Tech. J.*, vol. 33, no. 7, pp. 1220–1231, 2015.

[11] V. N. Popok *et al.*, "Radiation-induced change of polyimide properties under high-fluence and high ion current density implantation," *Appl. Phys. A Mater. Sci. Process.*, vol. 78, no. 7, pp. 1067–1072, 2004, doi: 10.1007/s00339-003-2166-9.

[12] V. N. Popok, "Ion implantation of polymers: Formation of nanoparticulate materials," *Rev. Adv. Mater. Sci.*, vol. 30, no. 1, pp. 1–26, 2012.

[13] H. Derivatives, J. Louis, and A. G. Macdiarmid, "Synthesis of Electrically Conducting Organic Polymers," *Polymer (Guildf).*, vol. 36, no. 578, pp. 578–580, 1977, doi: 10.1039/C39770000578.

[14] C. Prasanna, “Basics of Conducting Polymers (CP),” in *Basics of Conducting Polymers (CP)*, SpringerLink, 1999, p. 20.

[15] P. Mondal, C. Guo, and J. L. Yarger, “Water soluble gold-polyaniline nanocomposite: A substrate for surface enhanced Raman scattering and catalyst for dye degradation,” *Arab. J. Chem.*, vol. 13, no. 2, pp. 4009–4018, Feb. 2020, doi: 10.1016/j.arabjc.2019.05.004.

[16] B. U, P. I, M. G. Ć, Mitrić M, Scott P. Ahrenkiel, and Vodnik V, “No Title,” *ACS Appl. Mater. Interfaces*, vol. 7 (51), p. 28393, 2015.

[17] N. V. Blinova, J. Stejskal, M. Trchová, I. Sapurina, and G. Ćirić-Marjanović, “The oxidation of aniline with silver nitrate to polyaniline-silver composites,” *Polymer (Guildf).*, vol. 50, no. 1, pp. 50–56, 2009, doi: 10.1016/j.polymer.2008.10.040.

[18] J. M. Kinyanjui, D. W. Hatchett, J. A. Smith, and M. Josowicz, “Chemical Synthesis of a Polyaniline/Gold Composite Using Tetrachloroaurate,” 2004, doi: 10.1021/cm049478i.

[19] V. Sridevi and S. Malathi, “Synthesis and Characterization of Polyaniline/Gold Nanocomposites,” *Chem. Sci. J.*, vol. 2, no. January 2011, 2011, doi: 10.4172/2150-3494.1000018.

[20] H. J. Kim *et al.*, “Fabrication of Nanocomposites Complexed with Gold Nanoparticles on Polyaniline and Application to Their Nerve Regeneration,” *Cite This ACS Appl. Mater. Interfaces*, vol. 12, p. 30760, 2020, doi: 10.1021/acsami.0c05286.

[21] S. Mahalakshmi and V. Sridevi, “Conducting, crystalline and electroactive polyaniline-Au nanocomposites through combined acid and oxidative doping pathways for biosensing applications: Detection of dopamine,” *Mater. Chem. Phys.*, vol. 235, Sep. 2019, doi: 10.1016/j.matchemphys.2019.121728.

Chapter 4

Preparation of Cu-Poly Aniline nanocomposite by Mechano-synthesis route (Ball-Milling) and checking frequency and temperature dependent electrical conductivity and dielectric relaxation

4.1 Introduction:

In earlier chapters we described preparation of metal-polymer nanocomposites by the method of ion implantation and chemical route of fabrication respectively. In the former case conducting polymer films have been prepared and then, metal ion beam was implanted into it to obtain the composite. In the later case by means of chemical oxidation reduction method both polmerization of aniline monomer and preicipitation of metal from metal salt into the polymer took place simultaneously.

In this chapter and next chapter we present the mechano-route of fabrication of polymer-metal nanocomposite by using planetary ball-milling system.

Preemphasis of the work:

Polymers are generally known as insulators, but in last two decades a huge attention has grown to synthesize and fabricate conducting polymer composites, metal-polymer systems etc.

- ✓ To exhibit high electrical conductivity polymers should have linear backbone and alternate single and double bonds and large concentration of conjugated π-electrons [1], [2].

- ✓ Among various polymers (polypyrrole, polythiophene, polyacetelene) poly-Aniline has emerged as a popular one because of its unique electro-chemical and optical properties and aspects like light weight, cost-effective, easy to synthesize etc.

- ✓ It is also environmentally stable and due to alignment of chains mobility of charge carriers are very high; it has strong absorption coefficient in the visible part of the spectrum.

- ✓ Its optical and electrical properties change withnature and amount of doping. Depending on the oxidation states, PANI has three different forms, leucoemeraldine PANI, emeraldine PANI and pernigraniline. Its conducting form is known as emeraldine PANI; the name suggests the colour of PANI in this form.

- ✓ PANI has the potential to replace its inorganic counterparts in semiconductor applications like, automotive dash play displays, light emitting diodes (LEDs), solar cells, sensors, lightweight batteries, polymer actuators, corrosion protection agents, molecular devices etc.[3], [4].

- ✓ Among various oxidation states of PANI, emeraldine salt state exhibits higher conductivity (100 $Ohm^{-1}cm^{-1}$) compared to other traditional polymers ($<10^{-9}$ $Ohm^{-1}cm^{-1}$) but lower than that of the metals ($>10^{4}$ $Ohm^{-1}cm^{-1}$).

- ✓ The lone pair electrons in Nitrogen atom make it suitable to be attached with various kinds of dopants. The conductivity of PANI can be tuned by using different synthesis route (chemical, physical, electrochemical etc.).

- ✓ Conducting polymers find their applications in various fields like sensors, capacitors, transistors, thermo-electric devices, data storage devices, bio-medical applications like neural nerve recordings, stimulation of nerve generation etc.

- ✓ Charge conduction in conducting polymers happen due to presence of solitons, polarons and bi-polarons which form during polymerization or doping. As conducting polymers have a strong sigma bond at single bond position and one conjugated π bond at double bond positionalong its backbone, by introducing a dopantion can help in neutralizing the unstable backbone and hence carry the charge. Thus potentials across conducting polymer films depend strongly on dopant charge and mobility.

- ✓ Metal nanoparticles exhibit distinguishable optical and electrical properties than their bulk counterparts. Not every nanoparticle can sustain in every environment. Inclusion of metal nanoparticles into polymer matrix can change their opto-electrical properties severely [5], [6],[7], [8] and make them more efficient for applications.

- ✓ Poly-Aniline has the strong ability of binding with metal ions due to presence of secondary and tertiary amines in the backbone structure.

- ✓ The incorporation of various metal nanoparticles which can sustain in the polymer matrix like, Ni, Co, Fe, Cu, Au, Ag, etc. with conjugated PANI shows enormous change in electrical conductivity, thus we can tailor the electrical property by incorporating metal clusters [9], [10],[11], [12],[13], [14].

- ✓ On the other hand, metals included in matrix can act as centres for phonon scatterings thus further reduce thermal conductivity through the material. But the most significant

challenge lies in finding a suitable solvent for PANI which does not oxidize metal nanoparticles Ni, Cu, Ag etc. For this reasons applications are limited to Au, Pt like costly noble materials.

To fabricate PANI- metal nanocomposites having exotic properties, metal and metal-oxides have been incorporated into conducting PANI [7], [8]. The optical, electrical and dielectric properties of PANI vary significantly with the percentage of metal incorporation into PANI as well as shape and size of the metal particles. Actually the doped or incorporated metal clusters could act as conducting junction between the PANI chains leading a drastic increase of the electrical conductivity of the nanocomposites .

About this work:

In this work we report Cu incorporated PANI prepared by mechanical alloying method with HCl doped PANI in a typical Ball-Milling system. We reconnoitre the probabilityof enhancing the electrical conductivity of PANI by incorporating Cu small clusters, as copper is a good conductor like Ag, Au; and on the other hand, it is cost effective also. This method is our preferred method, as it provides overall homogeneous mixture using only composite materials and it is also much less expensive than plasma vapour or ion beam implantation method. The frequency and temperature dependent electrical conductivity as well as the dielectric properties of such Cu incorporated PANI have been extensively investigated.

4.2 **Experimental Details:**

4.2.1. Synthesis of Cu incorporated Polyaniline (PANI) nanocomposites

Materials used:

Aniline, HCl, Ammonium per Sulfate [(APS) [$(NH_4)_2S_2O_8$], readily available Cu powder (particle size 0.4-0.5 µm) were purchased from Merck. All reagents used in our experiment were of analytical reagent grade.

Procedure:

HCl doped PANI was synthesized by standard in-situ polymerization and the process is briefly described as follows:

i. 2ml of aniline monomer and 40ml (1M) HCl were added together and mixed under continuous stirring at low temperature bath (0-5^0 C).

ii. 2.4gm APS dissolved in 40ml HCl (1M) was added drop wise and polymerization was conducted at 0-5^0 C under stirring for 12 h.

iii. A deep green precipitate was obtained after the completion of polymerization. The precipitate was washed by deionized water and acetone consecutively until the pH value reached to 7 to remove the untreated acid and oligomers.

iv. Then the resultant was dried in vacuum at 60^0 C to get dry powder of HCl doped PANI. Incorporation of Cu nanoparticles in PANI were done using mechano-synthesis route.

The method of Ball-Milling:

1) Cu nanoparticles and PANI were mixed in desired percentages (10%) and ball-milled in planetary ball mill at 500rpm in steel-chrome milling jar filled with steel chrome balls. Sample to ball ratio was 1:40.

2) Anhydrous isopropyl alcohol was added as milling medium to improve homogeneity in the mixture during milling time.

3) Ball milling was done for 12 hours with 50% rest time giving total 6 hours of milling. This method provided enough time to dissipate the generated heat so that the jar temperature never went above 50^0 C.

4) After completion of milling, the products were collected in colloidal form and slowly dried at 50^0 C to get fine powder of Cu-PANI nanocomposites.

4.2.2 Characterizations

1. The optical absorbance spectra were recorded using Optizen pop spectrophotometer over the spectrum range of 400-850 nm at room temperature.

2. Then samples were prepared for FTIR measurements. The samples were compressed to form pellets (1.0 mm thick and 8.0 mm diameter). The pressure of the hydraulic press was kept at 10 tons/ $inch^2$. The FTIR spectra, (4000 - 400 cm^{-1}) of these samples with KBr pellets were obtained using RX1 Perkin Elmer FTIR spectrometer.

3. In another set of measurement the pellets were kept between two circular copper electrodes and temperature dependent dielectric measurements were carried out. The

frequency varied from 10Hz to 10MHz and temperature varied from193K to 333K using LCR meter model Hioki IM3536.

4.3. Result and discussions

4.3.1 UV-Vis study

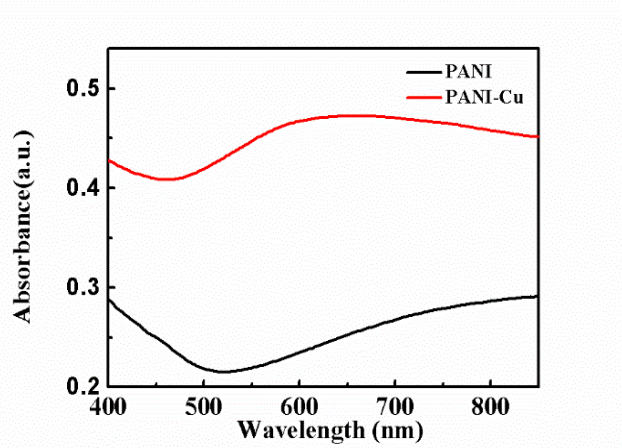

Fig. 4.1: UV-Vis spectra of PANI and Cu-PANI nanocomposite

Possible explanations for optical study:

Fig. 4.1 shows the UV-Vis spectra of PANI and Cu-PANI composites. We have analysed for the characteristic region between 400-850nm. Pristine PANI shows very small peaks around 430nm and a broad hump near 800nm which are due to Π-band – polaron band transition and again polaron band-Π* band transitions respectively [5], [6]. Moreover, both the curves depict the amorphous nature of the composites. There is broad surface plasmon absorption peak in Cu-PANI composite which may be due to the distribution of particle size and overlap of the characteristic regions of PANI and Copper nanoparticles [17], [18], [19]. Careful observation shows presence of absorption peak at 560nm which is the surface plasmon characteristics of Cu nanoparticles.

4.3.2 FTIR analysis:

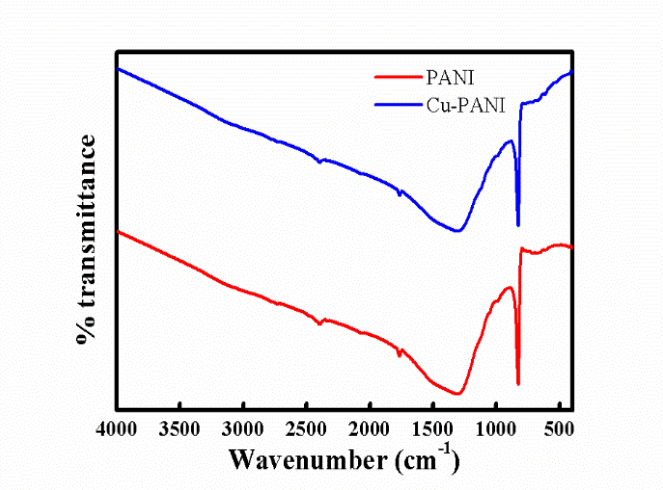

Fig. 4.2: FTIR spectra of PANI and Cu-PANI nanocomposite

Fig. 4.2 represents the FTIR spectra of PANI and Cu-PANI nanocomposite.

- A small peak at 509 cm^{-1} is present in both PANI and Cu-PANI, which are due to the periodic vibration of amine.
- The strong peak at 825 $cm^{-1}$was due to the in-plane and out-of-plane C–H bending modes.
- A peak at 1561 cm^{-1} corresponds to the stretching vibration of N-Q-N bond.
- In Cu-PANI all these characteristic peaks of PANI are present with slight deviation from their actual position.
- The peak at 996 cm^{-1} in Cu-PANI nanocomposite might be due to the presence of copper[5], [6], [20], [21].
- As observed from the spectra, there is no significant change in the structure of PANI because of Ball-Milling.
- A minute shift may be due to the incorporation of Cu without any bond formation with the PANI-chain in the latter case.

4.3.3 Dielectric studies

To check whether our composite material is suitable for high frequency applications, we need to perform dielectric measurements. The dielectric properties reveal a material's electric and magnetic energy storage and dissipating capacity and nature, thus very important for optical and electronic studies. The complex dielectric permittivity, Ɛ*, of a material is given by Eq. (1) [22], [23] as follows:

$$\text{Ɛ}^*(f) = \text{Ɛ}'(f) - j\,\text{Ɛ}''(f) \quad (1)$$

Where, Ɛ′(f) and Ɛ″(f) are the real and imaginary parts of complex dielectric constant respectively. Here, Ɛ′(f) is the amount of electrical potential energy storedand Ɛ″(f) is the amount of energy dissipated due to polarization. These two factors again can be obtained by using the following equations (2, 3)

$$\text{Ɛ}'(f) = \frac{C_p d}{\varepsilon_0 A} \quad (2)$$

$$\text{Ɛ}''(f) = \text{Ɛ}'(f) \tan\delta \quad (3)$$

Here,C_p is the capacitance of the pellet, $\mathcal{E}_0$ (8.85 x 10^{-14} F/cm) is the dielectric permittivity in vacuum, A is the effective surface area of the pellet and d is the thickness of the pellet.

- The frequency dependence Ɛ′(f) for Cu incorporated PANI pattern (Fig. 3(a)) depicts that Ɛ′(f) decrease gradually with increasing frequency as contribution from polarization effects diminish.

- At low frequency, it has been observed that Ɛ′(f) is increased with increasing temperature.

- The increase of Ɛ′(f) of the Cu incorporated PANI composite compared to pure PANI may be due to the incorporation of metal ions within PANI matrix which may be due to increase in conductivity and higher polarizability of Cu ions.

- Cu ions enhances *space charge polarization* which in turn enhances Ɛ′(f).

- At low frequency region *ionic polarization* prevails which was reflected in the small change in Ɛ′(f) with increasing in temperatures [22], [24], [25], [26].

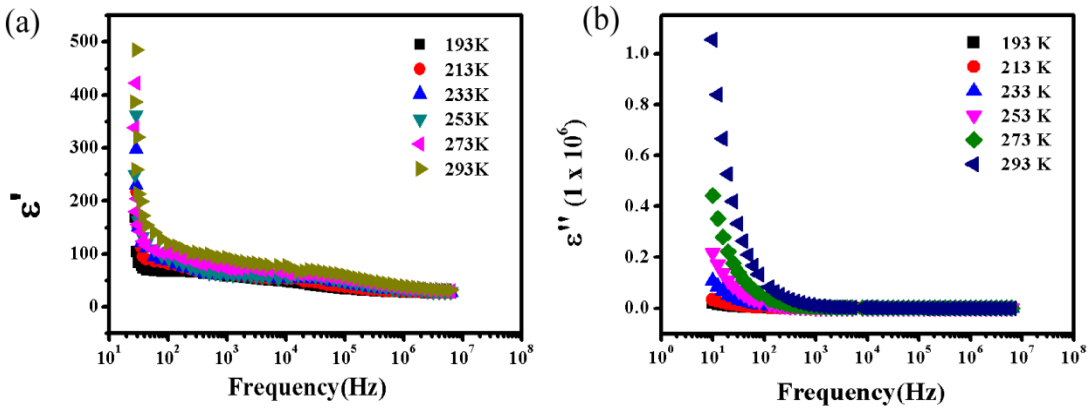

Fig. 4.3(a) ε ′ vs Frequency of Cu incorporated PANI composites, Fig. 4.3(b) ε″ vs Frequency of Cu incorporated PANI composites

- In Fig. 4.3(b), it was observed for all the samples that ε″(f) were decreasing with increasing frequency at all temperatures.

- It was also been observed that at low frequency region, ε″(f) increases faster with temperature.
- This may be the effects of disorder in polymer chain occurred due to metal nanoparticles incorporation and effects of boundary conditions.

- The metal nanoparticles put a break in long chains of PANI in case of Ball-Mill method, thus space charges got limited within short polymer chain.

- The dieletric loss factor was higher at low frequency region becauce of polarizations. On the other hand it was much less at higher frequency due to diminishing effects of ionic and orientational polarizations.

- This effected in decrease of ε″(f) with increase in frequency for all temperature [22], [23], [24].

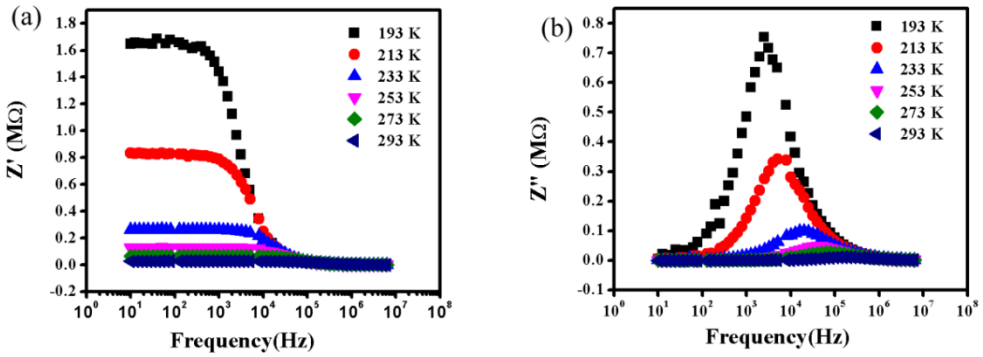

Fig. 4.4(a) Variation of real part of Z (Z ′) with frequency and Fig. 4.4(b) variation of imaginary part of Z (Z″) with imaginary part of frequency of Cu incorporated PANI

4.4 *Complex impedance study*

- The study of complex impedance property of Cu-PANI nanocomposite have been carried out in a frequency range of (10 Hz – 10 MHz) by varying the temperature in the range (193 K – 293 K) using complex impedance spectroscopy (CIS).

- The CIS technique is a very useful method to observe the ionic movements of the ions and also gives insight into capacitive and resistive behavior of the material.

- The variation of temperature dependent real part of impedance Z′(f) as a function of frequency for Cu-PANI nanocomposite is shown in Fig. 4.5

- The nature of variation of Z′(f) with frequency followed a sigmoidal type variation for Z′(f) with increase in frequency.

- It has been also observed that the value of Z′(f) decreases with increasing frequency and temperature which may be because of the increase in ac conductivity which follows the Negative Temperature Coefficient of Resistance (NTCR) property of the semiconductor.

- Greater values of Z′(f) at lower frequency indicates large polarization in the composite materialand at higher frequency, value of Z′ decreases which implies the inter- chain transport and disorder in polymer chain contribute to the total resistance which leads to increase in ac conductivity with increasing frequency and temperatures.

- The curves plotted at different temperatures reveal that the magnitude of total impedance (|Z*|) is strongly dependent on temperature.

- Z″(f) curves show distinct relaxation peaks for each set of temperature. The gradual rise in relaxation peak with temperature reveals relaxation behaviour of the composite material.

- The relaxation peaks appear when hopping frequency of the localized electrons closely matches with that of external applied field. This implies the presence of immobile ions at lower temperatures and disordered chains at higher temperatures.

- From Fig. 4.4(b) we can also observe that shifting and broadening of relaxation peaks towards higher frequency region at higher temperatures, which is mainly due to temperature depended electrical relaxation property of the composite. The peak frequency (ω_m) increases with increase in temperature and follows the Arrhenius law (Eq. 4),

$$\omega_m = \omega_0 \exp(-E_a/K_BT) \qquad (4)$$

Where ω_0 is the pre-exponential factor and E_a is the activation energy. We have calculated the activation energy from Fig. 4(b) (Eq. 4) and the value is E_a = 0.223 eV [22], [23], [27], [30].

- The frequency dependence of imaginary part of impedance, Z″(f) vs real part of impedance, Z'(f) at different temperatures of the samples are shown in Fig. 5 in the form of Cole-Cole plots.

- In a polymer composite material, disorder in chain and inter-chain transport – all have individual contributions to the total impedance [22], [24], [27].

- In the Cole-Cole plot the semicircles for higher frequency regions and lower frequency regions each have different interpretations for analysing complex impedances.

- Semi-circles in the higher frequency regions represent contribution of a polymer chain and that of lower frequency regions for chain-boundary contributions.

- In our case, we cannot quantitatively distinguish contributions from a polymer chain to chain-boundaries as curves are closely over lapped.

- A single depressed semi-circle in Fig 5 is a resultant of contributions from chains and chain-boundaries and contributions from chain-boundary resistance is more.

- The contributions from each of the aspect can be estimated by using Maxwell-Wagner equivalent circuit model.

- The equivalent circuit is a parallel combination of various Resistors (R) and capacitors (C). The overall frequency dependence impedance (Z*) is given by solving the below mentioned Eq. (5) [22]

$$Z^*(f) = Z'(f) + j\,Z''(f) \qquad (5)$$

Where, the frequency dependence real part of impedance $Z'(f)$ and imaginary part of impedance $Z''(f)$ can be expressed in Eq. (6, 7)

$$\mathbf{Z'(\omega) = \frac{Rc}{[1+(\omega RcCc)^2]} + \frac{Rcb}{[1+(\omega RcCc)^2]}} \qquad \mathbf{(6)}$$

$$\mathbf{Z''(\omega) = \frac{\omega CcR^2c}{[1+(\omega RcCc)^2]} + \frac{\omega CcbR^2cb}{[1+(\omega RcbCcb)^2]}} \qquad \mathbf{(7)}$$

Where, $\omega = 2\pi f$, R_c = chain resistance, C_c = chain capacitance, R_{cb} = chain boundary resistance and C_{cb} = chain boundary capacitance [24].

- As observed, from the Cole-Cole plot the diameters of the semicircles are gradually decreasing with increasing temperatures.

- The intersections of the curves with the real axis i.e., Z'-axis lower in value with the increase in temperature. This implies increase in dc conduction with the increase in temperature which in turn confirms temperature dependent semiconductor nature of the composite.

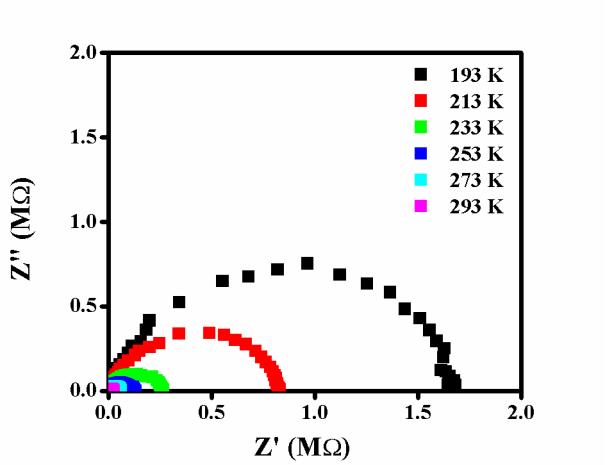

Fig. 4.5 Cole-Cole plots of Cu incorporated PANI composites

4.5 AC conductivity Study

To explain the effect of Cu nanoparticles on the electrical conductivity of PANI composites, the electrical conductivity measurement has also been done. Following are the observations:

- Fig. 4.6 reveals the variation of ac conductivity for Cu incorporated PANI nanocomposites.

The increase in ac-conductivity of the composite can be explained as the result of well dispersed Cu nanoparticles within the PANI matrix.

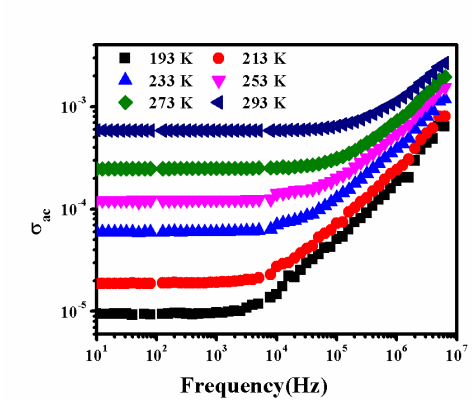

Fig. 4.6 Variation of ac conductivity with frequency of Cu incorporated PANI composites

- The metal nanoparticles may act as bridging elements for charge conduction and offer better inter-chain overlaps between PANI chains.

- The conductivity plot showed increase in conductivity with the frequency for the composite material. A sharp increase also observed beyond 10 KHz.

- As the ac conductivity of any material is dependent mainly on two factors, ----1) interface charge polarization and 2) intrinscic dipole polarization. Thus, in this type of metal-polymer composite mobile charges accumulate at the interface and they form large dipoles near the cluster interface.

- This large amount of metal clusters creates polarization and in turn affects ac conduction [23], [24], [25], [31], [32].

4.6 Conclusion

- ❖ We have successfully synthesized the metal incorporated polyaniline (PANI) nanocomposites by chemical oxidative method.

- ❖ The formation of nanocomposites and the incorporation of these metals into the PANI matrix have been confirmed by FTIR, UV-Vis analysis.

- ❖ The UV-vis studies suggest that the absorption mechanism is due to direct allowed transition. The optical band gap of metal incorporated PANI composites decrease compare to the pure PANI.

- ❖ The temperature and frequency dependent electrical conductivity and dielectric properties have been studied extensively and the conduction process has been explained with the help of Mott theory.

- ❖ Mott theory gives an insight into hopping mechanism for localized states within the sample.

- ❖ The Cu incorporated PANI nanocomposites display drastic increase of electrical conductivity and dielectric properties.

4.7 References:

[1] H. Derivatives, J. Louis, A.G. Macdiarmid, Synthesis of Electrically Conducting Organic Polymers :, (1977) 578–580.

[2] A. Azha, A. Rahman, A. Ali, M. Habrul, U. Othman, Effect of bismuth telluride concentration on the thermoelectric prop- erties of PEDOT : PSS – glycerol organic fi lms, 66 (2015) 293–298. doi:10.1016/j.physe.2014.10.032.

[3] S. Srivastava, M. Haridas, J.K. Basu, Optical properties of polymer nanocomposites, 31 (2008) 213–217.

[4] V. Torrisi, F. Ruffino, Metal-Polymer Nanocomposites: (Co-)Evaporation/(Co)Sputtering Approaches and Electrical Properties, (2015) 378–424. doi:10.3390/coatings5030378.

[5] A. Roy, A. Ray, S. Saha, S. Das, Investigation on energy storage and conversion properties of multifunctional PANI-MWCNT composite, Int. J. Hydrogen Energy. 43 (2018) 7128–7139. doi:10.1016/j.ijhydene.2018.02.153.

[6] A. Roy, A. Ray, P. Sadhukhan, S. Saha, S. Das, Morphological behaviour , electronic bond formation and electrochemical performance study of V 2 O 5 - polyaniline composite and its application in asymmetric supercapacitor, Mater. Res. Bull. 107 (2018) 379–390. doi:10.1016/j.materresbull.2018.08.013.

[7] D.A.D. Corte, C. Torres, S. Correa, E.S. Rieder, D.F. Malfatti, The hydrogen evolution reaction on nickel-polyaniline composite electrodes, 7 (2011) 3–10. doi:10.1016/j.ijhydene.2011.11.037.

[8] W. Martı, Characterization of composite materials of electroconductive polymer and cobalt as electrocatalysts for the oxygen reduction reaction, 34 (2009) 694–702. doi:10.1016/j.ijhydene.2008.11.006.

[9] R. Liu, H. Qiu, H. Zong, C. Fang, Fabrication and Characterization of Composite Containing HCl-Doped Polyaniline and Fe Nanoparticles, 2012 (2012). doi:10.1155/2012/674104.

[10] A. Liu, L.H. Bac, J. Kim, J. Kim, Preparation and Comparative Study of Polyaniline / Copper and Polyaniline / Silver Composites by Electrical Explosion of Wire, (2013).

[11] H.P. De Oliveira, DNA / Polyaniline / gold nanocomposites : an electrical overview, (2015) 1070–1073.

[12] P. Bober, J. Stejskal, M. Trchová, J. Proke, Polyaniline e silver composites prepared by the oxidation of aniline with mixed oxidants , silver nitrate and ammonium peroxydisulfate : The control of silver content, 52 (2011) 5947–5952. doi:10.1016/j.polymer.2011.10.025.

[13] R.S. Biscaro, R. Faez, M.C. Rezende, Reactive doping of PAni-CSA and its use in conducting coatings, (n.d.).

[14] J.E.P. Silva, D.L.A. De Faria, S.I. Co, D. Torresi, Influence of Thermal Treatment on Doped Polyaniline Studied by Resonance Raman Spectroscopy, (2000) 3077–3083.

[15] M.B. Radoičić, M. V. Milošević, D.S. Miličević, E.H. Suljovrujić, G.N. Ćirić-Marjanović, M.M. Radetić, Z. V. Šaponjić, Influence of TiO<inf>2</inf> nanoparticles on formation mechanism of PANI/TiO<inf>2</inf> nanocomposite coating on PET fabric and its structural and electrical properties, Surf. Coatings Technol. 278 (2015) 38–47. doi:10.1016/j.surfcoat.2015.07.070.

[16] A. Dey, S. De, A. De, S.K. De, Characterization and dielectric properties of polyaniline–TiO $_2$ nanocomposites, Nanotechnology. 15 (2004) 1277–1283. doi:10.1088/0957-4484/15/9/028.

[17] S. Nurzulaiha, M. Zuber, D. Kamarun, H. Zaki, Synthesis and Characterization of Polyaniline Coated Gold Nanocomposites, 020010 (2015). doi:10.1063/1.4928827.

[18] U. Bogdanovic, I. Pas, C. Gordana, M. Mitric, S.P. Ahrenkiel, Interfacial Synthesis of Gold − Polyaniline Nanocomposite and Its Electrocatalytic Application, (2015). doi:10.1021/acsami.5b09145.

[19] L.M.A. Monzon, K. Ackland, The role of polyaniline in the formation of iron-containing nanocomposites, (2013). doi:10.1007/s11051-013-1533-5.

[20] S. Kundu, B. Satpati, T. Kar, S.K. Pradhan, Microstructure characterization of hydrothermally synthesized PANI/V2O5·nH2O heterojunction photocatalyst for visible light induced photodegradation of organic pollutants and non-absorbing colorless molecules, J. Hazard. Mater. 339 (2017) 161–173. doi:10.1016/j.jhazmat.2017.06.034.

[21] Comparative study of conducting polyaniline / copper and polyaniline / nickel composites in the presence of surfactants Aysegul Uygun a ∗ and Erhan Aslan b, (2010) 1162–1167. doi:10.1002/pi.2844.

[22] A. Ray, A. Roy, S. Bhattacharjee, S. Jana, C.K. Ghosh, C. Sinha, S. Das, Correlation between the dielectric and electrochemical properties of TiO 2 -V 2 O

5 nanocomposite for energy storage application, Electrochim. Acta. 266 (2018) 404–413. doi:10.1016/j.electacta.2018.02.033.

[23] A. Ray, A. Roy, S. De, S. Chatterjee, S. Das, Frequency and temperature dependent dielectric properties of TiO_2-V_2O_5 nanocomposites, J. Appl. Phys. 123 (2018) 104102. doi:10.1063/1.5012586.

[24] P. Maji, A. Ray, P. Sadhukhan, S. Chatterjee, S. Das, Study on charge transfer mechanism and dielectric relaxation of cesium lead, 124102 (2018). doi:10.1063/1.5026038.

[25] T. Foo, J. Hassan, Z. Abd, S. Azis, Results in Physics Electrical conductivity and dielectric studies of MnO 2 doped V 2 O 5, 6 (2016) 420–427.

[26] S.C. Tjong, Y.C. Li, R.K.Y. Li, Frequency and temperature dependences of dielectric dispersion and electrical properties of polyvinylidene fluoride/expanded graphite composites, J. Nanomater. 2010 (2010). doi:10.1155/2010/261748.

[27] A. Dhara, S. Sain, S. Das, S.K. Pradhan, Microstructure, optical and electrical characterizations of Mn doped ZnS nanocrystals synthesized by mechanical alloying, Mater. Res. Bull. 97 (2018) 169–175. doi:10.1016/j.materresbull.2017.08.060.

[28] Z. Abbas, M. Farooq, M. Azhar, I. Shakir, M. Shahid, M. Naeem, Impacts of neodymium on structural , spectral and dielectric properties of LiNi 0 . 5 Fe 2 O 4 nanocrystalline ferrites fabricated via micro-emulsion technique, Phys. E Low-Dimensional Syst. Nanostructures. 73 (2015) 169–174. doi:10.1016/j.physe.2015.06.001.

[29] M. Irshad, M. Azhar, S. Ahmad, I. Ali, G. Murtaza, M. Naeem, A. Aziz, A. Manzoor, Improved electrical , magnetic and dielectric properties of polypyrol (PPy) substituted spinel ferrite composites, Phys. E Low-Dimensional Syst. Nanostructures. 93 (2017) 313–317. doi:10.1016/j.physe.2017.07.001.

[30] D. Rettenwander, G.J. Redhammer, M. Guin, A. Benisek, H. Krüger, O. Guillon, M. Wilkening, F. Tietz, J. Fleig, Arrhenius Behavior of the Bulk Na-Ion Conductivity in Na3Sc2(PO4)3Single Crystals Observed by Microcontact Impedance Spectroscopy, Chem. Mater. 30 (2018) 1776–1781. doi:10.1021/acs.chemmater.8b00179.

[31] M.R. Das, A. Mukherjee, P. Mitra, Structural, optical and ac electrical characterization of CBD synthesized NiO thin films: Influence of thickness, Phys. E Low-Dimensional Syst. Nanostructures. 93 (2017) 243–251. doi:10.1016/j.physe.2017.06.018.

[32] S. Sinha, S.K. Chatterjee, J. Ghosh, Dielectric relaxation and ac conductivity behaviour of polyvinyl alcohol – HgSe quantum dot hybrid films, (n.d.). doi:10.1088/0022-3727/47/27/275301.

Chapter 5

Study on dielectric relaxation of Ni doped PANI

5.1 Introduction:

In this work, we have explored the possibility of improving the electrical conductivity of PANI by incorporation of Ni particles. PANI/Ni nanocomposites have been prepared by mechanical route of synthesis using Ball-mill. The electrical properties of these PANI/Ni composites have been investigated by using complex impedance, dielectric permittivity and AC conductivity.

PolyAniline possesses magnetic properties [1]. Because of its aromatic amine unit PANI provides exotic organic magnets [2], [3], [4]. In this particular work we tried to incorporate some coinage metals which are equally ferromagnetic into the PANI. Nickel is one such material. The objectivewas to develop novel kind of material which could emerge as organic magnetic material with a high amount of utility in the field of engineering and technology. For various limitations, we had to restrict our work to optical and dielectric studies of the composite material.

Most of the earlier reports follow chemical route of fabrication, radiolysis [5] etc. where it is difficult to keep Nickel in its purest form into the composite material. In most of the cases due to its high reactivity Ni gets oxidized. It is comparatively easy to incorporate Nickel Oxide (NiO) into PANI. PANI-NiO finds its use as supercapacitors and other energy storage devices [6], [7], [8], [9].

Our approach is a novel route of fabrication, i.e. mechanical route of fabrication by means of Ball-Mill method where PANI and Ni powders are mixed together and crushed in a planetary Ball-Mill system. Ball-Mill is a fast, cost effective, green technology which finds its growing use in material science and hybrid technology area rapidly [10], [11].

5.2 Experimental Details:

Aniline, HCl, Ammonium persulfate ($(NH_4)_2S_2O_8$) (APS), Ni nanoparticles etc. were purchased from Merck. All other reagents used in our experiment were of analytical reagent grade and were used without further purification. HCl doped PANI was synthesized by standard in-situ polymerization and the process is briefly described as follows:

- In a typical synthesis process, 2 ml of aniline monomer and 40 ml (1M) HCl were added together and mixed under continuous magnetic stirring at low temperature bath (0-5^0 C).

- 2.4 g Ammonium persulfate dissolved in 40 mL HCl (1 M) was added dropwise and polymerization was conducted at 0– 5^0 C under stirring for 12 h.

- A deep green resultant was obtained after the completion of polymerization. The resultant was washed with water and ethanol until the pH value reached to 7.

- Then the resultant was dried in vacuum at 60^0 C to get dry powder of HCl doped PANI.

5.2.1 Incorporation of Ni into PANI:

Incorporation of nickel nano-particles in PANI were done by mechanical route[12], [13],[14].

- Nickel powder containing particles in the μm and PANI were mixed in desired percentage and ball milled in planetary ball mill at 500 RPM in steel-chrome milling jar filled with several steel chrome balls.

- Sample to ball ratio was 1:40. Anhydrous isopropyl alcohol was added as milling medium to improve homogeneity in the mixture during milling. Ball milling was done for 12 hours with 50% rest time giving total 6 hours of milling time.

- This method provided enough time to dissipate the generated heat so that jar temperature never went above 40^0 C. After completion of milling, the products were collected in colloidal form and slowly dried at 50^0 C to get fine powder of PANI – metal nano composites.

5.3 Result and Discussion:

After obtaining the homogeneous mixture, it has been under gone various studies were carried out to check the utility of the composite material.

5.3.1 UV-Vis study:

Fig.1 shows the UV –Vis absorption spectra of PANI and PANI/Ni nanocomposite. A broad adsorption peak around 458 nm appeared in absorption spectra of both PANI and PANI/Ni. This adsorption peak is associated with the π-π^* transition of PANI. This peak makes the other peak associated with Ni nanoparticles very small.

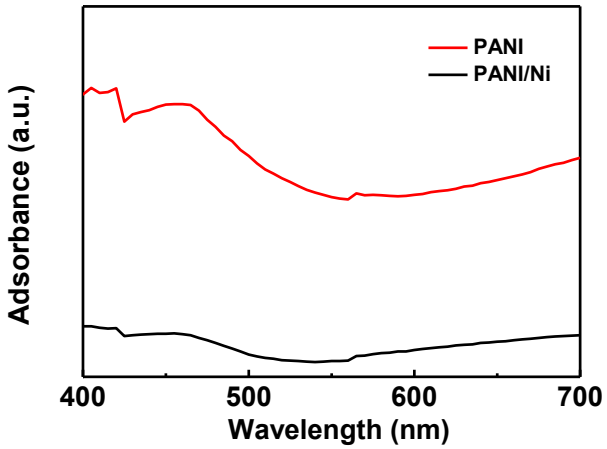

Fig. 5.1 UV-Vis Spectra of PANI and Ni doped PANI

5.3.2 XRD Analysis:

- The crystalline structure of the PANI/Ni composite is confirmed by XRD analysis as shown in Fig.2.
- The diffraction peaks at 2Θ = 21.4°, 23.8°, 32.5° and 41.1°represent the cubic structure of Ni for the diffraction planes (111), (200), (220) and (222), respectively.
- This result is well matched with standard spectrum of crystalline nickel (JCPDS NO. 73-1393). The sharpness and intensity of the peaks reveal the presence and large population of the crystallite planes [15].
- Since amount of PANI is much more than Ni in weight percentage, diffraction pattern is dominated by PANI signatures.

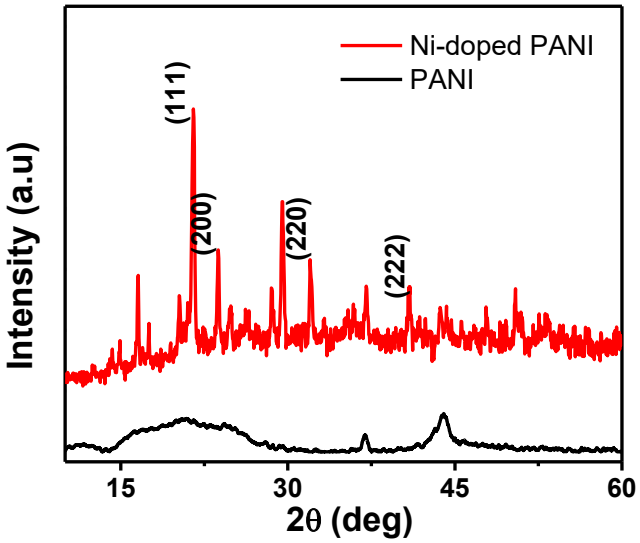

Fig. 5.2: XRD spectra of PANI and Ni doped PANI

5.3.3 FTIR Analysis:

The KBr pellets containing the materials are each placed inside FTIR spectrometer and measurements are carried out using Perkin-Elmer FT-IR spectrum RX1 spectrometer.

- Fig. 5.3 represents the FTIR spectra of PANI and PANI/Ni nanocomposite.
- A small peak at 509 cm^{-1} corresponds to vibration in amine molecule. The peak at 795 cm^{-1} is due to N-H bending of secondary amine.
- The peak at 1043 cm^{-1} is because of presence of water molecules due to natural humidity and corresponds to bending vibration of O-H bond.
- Peaks at 1226 cm^{-1} and 1286 cm^{-1} for PANI corresponds to C-H of benzenoid and quinoid ring of PANI.
- Two broad bands at around 1398 $cm^{-1}$and 1300 cm^{-1}correspond to C-N stretching vibration mode of quinoid ring.
- A peak at 1561 cm^{-1} corresponds to the stretching vibration of N-Q-N bond.
- In PANI/Ni all these characteristic peaks of PANI are present with slight deviation from their actual position.
- The peak at 996 cm^{-1} in PANI/Ni might be due to the presence of nickel.

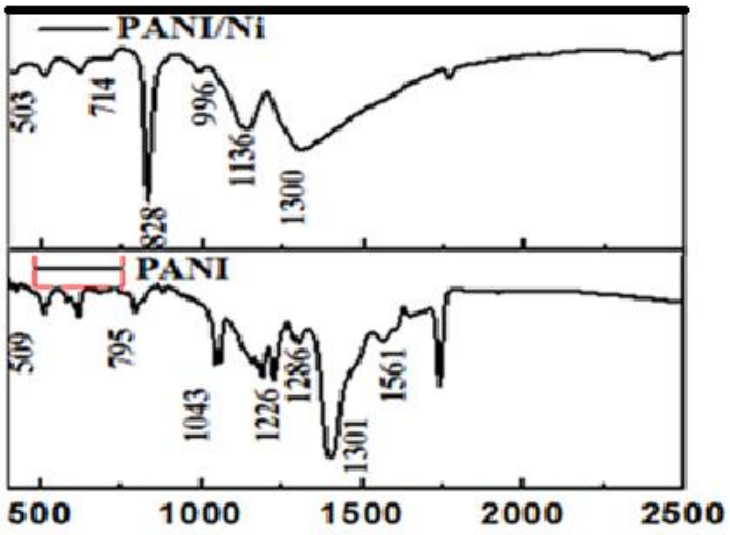

Fig. 5.3: FTIR spectra PANI-Ni and PANI

5.3.4 Dielectric Study:

The dielectric spectroscopy is a technique to obseverve the ac conduction mechanism and dielectric relaxation withina material by varying the temperature and frequency. In this technique, the parameters mainly considered are *complexim*pedance, *dielectric permittivity*, *electrical modulus* and *ac conductivity*.

- The non-localized (i.e. long range conductivity) and localized (i.e. dielectric relaxation) conductivity within the material, can be distinguished by the absence or presence of relaxation peak in frequency dependent imaginary modulus plot.

- Also a correlation between space charge effects and non-localized conductivity can be done depending on the presence of a peak in Z′ vs f plot.

- Activation energy and relaxation time plays crucial factors for a specific transportation mechanism.

- To analyse the whole dielectric properties, we demonstrate different electrical parameter based on single measurement.

- The frequency dependence representation of real part of dielectric impedance (Z') for nickel doped PANI has shown in Fig. 5.4(a).

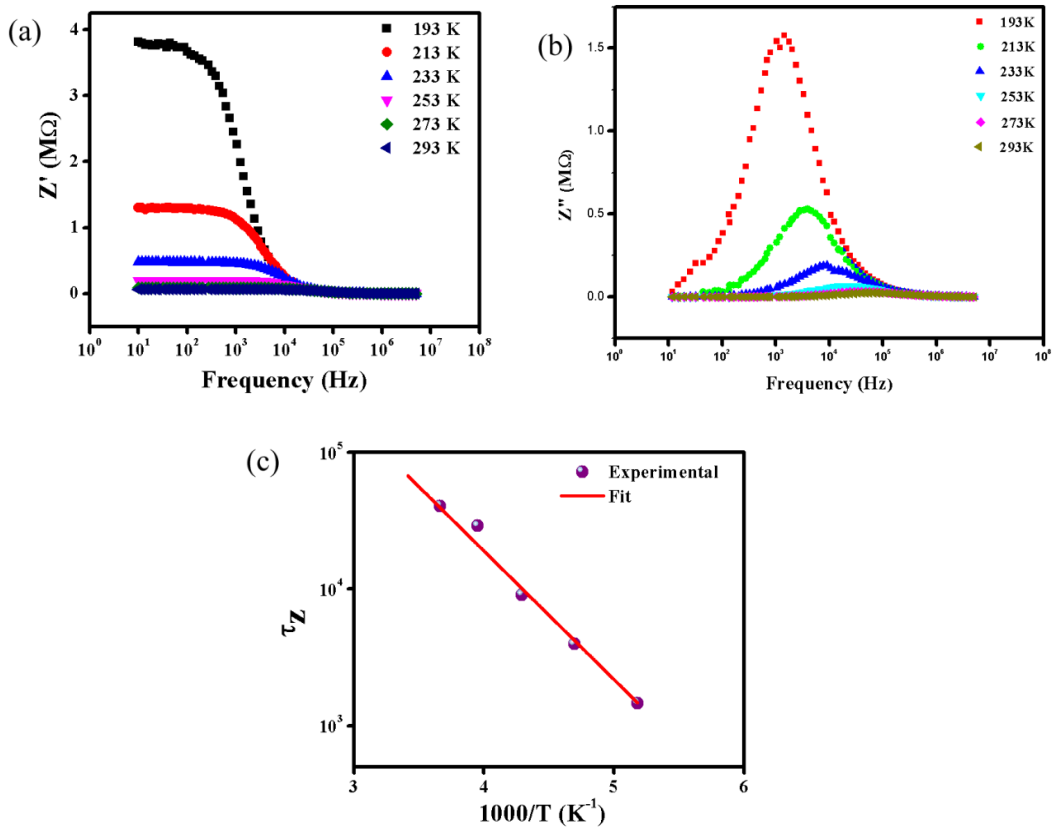

Fig. 5.4(a) Real impedance plot, (b) complex impedance plot, (c) Arrhenius plot

- From the above plot it has been observed clearly that at low frequency the value of $Z'(\omega)$ was high and decreased with increase of frequency.

- This was due to the combined effect of dipolar, electronic and orientation polarization which contributed significantly on the overall impedance.

- Also at higher frequency, no significant variation has been observed in the value of Z' indicating presence of space charge.

- It was observed that greater value of ac conductivity in high frequency domain may be due to the modified barrier properties and release of space charge.

- Fig.4b shows the frequency dependence imaginary part (Z'') of dielectric impedance for a frequency range 10 KHz- 5 MHz.

- The entire curve associated a peak, conventionally known as “Relaxation peak”, at high frequency region.

- The above said plot has two salient features, i) a loss peak, ii) peak broadening.

- The appearance of a single symmetric peak (“*relaxation peak*”) through out the spectrum confirmed the occurrence of dielectric relaxation. The broadening of the peak revealed distribution of relaxation time and frequency corresponds to maximum loss peak is known as mean relaxation frequency.

- We have estimated the relaxation time (τ_p^z) using the relation $\omega_p^z \tau_p^z$, where ω_p^z the relaxation frequency from Z" vs frequency plot. It has been observed that relaxation time changes with temperature and follows the Arrhenius law $\tau^z = \tau_0^z \exp(E^z/K_B T)$, where τ_0^z is pre-exponential factor and K_B, T represented Boltzmann constant and absolute temperature, respectively.

- The calculated value of activation energy (E^z) is 0.253 eV, obtained from linearly fitted Arrhenius plot has shown in Fig.4c.

- The calculated value of *‘Full Width at Half Maxima’* (FWHM) of (Z") plot is greater than $log((2+\sqrt{3})/(2-\sqrt{3}))$or 1.141 which reveals the deviation from ideal-Debye type relaxation process.

- The long range of charge transport was mainly contributed to the transportation below the maximum loss peak frequency and above relaxation frequency, because of localized motion of carriers within potential well.

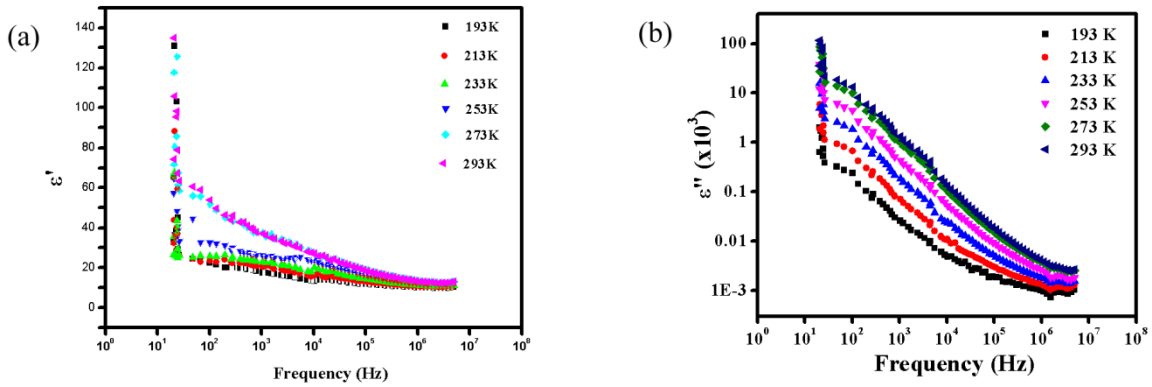

Fig. 5.5(a) Real permittivity plot, (b) complex permittivity plot

- Often analysis of relaxation mechanism through conventional techniques appears difficult because of the fact that the contribution from the dc conductivity prevails relaxation process. So, we have extensively investigated on the frequency dependent dielectric permittivity for Ni doped PANI.

- The frequency dependent dielectric permittivity can be expressed according to Mott's expression $\varepsilon^* = \varepsilon' - j\sigma''$, where real part of dielectric permittivity (ε') stands for ability of the material to store energy and imaginary component (ε'') represent entire energy loss inside the material. The real and imaginary part of complex dielectric permittivity can be calculated using the following equations 1(a,b) :

$$\varepsilon'(\omega) = \frac{Z''}{\omega C_o (Z'^2 + Z''^2)} \text{.....1(a)}$$

$$\varepsilon''(\omega) = \frac{Z'}{\omega C_o (Z'^2 + Z''^2)} \text{.....1(b)}$$

Where, $\omega = 2\pi f$ and $C_o = \varepsilon_o A/t$ (ε_o is free space permittivity, A is cross sectional area and t is thickness of the pellet).

- The frequency dependent real part of dielectric permittivity $\varepsilon'(\omega)$ for both sample has shown in fig.5a.

- The variation of $\varepsilon'(\omega)$ with frequencies is same for all the temperatures i.e. high at low frequency and decreases with increase in frequencies.

- At lower frequency, $\varepsilon'(\omega)$ is varying drastically (i.e. dispersion) and the "relaxed" permittivity mainly arising from dipole orientation.

- There were significant contributions from different polarizations such as orientational, interfacial and deformational (ionic and electronic) polarization in different frequency domain. Which effected in the decrease of $\varepsilon'(\omega)$ with frequency.

- With increase of frequency, under application of time reversal alternating field, contribution of oscillating charge carrier to dielectric permittivity become relatively less, results lowering tends of $\varepsilon'(\omega)$.

- At high frequency, the value of $\varepsilon'(\omega)$ does not change significantly and this "unrelaxed" value of permittivity reflects the atomic and electronic polarization.

- In fig. 5(b), the variation of imaginary part of dielectric constant $\varepsilon''(\omega)$ with frequency for different sample is shown. From figure it is clearly observed that $\varepsilon''(\omega)$ decreases with increase of frequency for the sample.

- The ascensive nature of $\varepsilon''(\omega)$ at lower frequency by virtue of dc conductivity. In that region dielectric loss factor vary with ω^{-1} as we know $\varepsilon''= \sigma_{dc}/\varepsilon_o\omega$. At higher frequency, vibration of ion mainly contribute to loss factor and can be explained by charge hopping between potential barrier within defect states.

- No loss peak has observed in entire frequency range suggested charge hopping frequency and applied ac field frequency are not equal.

The variation of ac conductivity with frequency and temperature has investigated in frequency range of 10 KHz – 5 MHz. Here we calculated ac conductivity using the equation 2.

$$\sigma_{(ac)} = \varepsilon'' \omega\varepsilon_o \qquad (2)$$

- Where ϵ'' represent imaginary part of dielectric constant, ω is the angular frequency and ε_o represent permittivity at free space.

- Fig.6a represents frequency dependent ac conductivity in logarithmic scale. At lower frequency, ac conductivity is almost constant i.e. independent of frequency and found to increase rapidly after a certain frequency, which is conventionally called hopping frequency.

- The plateau type region extended towards higher frequency value as temperature increases. This plateau type nature mainly due to dc conductivity.

- Transportation of charge carriers between different localized states increases with frequency that's why ac conductivity increases at higher frequency. According to Jump relaxation model (JRM), after hopping, a localized ion cannot be in equilibrium with neighbours.

- According to the theory, to achieve the stability, the neighboring ions will also move. Sometime, the ion jumps backward (unsuccessful hop) direction to get partially relax configuration.

- At low frequency, dc conductivity is prominent mainly due to successful hop of long range translational motion of ions. With increase of the frequency, some hops become unsuccessful.

- Increase of the ratio of successful/unsuccessful hoping results in conductivity more dispersive at high frequency.

- We have interpreted the Nyquist plot (Z''- Z), depleted as in Fig.6b According to Debye theory, the material having single relaxation time gives rise to a single semicircle with centred on real axis.

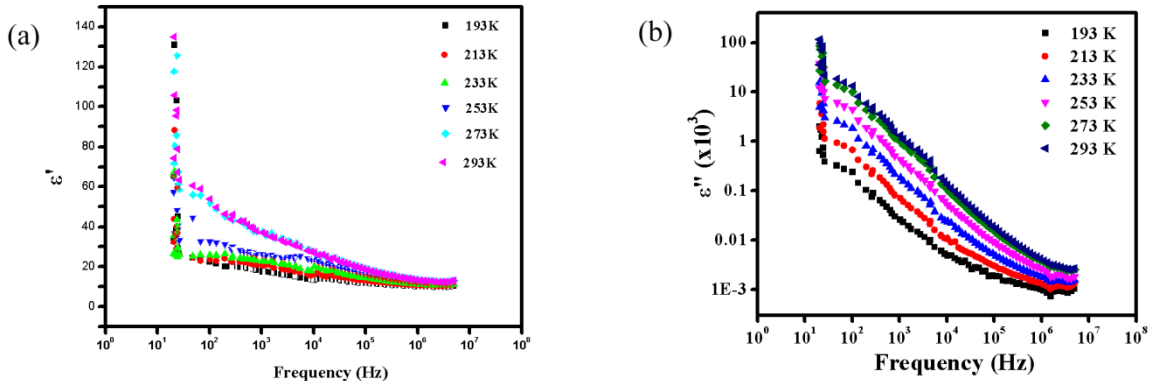

Fig. 5(a) Real permittivity plot, (b) complex permittivity plot

- But in practice, it can be treated as superimposition of two different semicircular arc contributed by intra-chain and inter-chain transportation at higher and lower frequency, respectively.

- The frequency dependent real and imaginary part of impedance can be expressed as equation 3(a,b).

$$\boldsymbol{Z'(\omega) = \frac{R_c}{[1 + (\omega R_c C_c)^2]} + \frac{R_{cb}}{[1 + (\omega R_{cb} C_{cb})^2]} \ldots\ldots\ldots\ldots\ldots (3a)}$$

$$\boldsymbol{Z''(\omega) = \frac{\omega C_c R_c^2}{[1 + (\omega R_c C_c)^2]} + \frac{\omega C_{cb} R_{cb}^2}{[1 + (\omega R_{cb} C_{cb})^2]} \ldots\ldots\ldots\ldots\ldots (3b)}$$

- Where, R_c = chain resistance, C_c = chain capacitance, R_{cb} = chain boundary resistance and C_{cb} = chain boundary capacitance.

Cole-Cole plot consists of a large semicircular arc at high frequency and a small tail at low frequency indicates that inter chain transport has more impact to the charge transport compared to disorder in chain. Also the suppressed semicircle centered at below the real axis suggests the clear deviation from ideal Debye type relaxation and distribution of relaxation time.

5.4 Conclusions:

Polyaniline (PANI) was prepared by a standard chemical polymerization technique. Nickel particleswere incorporated by using planetary ball milling method. X-ray diffraction spectra have been interpreted which assures the composite formation of Ni-doped PANI. A detailed investigation has been carried out on complex impedance, relative permittivity, complex modulus and ac conductivity for frequency range 10Hz-5MHz with different temperatures. The maximum loss peak in complex impedance spectra has been shifted with frequency which suggests the temperature dependent dielectric response of the material. Activation energy has been calculated using Arrhenius relation as 0.253 eV. The material obeyed non-Debye type relaxation mechanism which may be due to inhomogeneity presence within PANI. AC conductivity has been well interpreted using Jonscher's power law.

5.5 REFERENCES:

[1] M. E. Kompan, I. Y. Sapurina, V. Babayan, and N. E. Kazantseva, "Electrically conductive polyaniline-A molecular magnet with the possibility of chemically controlling the magnetic properties," *Phys. Solid State*, vol. 54, no. 12, pp. 2400–2406, 2012, doi: 10.1134/S1063783412120190.

[2] N. Martín, J. L. Segura, and C. Seoane, "Design and synthesis of TCNQ and DCNQI type electron acceptor molecules as precursors for 'organic metals,'" *J. Mater. Chem.*, vol. 7, no. 9, pp. 1661–1676, 1997, doi: 10.1039/a702314f.

[3] M. Properties, "Group-Substituted Poly(/n-aniline)s:," pp. 5618–5625, 1995.

[4] M. P. Struijk and R. A. J. Janssen, "Efficient synthesis of high-spin meta-para-oligoanilines .," vol. 103, pp. 3–6, 1999.

[5] A. M. Meftah, E. Gharibshahi, N. Soltani, W. M. Mat Yunus, and E. Saion, "Structural, optical and electrical properties of PVA/PANI/Nickel nanocomposites synthesized by gamma radiolytic method," *Polymers (Basel).*, vol. 6, no. 9, pp. 2435–2450, 2014, doi: 10.3390/polym6092435.

[6] B. S. Singu, S. Palaniappan, and K. R. Yoon, "Polyaniline–nickel oxide nanocomposites for supercapacitor," *J. Appl. Electrochem.*, vol. 46, no. 10, pp. 1039–1047, 2016, doi: 10.1007/s10800-016-0988-3.

[7] K. P. Gautam *et al.*, "Nickel Oxide-Incorporated Polyaniline Nanocomposites as an Efficient Electrode Material for Supercapacitor Application," *Inorganics*, vol. 10, no. 6, p. 86, 2022, doi: 10.3390/inorganics10060086.

[8] B. S. Anerao, A. M. Chaudhari, and S. B. Kondawar, "Synthesis and characterization of polyaniline-nickel oxide nanocomposites for electrochemical supercapacitor," *Mater. Today Proc.*, vol. 29, no. xxxx, pp. 880–884, 2019, doi: 10.1016/j.matpr.2020.05.107.

[9] S. Ahmad, M. M. Ali Khan, and F. Mohammad, "Graphene/Nickel Oxide-Based Nanocomposite of Polyaniline with Special Reference to Ammonia Sensing," *ACS Omega*, vol. 3, no. 8, pp. 9378–9387, 2018, doi: 10.1021/acsomega.8b00825.

[10] V. Monov, B. Sokolov, and S. Stoenchev, "Grinding in ball mills: Modeling and process control," *Cybern. Inf. Technol.*, vol. 12, no. 2, pp. 51–68, 2012, doi: 10.2478/cait-2012-0012.

[11] A. Stolle, T. Szuppa, S. E. S. Leonhardt, and B. Ondruschka, "Ball milling in organic synthesis: Solutions and challenges," *Chem. Soc. Rev.*, vol. 40, no. 5, pp. 2317–2329, 2011, doi: 10.1039/c0cs00195c.

[12] L. Takacs, "Self-sustaining reactions induced by ball milling," *Prog. Mater. Sci.*, vol. 47, no. 4, pp. 355–414, 2002, doi: 10.1016/S0079-6425(01)00002-0.

[13] T. H. El-Sayed, A. Aboelnaga, M. A. El-Atawy, and M. Hagar, "Ball milling promoted N-heterocycles synthesis," *Molecules*, vol. 23, no. 6, 2018, doi:

10.3390/molecules23061348.

[14] H. J. Fecht, E. Hellstern, Z. Fu, and W. L. Johnson, “Nanocrystalline metals prepared by high-energy ball milling,” *Metall. Trans. A*, vol. 21, no. 9, pp. 2333–2337, 1990, doi: 10.1007/BF02646980.

[15] H. S. Abdulla and A. I. Abbo, “Optical and electrical properties of thin films of polyaniline and polypyrrole,” *Int. J. Electrochem. Sci.*, vol. 7, no. 11, pp. 10666–10678, 2012.

Chapter 6

Conclusions & Future Scopes

6.1 Introduction

Although conducting polymer has multiple uses but its semiconducting properties increase manifold by inclusion of metal particles. There are many conducting polymers PolyAcetelene, PolyPyrrole, Polyvinylene. Among those PolyAniline (PANI) has been chosen for our work because of its oxidative dose dependent controllable optical and electrical properties. It can achieve its conductivity from insulator to semiconducting materials. PANI is conducting in its Emeraldaine Salt (ES) form. By doping ES Base with different acids and different pH we can obtain different conductivities. For example emarldine PANI gives more conductivity when doped with camphor sulfonic acid, compared to doped by hydrochloric acid. Again, when dissolved with *m*-Cresol its conductivity increases further. These wonderful aspects make PANI a good replacements of inorganic counterpart in many applications.

PANI film fabrication seems a challenging task. Different thicknesses of films provide different usefulnesses. Thick films in the range of μm to mm are useful for electrical conductions as they offer higher conductivity than the thin film ones. Thin films are particularly useful for optical purposes as thick films become opaque. To prepae thickfilms dropcasting method is used. To fabricate thin films, mainly two methods are used to obtain uniform thin films – 1) Dip coating, 2) Spin Coating. In our lab we used Spin coater for thin film fabrication. In both the cases of film fabrications a smooth, thick and homogenous solution is required. To prepare such solution continuous stirring for almost 72 hours required. The substrates for films can be anything from laboratory grade glass slides to n-type Silicon wafer. Glass slides are useful for optical studies. Alumimium, copper like substrates are used observe Schottky junction behaviour. ITO coated glass slides can be used for electrical studies. And finally silicon wafers are used mainly structural studies like cross-sectional FESEM. Various trial and error methods are used to optimize thin films.

PANI blended with metal nanoparticles show enhanced opto-electric properties. Metal nanoparticles are used, specially noble metals like gold, silver, copper and coinage metal like nickel used for our purposes. These metals posses SPR peaks at visible range as well as good conductivity at nanoparticle form. there are few ways of incorporating metal nanoparticles into conducting polymers, like a) sol-gel method, b) chemical-route of fabrication, c) vapor depositions, d)metal ion implantations, e) Ball-milling method etc.

- In sol-gel method two different solutions containing polymer and nanoparticles are mixed together. But PANI being insoluble in water this method can be discarded easily.

- Chemical route of fabrication involves costly chemicals and sufficient knowlwdge of chemistry. Moreover study from earlier reports could not provide satisfying outcome of the result.

- Our novel approach is to incorporate metal inclusion into conducting polymer matrix by the method of ion implantation.

- The novelty of this method is that we can implant at a specific depth. Amount of metal inclusion is much more than chemical route of fabrication.

- With the method of ball-milling or mechanical route metal incorporation can be achieved in the bulk which not very helpful while working with the thin film.

6.2 Questions aroused

while dealing with the problem, in our present work, few questions arised in our mind,

i. *What is the need of conducting polymer metal nanoparticle composites, does it really help in advanced electronic device?*

ii. *What are the possible routes of incorporating nanoparticles into the material? What are the drawbacks of each method.*

iii. *Finally can we tune the optical and electrical properties of the composite material according to our need?or if the changes in optical and electronic properties are acceptible or not.*

iv. *What are the possible use of the obtained material?*

6.3 Chapterwise summary of findings

1. **Chapter 1**comprises introduction chapter where we get to know the works done so far on conducting polymers especially Polyaniline (PANI) and metal nanoparticles nanocomposites. There are many striking features of conducting polymer PANI, metal nanoparticles, like gold, silver etc. like noble metals and Nickel like coinage metals too and altogether their composite materials also show exotic properties. These properties are feedstock growing research trends with them. We grasped from literature review that although there are many methods of incorporating metal nanoparticles into conducting polymers like, sol-gel, vapour deposition, *in-situ* chemical polymerization etc. we chose ion implantation and mechanical route of fabrication considering few of their strong advantages. After having a deep thought considering the characteristics like environmental stability, Surface Plasmon Effects (SPR) we select Gold, Silver and Nickel as our working nanoparticles.

2. **Chapter 2** firmly investigates on the method of metal ion implantation and thin film fabrication. First of all we stress on optimization of thin film fabrication of PANI dissolved in different solvents. We then have a prior calculation before ion implantation, i.e, SRIM ananlysis to determine desired energy. Then Au and Ag ions are implanted with varying doses and their optical, electrical and structural studies have been done. Although ion beams are capable of incorporating high amount of metal inclusions with utmost purity, but it creates considerable amount of damage within the material which reflects in the optical and electrical studies of the composite material. So, a trade off is required between dose/energy and conductivity or reflectivity. Moreover, the depth of distribution of metal clusters can be controlled with ion beam implantation.

3. **Chapter 3** is dealing with thick film. Thickness of the films are optimized by controlling the drop size and diffeent paprameters of *Spin coater*. Thick films are in µm to mm range and MeV range implantation energy is applied on them. For thin films energy is restricted to below 100KeV. Silver and Nickel ions are implanted. Then they are gone through various structural, optical and electrical studies. Cross-sectional FESEM reveals formation of metal clusters into the voids created by ion beam bombardment. With doses, the amount of metal inclusions increase. At higher doses carbonifications restrict the electrical conductivity. Due to graphite formation, metallic lustre apppears at higher doses.

4. In **Chapter 4** Copper (Cu) incorporated Polyaniline (PANI) composites have been successfully synthesized by mechanical mixing method in a Ball-Milling system. The

ball-milling is a fast, cost effective and green method. The prepared composites have been characterized by UV-Vis, FTIR spectroscopy.The UV-Vis study shows that the optical band gap of PANI decreases due to incorporation of Cu particles. The temperature (193K- 333K) and frequency (10Hz- 10MHz) dependent electrical conductivity shows that the conductivity of PANI increases after Cu incorporation. The ac-conductivity of the composites is ascribed to correlated barrier hopping charge transport mechanism. The Cu-PANI composite shows higher ε′ value at all frequencies. Over all dielectric studies indicate that the Cu incorporated PANI has better ability to store electrical energy and can be used in as energy storage devices and thermoelectric devices.

5. In **Chapter 5**, PANI has been prepared in the same way as the earlier chapter. Method of Ball-Milling is appied with the same intention as the earlier chapter. Nickel here incorporated because it has ferromagnetic property and earlier reports show that PANI too possesses some magnetic properties, so the summation from both material can further enhance the magnetic property. X-ray diffraction spectra have been interpreted which assures the composite formation of Ni-doped PANI. The maximum loss peak in complex impedance spectra has been shifted with frequency which suggests the temperature dependent dielectric response of the material. Activation energy has been calculated using Arrhenius relation as 0.253 eV. The material obeyed non-Debye type relaxation mechanism which may be due to inhomogeneity presence within PANI. AC conductivity has been well interpreted using Jonscher's power law.

6. In the last last chapter we reconnoiter all the findings of our works plan for the future research.

6.5 Recommendations

The work of opto-electric property studies by the method of ion implantation can be recommended in the following applications:

- Thin films on different substrates and free standing films can be optimized by the method of drop casting and spin coating.

- Ion implantation can change the structure of a polymer and the void spaces actually help in agglomeration of nanoparticles, so by the method of ion implantation we can incorporate metal particles into the matrix at which out numbers conventional chemical route of sysnthesis.

- By controlling the energy of the implantaion, we can actually control the depth of the nanoparticle layer. Which is a very important outcome from this research.

- The composites have enhanced electrical and dielectric properties at some specified dose and energy which can be used in many practical applications.

6.6 Future scopes of research

There are many further investigations can be continued based on the present outcomes:

i) *Change in conductivity and dielectric properties with the thicknesses of the free-standing films need to be observe as well as the semiconducting property as PANI is considered to be p-type in nature.*

ii) *If the p-type nature of PANI changes with the ion implantation.*

iii) Considerable amount of research is required to check the formation of metal nanoparticles with the dose, energy, species of metal. Any change in degassing, carbon cluster formation when implantation is taking place at room temperature and in cool environment i.e, liquid nitrogen chamber.

iv) Cross-sectional TEM analysis is required confirm the sizes of the nanoparticles formed through this method.

v) What happens to the ferromagnetic property when imbibed with coinage metals.

vi) We can check any change in opto-electric, photoluminescence properties of the composite films when electric and magnetic fields are applied across them.

vii) The incorporation of metal nanoparticles can increase the conductivity of the composite material by increasing the electron hopping. At the same time these particles can reduce the thermal conductivity by phonnon scattering which gives rise to overall increase in thermal coefficient or Seebeck coefficient. So these kind of composites can act as good thermoelectric material.

viii) All the above studies can be done by incorporating rare-earth elements into the conducting polymer.

6.7 Conclusions

In conclusion we can say that the method of ion implantation and Ball-mill can produce polymer-metal nanocompites. The method of ion implantation can be applied successfully for film technology where as the Ball-mill can produce composite materials in bulk. Both the kinds of materials have their own kind of application areas. There are lots scopes remain for future studies. Already cultivated features show that the above two methods can improve the opto-electric and dielectric properties of the composite material than the individual ones.